TAMPEREEN TEKNILLINEN YLIOPISTO
TAMPERE UNIVERSITY OF TECHNOLOGY

JOONAS AHOPELTO

INNOVATIVE AND ECONOMIC UTILIZATION OF STAINLESS STEEL IN LOAD BEARING STRUCTURES

Master of science thesis

Examiner: Senior research fellow Kristo Mela
Examiner and topic approved by the Vice Dean of the Faculty of Engineering Sciences on 1st November 2017

ABSTRACT

Joonas Ahopelto: Innovative and economic utilization of stainless steel in load bearing structures
Tampere University of Technology
Master of Science Thesis, 92 pages, 8 Appendix pages
July 2018
Master's Degree Programme in Mechanical engineering
Major: Analyzing of machines and structures
Examiner: Senior research fellow Kristo Mela

Keywords: stainless steel, energy absorption, fire design

In this work properties of ferritic, austenitic and duplex stainless steels were studied. The objective was to obtain the good properties of stainless steels by performing an inclusive overview on the published material on stainless steels. Based on the findings, energy absorption and elevated temperature properties were chosen to be studied in more detail. Finite element models were developed for the axial crush of single tube and bitubular structures, and the prediction of the models were compared to available experimental results. Elevated temperature properties of stainless steels and carbon steel were studied by performing mass and cost comparisons according to available fire design rules (Eurocode, Design Manual for Structural Stainless Steel).

Energy absorption of an axially loaded tube was simulated in explicit dynamics. Simulation model of a single tube axial crush gave good predictions for stainless steel and aluminum, and the error of the models compared to experimental results were around 10%. However, the simulation of the crush of a bitubular structure had a larger error (29%) in energy absorption when compared to the experimental data. At least a part of the reason for the excessive error was assumed to be the interaction between the two tubes, because the single tube model with the same material model and boundary constraints gave only 10% error. Because of the excessive error and uncertainty about the effects of the calculation parameters on the results when the dimensions or boundary conditions are changed, further parametric studies were not performed.

In fire design both mass and overall costs of carbon steel and stainless steel members were studied. The costs of the fire protection are not unequivocal, but the aim was to use descriptive values of general cost level. Also, the price of stainless steels fluctuates greatly affecting the total costs. The mass comparison was performed with only unprotected columns, whereas in cost comparison mild steel columns were calculated with and without fire protection. The studies showed that in the example loading situations with fire reduction factor of 0.35–0.57, the stainless steel columns were 21–46% lighter than unprotected carbon steel column in 15 min standard fire. The differences in masses were higher in 30 min standard fire. Though, unprotected carbon steel may not be used with R30 requirement. The studies on overall costs, excluding the life-cycle costs, showed that austenitic stainless steels EN 1.4301 and stabilized EN 1.4571 were at best 26% and 45% more expensive than the cheapest mild steel member with fire protection in chosen example situations. If the life-cycle costs were taken into account, it would give the stainless steels an advantage, as the need for maintenance is low compared to the painted carbon steels.

TIIVISTELMÄ

Joonas Ahopelto: Ruostumattoman teräksen innovatiivinen ja taloudellinen käyttö kantavissa rakenteissa
Tampereen teknillinen yliopisto
Diplomityö, 92 sivua, 8 liitesivua
Heinäkuu 2018
Konetekniikan diplomi-insinöörin tutkinto-ohjelma
Pääaine: Koneiden ja rakenteiden analysointi
Tarkastaja: Yliopistotutkija Kristo Mela

Avainsanat: ruostumaton teräs, energian absorbointi, palomitoitus

Tässä työssä tutkittiin ferriittisten, austeniittisten ja duplex ruostumattomien terästen ominaisuuksia. Tavoitteena oli löytää ruostumattomien terästen hyvät ominaisuudet kattavalla ruostumattomista teräksistä julkaistun kirjallisuuden tutkimuksella. Energian absorptio ja korkeiden lämpötilojen ominaisuudet valikoituivat tarkempaan tarkasteluun. Yhden ja kahden putken aksiaalisesta kasaan puristuksesta tehtiin elementtimenetelmäohjelmistolla simulointimallit, joiden tuloksia vertailtiin kokeellisiin tuloksiin. Ruostumattoman teräksen kohotetun lämpötilan ominaisuuksia tutkittiin massa- ja kustannusvertailussa yhdessä hiiliteräksen kanssa saatavilla olevien suunnitteluohjeiden mukaan (Eurokoodi, Design Manual for Structural Stainless Steel).

Kasaan puristetun putken energianabsorptiota simuloitiin eksplisiittisellä dynamiikalla. Ruostumattoman teräksen ja alumiinin yhden putken simulointi antoi hyviä tuloksia, ja energian absorptio vastasi noin 10 % virheellä kokeellisia arvoja. Kuitenkin kahden alumiiniputken mallissa ero energian absorptiossa kokeellisiin tuloksiin oli 29 %. Ainakin osasyy kasvaneeseen virheeseen otaksuttiin olevan kahden putken välinen vuorovaikutus, sillä yhden putken materiaalimalli samalla materiaalimallilla ja samoilla reunaehdoilla antoi vain 10 % virheen. Parametrista tutkimusta ei tehty epätarkkuuden takia. Lisäksi simuloinnissa oli epävarmuutta siitä, miten laskentaparametrit vaikuttavat tuloksiin geometriaa tai reunaehtoja muutettaessa.

Palomitoituksessa tehtiin sekä massa- että kustannusvertailua hiiliteräkselle ja ruostumattomalle teräkselle. Palosuojauksen kustannukset eivät ole yksiselitteisiä, mutta tavoitteena oli valita yleistä tasoa kuvaavat kustannusarvot. Ruostumattoman teräksen hinnassa on myös voimakasta heilahtelua, joka vaikuttaa merkittävästi ruostumattoman teräspilarin kokonaiskustannuksiin. Massavertailu tehtiin ainoastaan suojaamattomilla pilareilla, kun taas kustannusvertailussa hiiliteräspilari laskettiin sekä palosuojaamattomana että palosuojattuna. Laskelmat osoittivat, että valituissa esimerkkiolosuhteissa palotilanteen kuorman pienennyskertoimen ollessa 0,35–0,57 ruostumattomat teräsputket olivat 21–46 % kevyempiä kuin S355-hiiliteräsputki 15 min standardipalossa. Erot 30 min standardipalossa olivat suuremmat. Tosin, suojaamatonta hiiliteräspilaria ei välttämättä käytettäisi R30-palovaatimukselle. Kokonaiskustannusvertailussa, elinkaarikustannukset pois lukien, austeniittiset EN 1.4301 ja stabiloitu EN 1.4571 olivat parhaimmillaan 26 % ja 46 % kalliimpia kuin halvin hiiliteräsputki. Jos elinkaarikustannukset otettaisiin huomioon, antaisi se ruostumattomalle teräkselle kilpailuetua, sillä ruostumattoman teräksen ylläpidon tarve on vähäistä maalattuun hiiliteräkseen verrattuna.

FOREWORD

This work was done at A-Insinöörit as a part of a project for Stalatube, which was the financier of this work. This thesis has given me a great opportunity to take a closer look at the properties of stainless steels and possible advantageous use in structural applications – to a subject which I was not very familiar with beforehand. Material science studies as a minor subject and major studies among mechanics of solids gave a solid ground to further study the stainless steels and applications in structural design.

I would like to thank especially Kenneth Söderberg and Tommi Purtilo from Stalatube for their support and guidance during the work, and examiner Kristo Mela for his comments. Here at A-Insinöörit instructors Ilari Pirhonen and Ville Laine, but also coworkers Lauri and Henry, have given valuable comments on the subject, and I'm very grateful for those. Thanks to my family and friends – Juha, Toni and Kasper among others – who have offered me also pleasant free-time activities while doing this work. Special thanks to my sister for the guidance in English in this work.

Now it's time to leave the university studies behind and continue the lifelong learning at work among structural analysis – after this thesis, with better knowledge on the stainless steels.

In Tampere, Finland, on 30th of July 2018

Joonas Ahopelto

CONTENTS

LIST OF SYMBOLS AND ABBREVIATIONS

AISI	American Iron and Steel Institute
ASTM	American Society for Testing and Materials
BRBF	Buckling resistant braced frame
CBF	Concentrically braced frame
CFST	Concrete filled steel tube
CFSST	Concrete filled stainless steel tube
CHS	Circular hollow section
CSM	Continuous strength method
DSM	Direct strength method
EBF	Eccentrically braced frame
EC3	Eurocode 3
EN	European norms
FEA	Finite element analysis
FEM	Finite element method, finite element model
LBA	Linear buckling analysis
LC	Load case
MRF	Moment resistant frame
PRE	Pitting resistance equivalent
RHS	Rectangular hollow section
SHS	Square hollow section

A	Ultimate elongation in EN 10088 *or* amplitude *or* cross sectional area
A_0	Reference amplitude
A_m	Surface area of the member which is subjected to fire
b	Width of the cross section
c	Geometry parameter for cross section classification *or* specific heat of stainless steel
c_a	Specific heat of steel
C_i	i = 1, 2, 3, material model constants
E	Modulus of elasticity
E_{sh}	Strain hardening modulus
$E_{p0,2,\theta}$	Tangent modulus at $f_{p0,2,\theta}$
E_θ	Modulus of elasticity at temperature θ
$f_{0,2}$	0.2% proof strength at room temperature
$f_{2,\theta}$	2% proof strength at temperature θ
$f_{p0,2,\theta}$	0.2% proof stress at temperature θ
f_u	Ultimate strength
f_y	Yield strength (design strength)
F_{mean}	Average crushing force in axial crush
F_{peak}	Peak force in axial crush
G_k	Permanent load
h	Height of the cross section
$\dot{h}_{net}$	Net heat flux on the fire exposed surfaces (Eurocode notation)

$\dot{h}_{net,d}$	Net heat flux on the fire exposed surfaces (Design Manual for Structural Stainless Steel notation)
$\dot{h}_{net,c}$	Net convective heat flux
$\dot{h}_{net,r}$	Net radiative heat flux
I	Second moment of area
$k_{E,\theta}$	Reduction factor for modulus of elasticity at temperature θ
$k_{p0.2,\theta}$	Reduction factor for 0.2% proof strength at temperature θ
$k_{p0,2,\theta,CF}$	Reduction factor for 0.2% proof strength of cold formed material at temperature θ
k_{sh}	Correction factor for shadow effect
$k_{y,\theta}$	Reduction factor for yield strength at temperature θ
m	Exponent defining material nonlinearity in room temperature
m_θ	Exponent defining material nonlinearity at temperature θ
$m_{\theta,2}$	Exponent defining material nonlinearity at temperature θ
M_L	Magnitude of an earthquake (Richter's scale)
$N_{b,Rd}$	Design buckling resistance
$N_{b,fi,t,Rd}$	Design buckling resistance at time t and uniform member temperature θ_a
N_{cr}	Critical load, Euler buckling
N_{Ed}	Design compressive load in room temperature
$N_{fi,Ed}$	Design compressive load in fire
n	Ramberg–Osgood parameter
n_θ	Exponent defining the material nonlinearity at temperature θ (Ramberg–Osgood parameter)
$Q_{k,i}$	Variable load
t	Thickness *or* time [min]
V	Volume of steel in fire design

α	Factor of inaccuracy
α_c	Convective heat transfer coefficient
γ_G	Load combination factor for permanent load
γ_{M1}	Partial safety factor for buckling resistance
$\gamma_{M,fi}$	Partial safety factor in fire
$\gamma_{Q,i}$	Load combination factor for variable load
$\Delta\theta_{a,t}$	Uniform temperature rise of the cross section
ε	Engineering strain *or* parameter for cross section classification in room temperature
ε_f	Emissivity of the fire
ε_m	Emissivity of the steel surface
ε_θ	Parameter for cross section classification in temperature θ
$\varepsilon_{p0,2,\theta}$	0.2% plastic (engineering) strain corresponding to $f_{p0,2,\theta}$
ε_u	Ultimate elongation
$\varepsilon_{u,\theta}$	Ultimate elongation at temperature θ
ε_y	Yield strain
η_{fi}	Reduction factor for fire load

θ	Member uniform temperature (Design Manual for Structural Stainless Steel notation)
θ_a	Member uniform temperature (Eurocode notation)
θ_g	Standard temperature–time curve
θ_m	Surface temperature of the member
θ_r	Effective temperature of the environment, can be taken as the gas temperature θ_g
$\bar{\lambda}$	Non-dimensional slenderness
$\bar{\lambda}_\theta$	Non-dimensional slenderness at member temperature θ
$\bar{\lambda}_0$	Limiting non-dimensional slenderness
ρ	Density of the steel (Design Manual for Structural Stainless Steel notation)
ρ_a	Density of the steel (Eurocode notation)
σ	Engineering stress *or* Stephan–Boltzmann constant in fire design
Φ	Factor for buckling resistance calculations (carbon steel)
ϕ	Factor for buckling resistance calculations (stainless steel)
ϕ_θ	Factor for buckling resistance calculations in fire (stainless steel)
φ_θ	Factor for the reduction factor for flexural buckling
χ	Reduction factor for buckling resistance at room temperature
χ_{fi}	Reduction factor for buckling resistance at fire
ψ_{fi}	Variable action fire load factor

1. INTRODUCTION

Stainless steels are a group of steels with at least 10.5% chromium content. Good corrosion and heat resistance, good durability and low maintenance requirements are general properties of stainless steels. As the sustainable development is becoming more important, the fully recyclable stainless steels are an attractive option. [1] In 2008 approximately 4 million tons of stainless steel or 14% of all produced stainless steels were used in structural applications worldwide. The ratio has remarkable differences between different countries. The annual growth in the use of stainless steel is around 5%. [2]

Today, stainless steels are used in different structural and architectural applications [2] but are also widely used in transportation as well as in oil and gas industry. In recent years the use of stainless steels in load bearing structures has increased because of their good mechanical properties. [1] For different requirements of mechanical properties, there are a wide range of different stainless steel grades to fit the needs [3]. Austenitic and duplex grades are the most used grades in structural applications for their good properties discussed later, but also because they have been researched and validated [1]. Ferritic stainless steels have been mostly used in indoor-applications, though some ferritic grades have been developed for the structural applications, too [2].

This work was done for Stalatube, which produces stainless steel tubes, I-beams and flat bars. The data of this work is meant to be used to guide Stalatube's product development. Thus, the goal of this work was to gather data and answer the research questions: what the good properties of stainless steels are, and what are the possible applications where they can effectively and economically be used. Also, information about how stainless steel compares to carbon steel in both mechanical performance and costs were to be studied. This work was primarily an extensive survey on the published research on stainless steel to gather the aforementioned information. Comparisons of stainless steel and carbon steel with respect to mechanical performance and structure mass can be relatively widely found on the literature, but information about the cost difference between these two materials seemed to be rare. This work presents a suggestive cost data comparison of axially loaded carbon steel and stainless steel members in room temperature and in fire, partially filling the gap in information about stainless steel costs relative to carbon steel costs.

First, a thorough review was carried out on the available material on stainless steel and key points of several studies were summarized in chapter 2. During the literary research, energy absorption properties and mechanical properties in elevated temperatures stood out and were selected to be studied in more detail in their own chapters. Energy absorption and crashworthiness properties were studied with further literature research in chapter 3.

In chapter 3.5 finite element models with ANSYS AUTODYN for both single tube and bitubular axial crush were developed, and the predictions of the models were compared to experimental data. Chapter 4 focuses on the fire design with stainless steel. First the elevated temperature properties of stainless steels are discussed, and then in chapters 4.3 and 4.4 studies of mass and overall costs with carbon and stainless steels are presented. Only unprotected mild steel was included in the mass comparison, but in overall cost comparison mild steel columns with and without fire protection were considered. The results of this work are discussed in chapter 5 and a brief summary is presented in chapter 6.

A high number of articles, reports and surveys are published about stainless steel, and therefore it is time consuming to obtain the subjects of interest from the publications. Here some publications are gathered in groups based on some of the main topics. Most of them are used in this work, but also around 20 studies are included here, but are not later cited in this work. Material behavior of stainless steel differs remarkably from the behavior of carbon steel. Strain rate and cold forming affects the mechanical properties, and especially the latter has a more remarkable impact on stainless steel than on carbon steel. Room temperature material behavior such as the stress–strain curve and the effects of strain rate and cold forming, for instance, are investigated in [4-22]. Design rules and codes for stainless steel (such as Eurocode, direct strength method) and their accuracy, experimental cross section capacity, buckling and fatigue are studied for example in [3, 23-43]. Bolted stainless steel connections are studied in [44-46]. To date, mechanical behavior of stainless steels in elevated temperatures is rather well studied. These studies, for instance, are focused on this subject: [46-58]. Overall, mechanical behavior of stainless steel in fire and after fire exposure is excellent.

Stainless steels, especially austenitic grades, have high ductility and ultimate strength, which are promising qualities for good energy absorption. Energy absorption can be critical in different kind of applications such as crashworthiness and protection from ballistic impact or from explosion. These properties are studied in [59-73]. Seismic design also benefits from excellent ductility and strain hardening and the use of stainless steel in seismic design has been examined in [74-77]. The benefits of using stainless steel in concrete filled steel tubes are studied in several papers in both room temperature and in fire, [78-85]. Several surveys, reviews and design manuals on stainless steels have also been published. Some are focused on a specific subject such as fire design or structural application possibilities and some are reviews of stainless steels in general. References [1-3, 86-89] belong to these categories, to name a few.

2. STAINLESS STEELS

Stainless steels in general are highly alloyed. In addition to chromium, alloying elements molybdenum, nickel and nitrogen are commonly used to control the grain structure, mechanical properties or corrosion resistance of the stainless steels. [88, 89] Titanium and niobium are also noted in EN 10088-4 to be used for stabilizing stainless steel grades [90]. Because of the different mechanical behavior of stainless steels and carbon steels, a few terms that arise with stainless steels but are not so important with carbon steels and they are explained here. Stainless steels don't have a clear yield point, and for that reason **0.2% proof strength** is used: it is the stress level measured at 0.2% plastic strain. When term yield strength is used for stainless steels, it usually means 0.2% proof strength. Cold forming or cold rolling can have a significant effect on the strength of stainless steels, because stainless steels experience work hardening. [3] **Work hardening**, also called **strain hardening**, describes the strength increase when the material goes through plastic deformation (permanent deformation).

Stainless steels can be divided into five groups: ferritic, austenitic, duplex, martensitic and precipitation-hardening grades. **Ferritic grades** are the most affordable stainless steels and have a stable price due to the low nickel content. [1] They are usually alloyed with 10.5–18% chromium content, and the grain structure is the same as in mild steels. This leads to lower ductility, deformability, weldability and corrosion resistance when compared to austenitic stainless steels. [88] Ferritic grades can be work-hardened but less than the austenitic grades [3]. They cannot be strengthened by thermal treatment, but they still have good strength and durability [1]. Ferritic grades have better workability and machinability than the austenitic grades [42], similar to S355 mild steel [3]. Ferritic stainless steels are also magnetic like the mild steels [88]. Toughness of the ferritic stainless steels is often poor in low temperatures, especially with thicker cross sections, though EN 1.4003 has a modified microstructure giving it a sufficient toughness, equivalent to carbon steels, in low temperatures [1, 87]. Ferritic stainless steels are usually used in indoor applications or in mild outside environments [3], and they have relatively minor usage in structural applications, because there have been less performance data and design guides available for ferritic stainless steels. EN 1.4003 and EN 1.4016 are the most used grades among ferritic stainless steels. [1]

Austenitic stainless steels have a modified face centered cubic grain structure and because of that they have high ductility, cold-formability and weldability [43, 88]. These grades are usually alloyed with 17–18% of chromium and 8–11% of nickel. In addition to chromium content, adding molybdenum can enhance the corrosion resistance. [88] Austenitic stainless steels also have high strain hardening [88], though the initial 0.2% proof strength value might not be very high. For instance, for the most used austenitic

stainless steel EN 1.4301 in cold-rolled condition, the minimum values in EN 10088-4 standard are for 0.2% proof strength 230 MPa, for tensile strength 540–750 MPa and for elongation at fracture 45% [90]. The corresponding values from the supplier are usually higher, and for example Outokumpu EN 1.4301 equivalent stainless steel Core 304/4301 has a 0.2% proof stress of 285 MPa, tensile strength of 640 MPa and ultimate elongation of 70% [91]. Nickel-free, high nitrogen (around 1 mass percent) austenitic stainless steels have also been studied for instance in [11]. There two nickel-free austenitic stainless steels with 0.82% and 0.96% nitrogen contents were tested. Both grades showed high strength and high ductility in room temperature: 0.2% proof strength was 500–600 MPa and ultimate elongation 47–62% with different tensile test crosshead speeds (0.5–40 mm/min). Ductility and tensile strength decreased, and 0.2% proof strength increased when crosshead speed was increased. [11] Austenitic grades cannot be strengthened by heat treatments [88].

Face centered cubic austenite can reform into body centered cubic martensite in low temperatures or when the specimen is exposed to high strain rates or large plastic deformation [43]. Chemical composition, strain path, grain size and stress state also influence the transformation behavior. If the strain rate is high enough, self-heating can prevent transformation from austenite to martensite and cause unstable plastic flow. [7] The transformation from austenite to harder martensite enhances the strength but lowers the elongation and is the main reason for the high strain hardening of the austenitic grades. The strain hardening effect can be seen also in cold formed tubes and profiles, where cold formed angles have enhanced strength properties. In an experimental study, the longitudinal compression 0.2-proof strength in of the corner area of a brake-pressed profile was measured to be up to 2.33 times the corresponding value of the flat area [43]. Austenitic stainless steels also have better toughness in low temperatures and are less prone to brittle fracture than the mild steels and ferritic stainless steels all the way to -40 °C service temperatures. [77] Austenitic grades experience anisotropic properties in some degree.

Duplex stainless steels have a dual-phase microstructure which consist of ferritic and austenitic phases. Duplex grades are usually alloyed with 21–26% of chromium, 4–8% of nickel, 0.1–4.5% of molybdenum [88] and 0.05–0.3% of nitrogen [3]. In annealed condition, they are approximately twice as strong as the austenitic grades, as the 0.2% proof strength is in general 450–550 MPa [90]. Duplex stainless steels also have good corrosion and stress corrosion cracking resistance [3, 88] and good fatigue properties [88]. Like austenitic and ferritic stainless steels, duplex grades cannot be strengthened with heat treatments, but they have work-hardening properties. Modern duplex grades have good weldability and with proper welding speeds and heat input also good corrosion resistance after welding. Because of the lower thermal expansion, duplex stainless steels have less warping than the austenitic grades when welded. [88]

Lean duplex grades have less nickel and molybdenum than ordinary duplex grades making them more economical [3]. Because of the lower nickel content, the lean duplexes

also have less price volatility. They still have high strength and appropriate corrosion resistance, and the localized corrosion resistance is comparable to the resistance of austenitic grades. [89] Common applications for duplex stainless steels are pressure piping systems for seawater, chemicals, oil and gas, storage tanks for corrosive fluids, pressure vessels and structural components in corrosive environments [92] – basically applications, where high strength and excellent corrosion resistance is needed.

Martensitic stainless steels have high strength and good wear resistance and hardness. On the other hand, the martensitic grades are less ductile than the steels in the three aforementioned groups. Common applications for martensitic stainless steels are cutlery, knives and other applications where the high hardness and wear resistance can be utilized. **The precipitation hardening grades** have very high strength, and can have austenitic, semi-austenitic or martensitic microstructure. These grades are usually used when high strength and moderate corrosion resistance are necessary: bolts and tension bars, for example. [3]

Nickel is used in alloying stainless steels. Nickel mostly affects on the correct formation of microstructure in austenitic and duplex stainless steels and enhances their mechanical properties. [89] Nickel is expensive, and the price has high fluctuation. The high costs and price fluctuation of the prices of austenitic and duplex stainless steels, that have a remarkable nickel content, are mainly caused by the nickel. [2] The price and the price fluctuation of stainless steels can be partly described with alloy adjustment factor (AAF), which correlates to the prices of the alloying elements. Nickel mainly controls the alloy adjustment factor, but molybdenum has also some effect on it. Steel manufacturers cannot directly control the AFF value. The mill price of stainless steel is affected also by the base production costs, which are determined by the manufacturer. [89] Also, further manufacturing costs are higher for stainless steel than for mild steel, and the total manufacturing costs of the stainless steel are estimated to be 30% higher. Compared to the mild steel, stronger strain hardening makes blanking, machining and pressing more difficult increasing the costs, and the welding consumables are more expensive for stainless steel than for the mild steel. [87]

2.1 Corrosion resistance

Stainless steels have good **corrosion resistance** and they are hygienic [2]. Mainly because of the high chromium content, stainless steels have a thin, approximately 5 µm thick passive layer, which is formed in any oxidizing environment, including air. The passive layer is transparent, tightly adherent, stable and insoluble, and it prevents the rest of the steel from reacting with the environment. The stability of the layer depends on the alloying elements of the steel, surface treatments and the nature of the corrosive environment. Increasing the chromium content increases the corrosion resistance and stabilizes the passive layer but adding of nickel and molybdenum have also an effect on it. [88]

Alloying of chromium, molybdenum and nitrogen also improve the pitting corrosion of the stainless steels in concentrated chloride and in chloride–sulphate solutions [93]. The corrosion resistance can be described with pitting resistance equivalent (PRE), which is calculated as equation (1) shows. The larger number the better corrosion resistance. By no means PRE should be used alone for selecting stainless steel grades with respect to corrosion resistance, but it is one way of ranking stainless steels considering corrosion resistance. Choosing right grade with respect to corrosion resistance require that several matters are considered: macro environment of the particular location and micro environment that can affect the long-term corrosion (cracks, covering from the natural rain wash), exposure to natural or man-made chloride sources, roughness of the steel surface and effects of manufacturing on the joints. Contamination from fragments of other material, especially carbon steel, can also affect the corrosion resistance of stainless steel. [89]

$$PRE = Cr\% + 3.3Mo\% + 16N\% \quad (1)$$

Choosing the right grade is not only about corrosion resistance. After clarifying suitable grades with respect to corrosion, environment and subjects that are in contact with the member, attention should be paid to mechanical properties. Necessary mechanical properties are determined by defining service loads, cyclic loads, vibration and seismic loads, effects of heating or cooling and ease of manufacturing. [88] Especially in case of duplex steels with high 0.2% proof strengths at around 500 MPa the formability should be taken into account.

2.2 Stress–strain behavior

Stainless steels have a **nonlinear stress–strain response** without a clear yield strength [1, 89]. They can also have significant differences in the behavior in tensile and compression [2]. Garner and Nethercot (2004) reported that in case of austenitic EN 1.4301 the 0.2% proof strength was 5% lower and 1.0% proof strength was 4% higher in compression than in tension, leading to a more rounded stress–strain relation in compression [21]. Compression and tensile stress–strain curves of ferritic stainless steels have no significant differences [87]. Wide plasticity between the proof stress and ultimate strength is common for stainless steels [89], and thus the stainless steel members have high plastic deformation capacity and redistribution on cross section and member level [77]. The manufacturer of stainless steel can easily adjust the proof strength and ultimate strength because of the more precise adjustments on the production chain. For the same reason the variations in proof strength and ultimate strength are small, under 4–5%. Low coefficient of variation on strength, 2–3%, ensures for instance the precise control of the fracture mechanism, for example weak beam–strong column in seismic design. [77]

Several stress–strain models have been proposed for stainless steels. Rasmussen (2003) presented a modified two-stage Ramberg–Osgood model, which is capable to predict the material behavior after the 0.2% proof strength rather accurately [22]. This material

model has also been adopted in EN 1993-1-4 annex C [94]. Equation (2) is the Rasmussen's model with Eurocode notations.

$$\begin{aligned}
&\varepsilon = \frac{\sigma}{E} + 0.002\left(\frac{\sigma}{f_y}\right)^n \; for\; \sigma \le f_y \\
&\varepsilon = 0.002 + \frac{f_y}{E} + \frac{\sigma - f_y}{E_y} + \varepsilon_u\left(\frac{\sigma - f_y}{f_u - f_y}\right)^m \; for\; f_y < \sigma \le f_u \\
&m = 1 + 3.5\frac{f_y}{f_u} \\
&E_y = \frac{E}{1 + 0.002\, n\frac{E}{f_y}}
\end{aligned} \tag{2}$$

where σ is engineering stress, ε engineering strain, E modulus of elasticity, f_y yield strength (0.2% proof strength), f_u ultimate strength, n Ramberg–Osgood parameter and ε_u ultimate elongation. Coefficient 0.002 in the equations is the 0.2% strain. Rasmussen proposed that the ultimate elongation can also be calculated from yield and ultimate strength, $\varepsilon_u = 1 - f_y/f_u$, but it is always smaller than the ultimate elongation presented in EN 10088-4 (ref. [90]). [94] Same expression as the Rasmussen's model was presented first by Mirambell and Real (2000) with little different notations and without expressions for m or ε_u [12]. However, these authors derived the same expression independently. [95, 96] In Design Manual for Structural Stainless Steel the same material model is included with little improvements on m and calculation of ε_u: [3]

$$\begin{aligned}
&m = 1 + 2.8\frac{f_y}{f_u} \\
&\varepsilon_u = 1 - \frac{f_y}{f_u} \le A \qquad \text{for austenitic and duplex grades} \\
&\varepsilon_u = 0.6\left[1 - \frac{f_y}{f_u}\right] \le A \qquad \text{for ferritic grades,}
\end{aligned} \tag{3}$$

where A is ultimate elongation in EN 10088-4 [90].

Based on the material constitutive equation presented by Rasmussen and Mirambell and Real, Gardner and Nethercot (2004) proposed a two-stage Ramberg–Osgood model, where 1% proof strength was used instead of ultimate tensile strength. With this modification the material model was able to describe also compression, where necking does not exist. Moreover, the strains in general applications are far from ultimate elongation, and thus using 1% strain and corresponding proof strength offer smaller deviations between the measured and modelled stress–strain relationships up to around 10% strains. [21] Quach et al. (2008) proposed a three-stage Ramberg–Osgood based material model, which uses only the three basic Ramberg–Osgood parameters. The benefit of this material

model is that it gives very accurate stress–strain relationship in tension, similar to Rasmussen's model, but it is more accurate in compression in the studied range up to 2% strain than the Rasmussen's model. Rasmussen's model tends to underestimate the stress levels in compression. [20]

Behavior of austenitic stainless steels at high strain rates may differ remarkably from the quasi-static loading. This behavior is called **strain rate sensitivity**. Effects of strain rate on austenitic grades were studied by Talonen et al. (2005). The strain rate sensitivity strongly depended on the stability of austenite. For example, the formation of α′-martensite was low in stable (with respect to martensite transformation) EN 1.4301 and the strain rate had only little effect on the work-hardening rate, whereas in case of unstable EN 1.4318 the work hardening behavior was closely related to the formation of α′-martensite. The proof strength of both EN 1.4301 and EN 1.4318 increased as the strain rate increased but the ultimate strength and elongation were strain rate depended and did not increase linearly. The maximum ultimate strength of EN 1.4301 was reached with maximum tested strain rate 200 s^{-1} whereas the maximum ultimate strength of less stable EN 1.4318 occurred at quasi-static loading. Ultimate elongation of EN 1.4301 was found to be more depended on the strain rate, and maximum elongation was reached in quasi-static tensile tests. Adiabatic heating at higher strain rates prevented the transformation induced plasticity effect (or TRIP) causing increased necking and thus lowering the ultimate elongation. The ductility of EN 1.4318 was increased at high strain rates. [6]

Similar tensile test results were gained by Lichtenfeld et al. (2006) in their experiments. In that study the yield strengths of AISI 309 and 304L were discovered to increase as the strain rate increased. The yield strengths in quasi-static loading were 291 MPa and 300 MPa and at 400 s^{-1} strain rate 541 MPa and 480 MPa for AISI 309 and AISI 304L, respectively, showing remarkable increase in yield strengths. The maximum ultimate strength of the more stable AISI 309 was reached at high strain rates, 400 s^{-1}, and the maximum ultimate strength of less stable AISI 304L was obtained at quasi-static tensile loading. The minimum ultimate strength of AISI 304L occurred at 0.125 s^{-1} which after the ultimate strength increased again when strain rate was increased. As the strain rate increased, the ultimate elongation of both AISI 309 and 304L were first decreased up to strain rate level 0.125 s^{-1} and were then increased to some extent. [5] The ultimate elongation results of [5] differ from the results of [6] above, where ductility of unstable grade increased when strain rate was increased. Otherwise the results match.

Stainless steels have **anisotropic mechanical properties**. The anisotropy of mechanical properties of austenitic stainless steels is not necessary to take into account, according to [13, 97]. Anisotropy is more remarkable for ferritic and duplex grades [13]. In experiments, ferritic stainless steels showed on average 12% higher 0.2% proof strength values in transverse than in rolling direction [87]. Austenitic EN 1.4301 has been reported to have lower yield strength in the transverse direction than in longitudinal direction, particularly at low strains while the ultimate tensile strength was similar in both direction. [52]

On the other hand, Chinese-made austenitic S31608 (EN 1.4401) has been reported to have 16% higher 0.2-proof strength and 9% higher ultimate tensile strength in the transverse direction than in the longitudinal direction [9] – opposite observation to [52]. Also, the Young's modulus of the Chinese austenitic grade was measured to be 4% higher in transverse direction than in longitudinal direction, and it was advised that the anisotropy should not be neglected in engineering applications [9]. In Lecce and Rasmussen's study, austenitic AISI 304 (similar to EN 1.4301) had 1% difference in 0.2% proof stress in longitudinal and transverse direction, whereas ferritic AISI 430 (EN 1.4016) had 8–9% difference, respectively [43]. Based on these results, at least the Chinese austenitic grades may show similar anisotropy than the ferritic steels in general.

2.3 Strength enhancements by cold forming

Stainless steel cross sections can be manufactured by cold forming in two different ways: press braking and cold rolling. In press braking a tool and die are used to form a sheet to the form of the tool–die pair, whereas in cold rolling the cross section is gradually formed by using rolls. [17] Stainless steels, especially austenitic grades, have enhanced strain hardening properties and thus they are very sensitive to cold forming, resulting in **increased strength in cold-worked areas**. Cruise and Gardner (2008) studied the effects of cold forming on austenitic EN 1.4301 in experiments, where both press braking and cold rolling were considered. In press-braked sections the increase in strength of flat surfaces was low, whereas in corner areas where large plastic deformation occurred, the increase in strength was significant, up to around twice the strength of the flat material. The effect of strain hardening was noticeable in corner area only. [17]

In cold rolled rectangular and square hollow sections not only the corners had increased strength, but also a part of the flat areas had some degree of enhancement in strength due to cold forming: first a circular hollow tube was manufactured and then crushed to RHS/SHS form. The increased 0.2% proof strength, maximum at the intersection of the flat face and corner, slightly decreased to the corner direction and linearly decreased towards the flat face. After the corner at a distance of around 4 times the thickness, the strength of the flat material was reached. It was proposed that when increased strengths are modelled, enhanced strength should be used at the corner of press-braked sections. In SHS and RHS sections the corner area strength can be modelled with a constant increased 0.2% proof strength at the area which includes the corner but is extended to 2 times the thickness beyond the corner. The proposed regions for strengthened areas are illustrated in Figure 1. Formulas for uniform strength of the press-braked corner, flat face of a SHS/RHS hollow section and corner area of a SHS/RHS tube were proposed. [17] In Becque and Rasmussen's study the 0.2% proof strength of corner in a cold-formed austenitic EN 1.4301 sheet was 2.25 times the original value in tension and 2.35 times the original value in compression. Ferritic EN 1.4003 and EN 1.4016 had corner 0.2% proof strength enhancement of about 1.6–1.7 times the value of the flat region. [33]

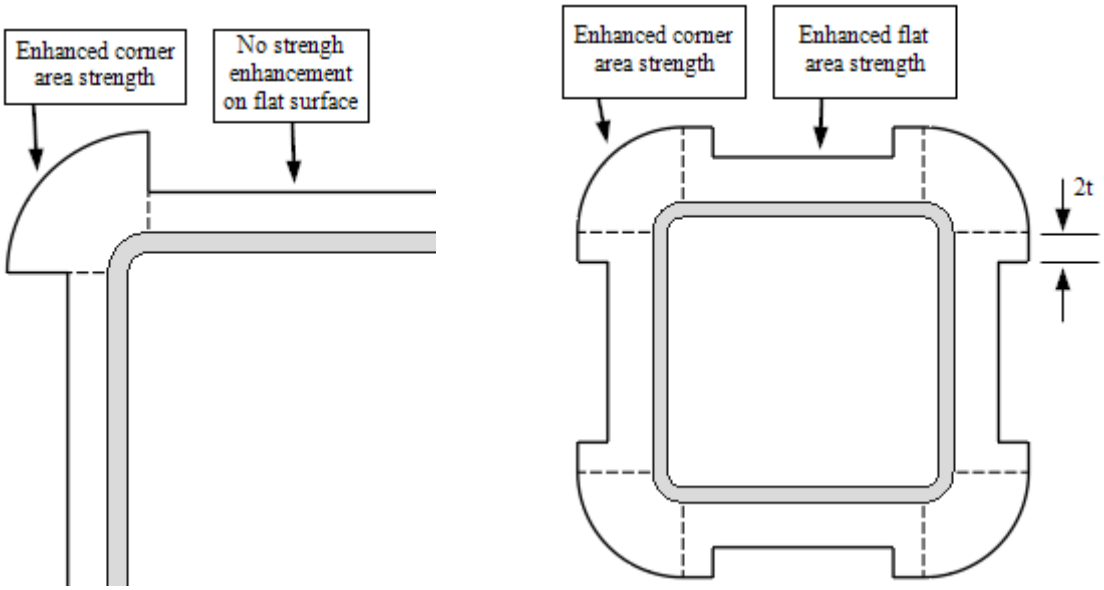

Figure 1. *Strength enhancements from cold working. Uniform increased 0.2% strengths proposed in [17] for press-braked (left) and SHS/RHS (right) cross sections.*

Formulas for corner 0.2% proof strength and ultimate strength are also presented for example in [14] and [16], where the region of the strengthened material was not studied. In numerical analysis carried out by Ashraf and Gardner, corner strengths were calculated with equations presented in [14], and the enhanced strength was applied to a range 1*t* and 2*t* beyond the curved area of the corner of press-braked and cold-rolled sections, respectively [98]. Term *t* is the thickness of the section. In [16] a whole cross section weighted average enhanced 0.2% proof strength was also proposed for both press-braked and cold-rolled box sections. Up to 49–84% increases in 0.2% proof strength and 43–35% increases in ultimate strength were measured in corner areas of high strength austenitic and duplex stainless steels in [4].

2.4 Design methods and design codes

Lack of experimental data from stainless steel and load bearing members manufactured from stainless steels is reflected in the codified design rules. Often the European code is overly conservative leading to inefficient design. For example, web crippling of austenitic and duplex stainless steel square and rectangular hollow sections were studied by Zhou and Young (2007), and Eurocode was found to be very conservative for end and interior loading conditions but also the scatter was large. Interior two flange loading with high-strength specimen had the most conservative predictions as the ratio of maximum load from numerical or experimental tests and Eurocode value was 5.68. At lowest the ratio was 1.56 for interior one flange loading of high strength specimen. Thus, the Eurocode was 56–468% conservative for web crippling. [31] Similar results were obtained in experiments by Young and Lui (2005) and Zhou and Young (2007), where the maximum mean value for the tested-to-predicted force ratio value was 5.50 for interior two flange

loading of high-strength stainless steel tube and 5.11 for AISI 304 austenitic stainless steel tube in similar loading conditions. [4, 26] Eurocode predictions for web crippling of ferritic EN 1.4003 stainless steel rectangular hollow sections were found to be very conservative, too. The experimental-to-predicted load ratios were up to over 4 for exterior two flange loading and over around 1.2–2.4 for interior two flange loading. [25]

In case of stainless steels, especially austenitic and duplex grades with high strain hardening capabilities, using 0.2% proof strength and ideally plastic material model will lead to excessively conservative capacity predictions in design. For this reason different design methods are developed for stainless steels. [37] It should be mentioned that in EN 1993-1-4 no design rules are given for plastic global analysis for stainless steels [94]. **Continuous strength method** (CSM) is a design procedure based on deformation and it considers the strain hardening effects in resistance calculations for stocky members. CSM is included for example in Design Manual for Structural Stainless Steel [3]. **Direct strength method** (DSM) considers all instabilities in a non-iterative way. It was first developed for carbon steels and was added to North American Specification AISI-S100-12. Attempts have been made to modify DSM to be used with stainless steels by accounting the nonlinear stress–strain behavior, but it has not been introduced in stainless steel design codes. [37] Arrayago et al. (2017) proposed a new full slenderness range DSM approach for stainless steel hollow sections. Resistance of the stainless steel section in compression, bending or combined compression and bending is predicted using only one strength curve for all loading conditions. Strain hardening and local buckling effects are considered. Comparing the predictions to a wide range of experimental data and parametric studies, the proposed method was found the be more accurate than the current design methods. On average, the proposed method was 7%, 13% and 10% conservative in cross section resistance predictions compared to reference data for compression, bending and combined loading, respectively. [37]

Ahmed and Ashraf (2017) proposed a design method based on the continuous strength method. The predictions of the model were compared to 132 SHS and RHS experimental or numerical buckling resistance test results from several different studies. In continuous strength method deformation capacity, as buckling strain of a section, is expressed in terms of cross section slenderness. This design base curve is used with a material model which takes nonlinearity of the material and strain hardening into account. The proposed model had excellent agreement with experimental and numerical test results. The ratio of buckling load predicted by the proposed CSM model and finite element method (FEM) or experimental results was between 0.92–1.06 with 0.98 mean value. Coefficient of variation was 0.03. In comparison, Eurocode 3 buckling load predictions were on average 0.89 compared to the FEM and experimental test results with coefficient of variation of 0.10. Thus, remarkable improvement, about 10%, was obtained for the buckling resistance with the proposed CSM method compared to the EC3 and the variation also decreased significantly. [40]

The CSM procedure in 4th edition of Design Manual for Structural Stainless Steel [3] uses a bilinear, elastic linear hardening material model. The elastic part is modelled up to yield strain ε_y which is determined from $\varepsilon_y = f_y/E$, where f_y is yield strength and E is Young's modulus. Linear hardening is modelled from yield strain to ultimate strain ε_u, which is defined as $\varepsilon_u = C_3(1 - f_y/f_u)$, where C_3 is a material model coefficient given in Design Manual for austenitic, ferritic and duplex grades and f_u is ultimate strength. The strain hardening modulus E_{sh} is extracted from equation (4):

$$E_{sh} = \frac{f_u - f_y}{C_2\varepsilon_u - \varepsilon_y}, \tag{4}$$

where C_2 is a material model constant. Next a base curve is determined. It defines the deformation capacity of the cross section, and it is required for determining the resistance and slenderness of the cross section. Then the resistance of the cross section in axial compressive loading, bending or combined compression and bending can be calculated with the given formulas. [3]

Design rules for welded austenitic EN 1.4301 and duplex EN 1.4462 I-section columns were studied by Yuan et al. (2015). Finite element model was developed, validated against experimental results and used for parametric study. They compared four existing design rules and proposals, including Eurocode 3 part 1-4 [94] and direct strength method. They found that Eurocode gave in general conservative buckling load predictions, and the ratio of Eurocode predictions to numerical results was 0.88 and 0.79 for austenitic and duplex grades, respectively. DSM model given in Eurocode format had corresponding values 0.87 and 1.01 for austenitic and duplex stainless steel columns, respectively. The authors proposed modifications for the Eurocode and DSM design, and remarkable improvements were obtained. These two modified methods predicted buckling loads 0.99 and 1.01 times the buckling load from FE results. Coefficient of variation remained approximately the same as in Eurocode, 0.05–0.07. [39]

In Theofanous and Gardner's three-point bending tests, moment resistance of lean duplex EN 1.4162 square and rectangular hollow sections were studied. A parametric study was performed with a validated finite element model. There continuous strength method was found to be more accurate than Eurocode 3 part 1-4 [94], American [99] and Australian/New Zealand [100] design codes for lean duplex. Eurocode class 2 and 3 slenderness limits were overconservative while the two other standards were more accurate in predicting moment resistance of duplex cross sections. [32]

2.5 Welded and bolted connections

Welding causes heating and cooling cycles to the material. In case of stainless steels, it affects the microstructure, especially with duplex grades. Suitable procedures and consumables should be used, and qualified welder are recommended to accomplish the welding. [3] Ferritic stainless steel grades are easily weldable, but welding parameters such as welding process and used consumables should be considered. [1] Austenitic fillers are recommended over the ferritic fillers because of the better toughness. Ferritic fillers can be considered, if it is necessary to have similar thermal expansion or appearance with base material or if nickel-free consumable is important. [1, 87]. Among ferritic grades EN 1.4003, EN 1.4509 and EN 1.4521 are the most suitable grades for autogenous welding, but the ultimate strength of the weld can be lower than of the base metal. The welds of the ferritic grades usually experience at least some degree of corrosion regardless of the grade used. [87] Stabilized ferritic grades with low carbon content should be chosen for welding to avoid the concentration of carbon and chromium to the grain boundaries, a phenomenon called sensitization. When austenitic or duplex grades are welded, low carbon grades with less than 0.03% carbon content should be used to avoid sensitization and intergranular corrosion. Modern austenitic and duplex grades have low carbon contents and thus the intergranular corrosion is uncommon. [3] Carbon steel and ferritic AISI 430 were welded together with and without filler material in [101]. Hardness of the weld with filler metal was approximately 2.75 times higher than of the weld without filler metal. In the heat affected zone of the ferritic stainless steel the hardness was 12% lower in case of weld with filler metal. Ultimate tensile strength 922 MPa of the weld with filler metal was around 40% higher than of the autogenous weld. [101]

Bolted connections should be designed considering the high ratio of ultimate strength f_u to yield strength f_y (0.2% proof strength $f_{0.2}$) of stainless steels to avoid excessive deformation. [1] Overestimating the rigidity of the joint can lead to larger displacement than expected in design and increased risk of failure, while underestimation of stiffness can cause larger forces to the structural members than designed. [102] To avoid the overestimation of the stiffness of a connection, EN 1993-1-4 uses reduced strength, which is calculated as $f_{u.red} = 0.5f_{0.2} + 0.6f_u$, where $f_{0.2}$ is 0.2% proof strength and f_u is the ultimate strength [94]. For ferritic stainless steels which have lower f_u/f_y ratios than austenitic grades, it is not as important to use the reduced values [1]. In 4th edition of Design Manual for Structural Stainless Steels, new more economical design rules for stainless steel bolted connections are given. Reduced strength is not used anymore, and the rules are expected to replace the current design rules in next revision of Eurocode. [3] The over conservatism of the Eurocode design of the stainless steel bolted connections were noticed also in a study by Salih et al. (2010), where parametric study with a validated numerical model was carried out for austenitic EN 1.4306 and ferritic 1.4016 stainless steels. Proper partial safety factor and a design formula for net section capacity of stainless steel bolted connections were proposed. [45]

2.6 Cyclic loading and fatigue

Zhou and Li studied **fatigue** behavior of hot rolled plates, cold rolled sheets and cold formed tubes made from austenitic stainless steel AISI 304 (close to EN 1.4301) and duplex stainless steel LDX2101 (EN 1.4462). Cyclic loading tests with ± 0.5%...± 2.0% strain amplitudes were performed. The hysteresis loops of the stainless steels showed good hysteretic behavior: the loops were plump, stable and symmetric relative to the origin. Except cold rolled LDX2101 samples, stainless steel showed non-Masing properties. It means that the hysteresis loops were symmetric relative to origin and hysteresis loops from different strain amplitudes did not coincide. Samples from cold formed lean duplex tubes experienced sudden fractures without necking, whereas all other samples had necking behavior. The lack of necking in case of cold formed duplex samples was assumed to show the effect of cold forming. In general, cycling loading was found to slightly increase the tensile strength of the specimen except for the cold formed duplex samples, which experienced a higher, approximately 80% increase in ultimate strength. Ductility of the stainless steels were decreased with cold working. Despite the effects on strength and ductility, the effect of hot or cold forming on the cycling hardening or softening was found to be minimal. In monotonic tensile tests austenitic stainless steels have better work hardening properties, and also in cyclic loading the strain hardening of austenitic AISI 304 was more pronounced than of the lean duplex LDX2101. [34] Chinese made austenitic S31608 was reported to have remarkable cyclic hardening with excellent cyclic behavior [9].

Nip et al. performed extremely low cycle fatigue and low cycle fatigue tests on structural carbon and stainless steels. Test coupons from cold formed carbon steel S235JRH, hot formed carbon steel S355J2H and cold formed austenitic EN 1.4301 and EN 1.4307 were studied. Axial loading with ±1%...±7% strain and bending loading with ±2%...±15% maximum surface strains were tested. Cold formed stainless steel showed significant cyclic hardening, and as the strain amplitude in cyclic tests was increased, the stresses increased up to level of 70% over the ultimate strength measured in monotonic tensile tests. The cyclic hardening of both hot and cold formed carbon steel was smaller, and the stress levels in cyclic test reached levels that were approximately 30% higher than the tensile strength in monotonic tensile test. The different grain structure of mild and austenitic stainless steel may be one reason for the differences cyclic behavior. The differences in fatigue life were small, but the hot formed carbon steel had marginally better fatigue life than cold formed carbon steel and cold formed stainless steel. [35] Paul et al. found in their study that austenitic AISI 304LN had cyclic softening or hardening depending on the load level in low cycle fatigue and ratcheting. With 300 MPa load level the material experienced softening whereas with 360 MPa and 420 MPa amplitudes cyclic hardening was noticed. Ratcheting is a progressive directional plastic deformation caused by asymmetric stress cycling. [29]

Cyclic loading of carbon steel and stainless steel tubular bracing members were studied by Nip et al. Cold formed carbon steel S235JRH, hot formed carbon steel S355J2H and cold formed austenitic EN 1.4301 and EN 1.4307 rectangular hollow sections were used. Yield strengths of the materials were similar, but the ultimate strengths and ultimate elongations were larger for the stainless steels. All the test braces had global slenderness under 2. Rotations and lateral displacement were restrained at both ends of the test specimen. The results showed that local and global slenderness had a significant impact on the fatigue life. The nonlinearity in load–displacement curve of stainless steel started earlier than of carbon steels, but the deterioration of the compressive resistance after the buckling was slower. All test specimen had similar failure behavior. First, after the local buckling the stresses and strains increased in corner areas. Localization of the strain leaded to initiation of a crack after a few non-elastic buckling and tensile yield cycles. Stainless steel retained better its compressive stiffness around 1% strain which delayed local buckling and fracture. Stainless steel braces with stocky cross sections (high global slenderness) had a remarkably higher fatigue life than the mild steel members. It also means that more energy was absorbed with stainless steel bracing before failure. Hot rolled carbon steel had a higher fatigue life than cold rolled carbon steel due to the reduced ductility in the corners of the cold rolled section. [30] It can be assumed, that similarly a hot formed stainless steel brace would outperform cold rolled stainless steel member in terms of fatigue life.

Table 1 gathers together the main properties of stainless steels for austenitic, ferritic and duplex (austenitic–ferritic) stainless steels. *It should be noted, that this table is only suggestive, and significant differences between different grades of each group are possible.*

Table 1. *Stainless steel properties (in annealed condition) as groups and properties of each group in general. Strength and ductility are minimum values according to EN 10088 [90].*

	0.2% proof strength (MPa)	Ductility, ultimate elongation (%)	Work hardening	Corrosion resistance	Elevated temperature resistance
Austenitic	200–240	>35–45	Very high	High	Very High
Ferritic	230–280	>18–25	Moderate	Moderate	Moderate
Duplex	400–500	>20–30	Moderate	Very high	Moderate

2.7 Applications in structural design

Tao et al. (2011) studied **concrete filled stainless steel tubes** (CFSST) in axial compression with a parametric numerical analysis. Square hollow section made from carbon and stainless steels with concrete filling were compared. Ferritic EN 1.4003, austenitic EN 1.4301 and EN 1.4404 and duplex EN 1.4462 were studied. Results suggested that concrete filled stainless steel columns perform better in axial loading than the carbon steel

counterparts. This is mainly due to the enhanced strain hardening properties of the stainless steels. Axial load bearing capacity of the concrete filled square stainless steel columns were up to around 20% higher than of carbon steel columns. Design equations for CFSST axial load resistance and ultimate strains were also presented. [84]

Circular CFSST tubes were also studied by Chen et al. (2017) in experiments, where static 4-point bending experiments with 18 CFSST and 9 empty circular hollow section tubes were made. Austenitic SUS 201 (equivalent to EN 1.4372) stainless steel was used as the material. Empty tubes failed by local buckling under the compression of the load points. The support from the concrete in CFSSTs prevented local buckling in loading points and enabled the enhanced utilization of the stainless steel properties. CFSST test specimen failed by global buckling. Between the two loading points in the middle, yielding of the tube and cracking of the concrete were observed. The effect of the strength of the concrete to bending resistance was relatively small, only 7% between C30 and C50 concretes (30 MPa and 50 MPa cubic strengths, respectively). Increasing outer diameter remarkably enhanced the bending resistance in both empty and concrete filled CHS tubes. Increasing thickness from 1.1 mm to 1.5 mm or from 1.5 mm to 2.0 mm increased the bending resistance of CFSST with C30 concrete approximately 30–50% and resistance of empty tubes 64–125%. Maximum moment–weight ratio of the filled tube was smaller than the ratio of the empty tube, which is due to the relatively heavy and low-strength concrete. [81]

CFSST stub columns were studied by Patel et al. (2014). A parametric numerical study with a validated fiber element model was carried out. During the validation it was noted, that the Rasmussen's two-stage Ramberg–Osgood model, which assumes that the stress–strain behavior is the same in tension and in compression, does not accurately predict the stub column axial load resistance, as it cannot describe accurately the strain hardening in compression which is stronger than in tension. Therefore, a three-stage model proposed by Abdella et al. [103] was used in the parametric studies. The three-stage model considers the more pronounced strain hardening in compression. The ratios of predicted axial load capacity to the experimental value were 81% and 97% for the two-stage and three-stage material models, respectively. Different analytical design methods were also compared to the experimental and numerical results. Eurocode 4 [104] was found to be conservative for the stub columns as it predicted on average 78% axial capacity compared to the experimental value. It does not take into account the significant strain hardening of the stainless steel. A design model based on Liang and Fragomeni's formula [105] was proposed and it showed excellent agreement with the experimental results, underpredicting the axial load capacity on average by only 3%. [83]

Seismic design for earthquakes is a possible application, where properties of stainless steels might be effectively utilized. Good ductility and energy absorption properties of stainless steels are an advantage during the earthquake, and in fire which often occurs after the earthquake, good elevated temperature properties are valuable. The amplitude of

the seismic waves in earthquake is often described with Richter scale, which is calculated as below:

$$M_L = logA - logA_0 \quad (5)$$

where A is the maximum registered amplitude at a given distance and A_0 is a function of attenuation from a reference earthquake. Thus, the magnitude is depended only on the seismic action itself, not on the damage caused by the earthquake. Soil gives some restrictions to the intensity of an earthquake, and this far Richter scale value 9 has never been exceeded. Most of the seismic standards consider the seismicity of the area, characteristics of the soil, the intended use of the structure and the consequences in case of earthquake and structural properties such as ductility and overstrength. [75]

In earthquakes structural members may experience low cycle fatigue, where a low number of large deformation cycles occur. The response of the structure then depends on the geometry and hysteresis behavior of the structure. [34] The peak accelerations and speeds of the ground vary in different earthquakes. If the origin of an earthquake is close to a structure or the ground is hard rock, cycles of the earthquake are short and the accelerations are high. If the soil is soft or the center of the earthquake is far away, the accelerations are smaller, but the velocities are higher and seismic cycles longer. Large accelerations and short cycles are more severe for stiff structures whereas larger velocities and longer cycles are more harmful for flexible structures. [77]

Eight concentrically braced frames (CBF) and nine eccentrically braced frames (EBF) were studied with pushover and inelastic response history analyses by DiSarno et al. (2008). In concentrically braced frames the midlines of the braces coincident at the centerline of the beam, whereas in eccentrically braced frames the midlines of the braces do not coincident at the centerline of the beam. Mild steel S275 with 275 MPa yield strength and stainless steel with 275 MPa proof strength were used in the study. About the material modeling and strain hardening in the study it was only reported that the strain hardening of stainless steel is nearly twice that of carbon steel, values 2.30 and 1.20, leaving the material models otherwise unexplained. When stainless steel was used for dissipative braces and non-dissipative columns in concentrically braced frame in static pushover analysis, the stainless steel–mild steel hybrid structure showed 33% enhancement in overstrength compared to the mild steel structure. The results showed that when the probability of exceedance of the earthquake was over 50% the seismic shear demand can be lowered by 40–45% by using stainless steel columns and braces in CBFs. If the probability of the exceedance of the ground motions was 10%, there was no remarkable advantage in using stainless steel. [77]

In eccentrically braced frames, where the links were dissipative, using stainless steel in non-dissipative braces and columns gave the same response than when stainless steel was

used for all members. In these two cases the frame had 34% enhancement in global overstrength with respect to the carbon steel frame. With stainless steel braces and links the increase in overstrength was 20%. No benefit was observed by using stainless steel links in EBF, but it was noted, that the energy absorption capacity of EBFs with dissipative stainless steel links was not fully utilized because of buckling of the braces. Braces with lower slenderness should be used to force the inelastic dissipation to the stainless steel links. Using stainless steel in beams of the frame structure showed no benefit. When all members in EBF were stainless steel, the base shear demand of the structure was decreased by about 50% compared to the carbon steel structure. When only stainless steel braces and columns or stainless steel braces and links were used, the reduction was 35%. Roof drifts were reduced by 35–40% with respect to the mild steel structure when stainless steel braces and columns or braces and links were used. The high material overstrength, f_u/f_y, and nonlinear stress–strain behavior made possible that the lateral resistance of the structure only increased also with large displacements. [77]

In a paper by Baiguera et al. (2016) was noted, that the traditional seismic design has two problems: the large inelastic deformation and damage in load bearing structures, and large lateral displacements after a strong earthquake. To facilitate the reparability of the structure, dissipative stainless steel fuse parts were proposed. The proposed structure is presented in Figure 2. After an earthquake the damaged fuses would be replaced, and the rest of the structure have remained in elastic state. Replacing the fuse parts would also center the structure back to the original state. Post-tensioned bars can result in self-centering moment resistant frames, as the recovering force eliminates the residual drifts. In the study stainless steel was used in dissipative hourglass-shaped pins and fuse parts in locations where plastic hinges were expected to form. A concentrically braced moment resistant frame (CBF–MRF) was used in the study. The use of proposed structure ensured large initial stiffness and low drifts and damage to the non-load bearing structure. It also eliminated structural damage as the plastic deformation was restricted to the stainless steel dissipative parts and fuses. It also showed remarkable decrease in residual drifts: the peak storey drifts were about the same as in a buckling resistant braced frame–moment resistant frame (BRBF–CBF), but the residual drifts were only 20-25% of the residual drifts of the BRBF-CBF (75–80% lower). [74] Toset (2014) proposed, that the ends of a structural member could be stainless steel while the midsection could be carbon steel. Thus, the costs would be lower compared to the members made completely from stainless steel, while the good plasticity properties would be utilized in plastic hinges occurring in stainless steel part. [75]

One proposed application for **ferritic stainless** is **decking for steel–concrete composite floor system**. Traditionally, composite floor slabs are made with corrugated galvanized steel deck. A study about the use of ferritic stainless in this application instead of galvanized carbon steel was performed and presented in final report of Structural Applications

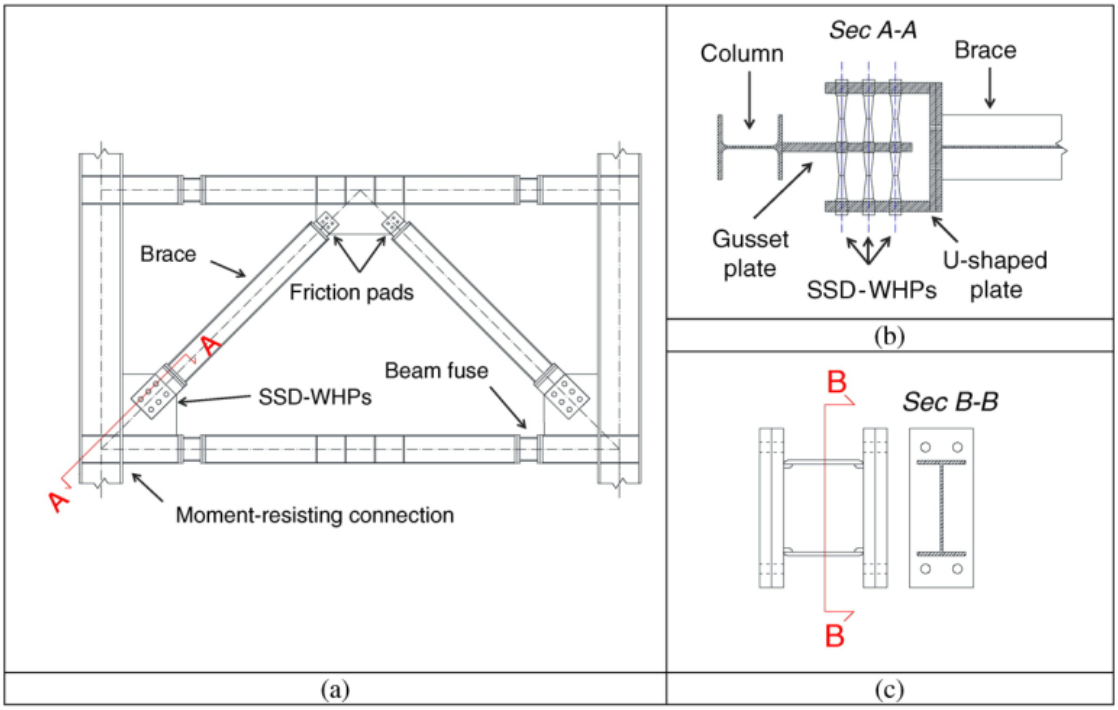

Figure 2. *Concentrically braced moment resistant frame with stainless steel dissipative pins and stainless steel fuses [74]. Figures: a) an overview, b) energy dissipative hour-glass shaped pins (with high post-yield stiffness, WHP) made from duplex stainless steel (SSD), c) beam fuse.*

for Ferritic Stainless Steels. One advantage of the stainless steel with respect to galvanized carbon steel is the appearance. By using ferritic stainless steel decking the composite slab can generally be considered to be visually more attractive and thus the slab is more likely left uncovered from the downside. This way the slab also participates in the heat exchange of the building. In the study, the mass of the slab absorbed energy from the space below at day time and released heat during the night when the external temperature dropped, providing smaller differences between the maximum and minimum temperatures of the building by passive heating. Overall, the EN 1.4003 stainless steel decking was found to have very similar behavior as galvanized carbon steel decking. The ferritic stainless steel composite slab performed better in elevated temperatures, but the room temperature moment resistance of the carbon steel slab was higher due to the higher yield strength (280 MPa and 350 MPa). Through deck welding was similar for stainless steel than for carbon steel deck. When it comes to appearance, shiny stainless steel surface is usually preferred. However, the shinier surface, the smaller is the emissivity of the stainless steel and the smaller is the effect of the slab as a passive thermal stabilizer. Thus, a balance between the good appearance and good heat exchange properties should be discovered. Opinions of several architects about the attractiveness of the exposed ferritic stainless steel slab were asked, and it had very positive feedback. [87]

Several studies have shown that stainless steels have good mechanical properties in elevated temperatures. The reduction of strength and modulus of elasticity of stainless steel

in high temperature are smaller than of the carbon steel and the emissivity of the stainless steel is also lower. [3, 106] These are beneficial in fire design of structures. Especially in case of austenitic stainless steels high tensile strength and ductility, leading to large area under the stress–strain curve, are promising when energy absorption is considered. For these reasons these two subjects, energy absorption and fire design, were studied more thoroughly in chapters 3 and 4.

3. ENERGY ABSORPTION

Energy absorption is a critical property in different kind of energy dissipating applications, where a structure member is designed to absorb energy from a loaded structure. Such applications are energy dissipating members in seismic design [75] and different kinds of crashworthiness and blast resistance applications [64], for example. In crashworthiness applications, two types of loading can be identified: quasi-static and dynamic loading. In quasi-static loading the loading or deformation is increased slowly enough so the effects of inertia, strain rate or the heat caused by the deformation, does not have to be considered. On the other hand, in dynamic loading, the effects of the aforementioned properties are necessary to take into account.

AISI 304 austenitic stainless steel was compared to common carbon steel "ES" and TRIP 1000 steel in case of **ballistic impact** by Rodríguez-Martínez et al. (2010). In true stress–logarithmic strain scale, ultimate tensile strengths of AISI 304, ES and TRIP 1000 were approximately 1000 MPa, 400 MPa and 900 MPa, respectively, whereas the corresponding ultimate elongations were 0.43, 0.19 and 0.39. The 2% proof strengths were about 375 MPa, 625 MPa and 210 MPa, respectively. AISI 304 and TRIP 1000 were compared in a low velocity impact test, where a striker with 18.787 kg total mass was dropped to a 1 mm thick plate. The maximum velocities of the striker that did not penetrate the sheet, were 2.6 m/s and 2.9 m/s for TRIP 1000 and AISI 304, respectively, meaning better ballistic properties for the austenitic stainless steel. AISI 304 sheets experienced larger displacements than the TRIP 1000 sheets in similar impacts because of the lower yield strength and higher strain level at ultimate strength. However, the maximum measured force was approximately the same because of the similar ultimate strengths. In high velocity tests with AISI 304 and ES carbon steel, the maximum speed of the projectile without penetration was 45 m/s and 75 m/s for carbon steel and stainless steel, respectively, and much better ballistic properties were discovered for AISI 304. It should be noted, that both yield and ultimate strength of the normal carbon steel were significantly lower than those of the stainless steel, and the ductility of the stainless steel was also little better. *Overall, AISI 304 was discovered to be an effective material for protecting structures from ballistic impacts*. [66]

Corrugated sheets made from austenitic stainless steel EN 1.4401 or duplex EN 1.4362 are commonly used in offshore applications as **blast shields** on topside modules to protect the structures and personnel from explosions. High strength, good ductility and high energy absorption of stainless steels with higher strain rate dependency than of carbon steel are suitable properties in blast shields. [2] There are two types of blast shields in offshore structures: bulkheads and corrugated walls, illustrated in Figure 3. Bulkheads are strong, usually 5…16 mm thick flat plates, sometimes supported by stiffeners. They are not very

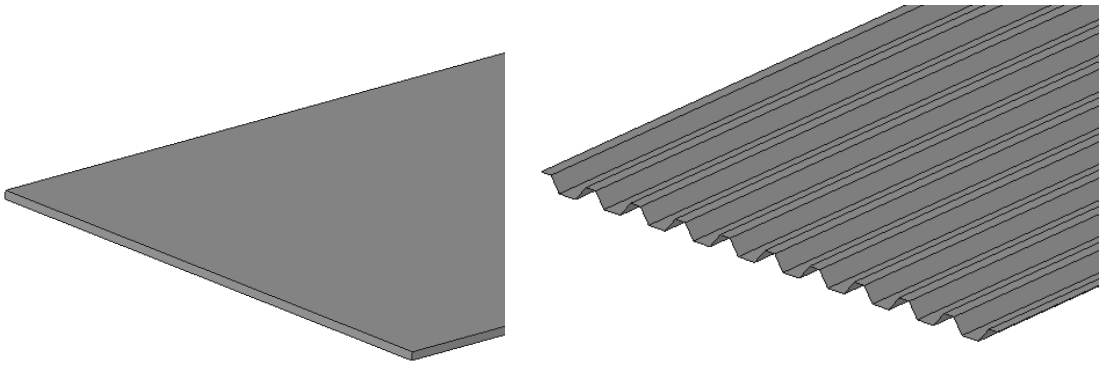

Figure 3. *Bulkhead on the left and corrugated wall on the right.*

flexible and experience a brittle failure. They are usually made from carbon steel. Corrugated walls are thinner than the bulkheads, usually 1…6 mm thick. Combined low thickness and corrugated structure enables large energy dissipation through large plastic deformation. Corrugated walls are usually made from carbon steel or stainless steel. *When bulkheads and corrugated walls made from the S355 carbon steel were compared in FE-analysis, the corrugated walls showed excellent performance*. A 2 mm thick corrugated plate experienced large plastic deformation and had the same deflection as a 16 mm thick bulkhead. The maximum (local) reaction force of the corrugated 2 mm plate was over twice as high as the reaction force of the 16 mm bulkhead. At the same time the plastic energy absorption of the corrugated plate was also over twice the value of the bulkhead. [107]

A series of experimental investigation, analytical modelling and numerical simulation was carried out with austenitic AISI 316L (~EN 1.4404) corrugated blast walls in [60, 68, 69] by Langdon and Schleyer. The effects of blast loading direction and flexibility of the connection to the main load bearing structures were also considered. The experimental results showed that flexible connections increased the deformation on the panel but also decreased the pressure which caused plastic deformation. It was also noticed that large tension forces were developed as the corrugated plate started to carry the load with tension. It is not desirable, because the tension can be transferred to the main frame structure and cause permanent damage. For that reason, it is important to design the wall for maximum energy absorption in bending and stretching while still limiting the maximum deformation in order to avoid contact with other gear. [60, 68, 69] In that point of view the excellent ductility and strain hardening of especially austenitic stainless steel may be beneficial: good energy absorption with plastic deformation is expected while the strain hardening can restrict the maximum deformation. In a study performed by Louca et al. (2004), *austenitic SS316 (EN 1.4401) was preferred over the duplex SS2205 (EN 1.4462) in blast shields*. The austenitic grade has better energy dissipation, which can prevent the formation of a sudden instability at high load levels, where plastic deformation is possible. [61]

Ship collisions with offshore structures or other ships are still relatively common nowadays, and proper design of structures in case of collisions is essential. When Lehmann and Peschmann (2002) studied a collision of two ships with a validated numerical model, use of austenitic stainless steels instead of carbon steel with approximately similar yield strength showed remarkable improvements in energy absorption. When only the inner shell of the ship was made from austenitic stainless steel, the energy absorption increased 93% compared to the ship made fully of carbon steel. *When both inner and outer shells were made of austenitic stainless steel instead of carbon steel, the energy absorption increased 220%.* [65] Not only the ships but also the offshore installations such as offshore drilling platforms are designed to withstand a collision with a ship. NORSOK N-004 standard allows three design procedures: ductile, strength and shared energy design. In ductile design the bow or side of the ship is assumed to be rigid and the platform to absorb all the energy. In strength design the installation is rigid and the ship absorbs all the collision energy with plastic deformation. In shared energy design both ship and installation are expected to have plastic deformation. [108] Using austenitic stainless steel with good ductility and energy absorption properties might be beneficial in load bearing structures of an oil platform when the collision is considered. Large plastic deformation before fracture of austenitic stainless steels allow good energy absorption before the failure. Corrosion resistance of stainless steel in such corrosive sea environment is also advantageous.

Crashworthiness of hollow section tubes was studied in more detail. Crashworthiness describes the energy absorption properties of the structure in impacts. The aim in crashworthiness applications is to protect the occupants – or other structures – in case of impact.

3.1 Measuring and comparing energy absorption

There are some often used parameters for describing the crashworthiness of the member. **Total energy absorption** is defined as the total energy absorbed in the crush of the specimen, and it describes the total energy absorption capabilities. **Mean crush force**, in some references called crush strength, is the mean force during the crush of the member, and it can be also calculated as the absorbed energy during the collapse divided by the displacement. **Peak crushing force** is the maximum load value at the load-displacement curve and in the case of a single tube, it is the force needed for the formation of the first fold. The peak crushing force should be minimized and be as close to the mean crushing force as possible for the smoothest deceleration. **Specific energy absorption** is defined as the absorbed energy per unit mass. [59]

The area under the stress–strain graph, as the **absorbed energy per unit volume**, is often used to compare the energy absorption properties. Some authors have suggested various kinds of strain limits for the comparison, for example 10% or 40% total strain, but Talonen and Hänninen (2006) suggested, that stress–strain curve up to a certain level, for

example 10% strain, is not sufficient criteria to compare energy absorption. Strain hardening can play a significant role also at higher strains, and in crush tests the folding of the austenitic stainless steel (EN 1.4301, EN 1.4318) hat and hexagon specimen produced remarkably higher local strains than 10%. Thus, the energy absorption cannot be described only by the stress–strain curve up to the 10% strains. It was also noted that the *energy absorption cannot be increased only by increasing the yield strength of the material, and the work-hardening must be taken into accoun*t. [63] In high-speed impacts where high speed causes the material to prefer fracture instead of plastic deforming, high yield strength was noted to be more important than good plasticity in austenitic stainless steels [70].

3.2 Properties affecting energy absorption

Geometry has a significant effect on the abilities of energy absorbing elements. A rule of thumb is that *the more corners there is in a polygon profile, the better the energy absorption is* [59]. Similar results were obtained by Yamashita et al. (2003) in the quasi-static and dynamic crush tests with aluminum and simulation of both aluminum and steel. The spherical length of the specimen was kept constant, and the crush strength or mean force increased as the number of the corners in the tube was increased. For example, hexagon tube performs better than square tube in terms of crush strength or mean force. When steel polygon sections with 4 and 12 corners and linear hardening rate of 100 MPa were compared, the crush strength of the 12-corner section was 50% and 10% larger than of the 4-corner section with thickness of 1.0 mm and 3.0, respectively. With linear hardening of 300 MPa the corresponding values were 55% and 15%, respectively. These results suggest, that *the effect of number of polygon corners is significantly larger with thinner section*. [109] According to Talonen and Hänninen, hexagon profiles outperform the hat-profile in energy absorption [63].

The studies with aluminum tubes mentioned above also suggested that the deformation patterns are more ordered with larger thicknesses or with larger number of corners (shorter side lengths). More ordered deformation patterns and increased energy absorption by increasing number of corners was explained by that shortening the side length increased the constraint on the deformation [109]. In other study Vinayagar and Kumar (2017) suggested, that the reason for the enhanced energy absorption by increasing the number of polygon corners was the increased number of plastic hinges and folds [59]. Sections with under 6 corners have irregular (unsymmetrical) folding patterns and thus should be avoided if regular and predictable folding pattern is desired. Strain hardening has also a significant effect on the folding behavior of the tube. Stronger strain hardening stabilizes the folding behavior and can cause the formation of a symmetric accordion folding instead of a diamond shape folding in circular sections. [109]

Axisymmetric accordion folding behavior was discovered only with thicker 3 mm CHS aluminum tubes and unsymmetrical diamond mode was observed with both 3 mm and lower thicknesses. The two folding modes, diamond and accordion, are presented in Figure 4. *The mean crush force for the axisymmetric accordion mode was higher than for the diamond shape mode*. [109] Opposite results regarding to the effect of thickness were obtained by Taherishargh et al. (2016) in their study, where increasing the ratio of the thickness to diameter changed the folding behavior of AISI 304 CHS tubes from concertina mode to mixed mode [67]. Thus, the effect of thickness on the folding behavior symmetricity and energy absorption is not self-evident. In these two studies different materials were used (aluminum and austenitic stainless steel), loading conditions may not be exactly the same or initial imperfections may have been different on the tubes, and these possibly had an effect on the folding behavior.

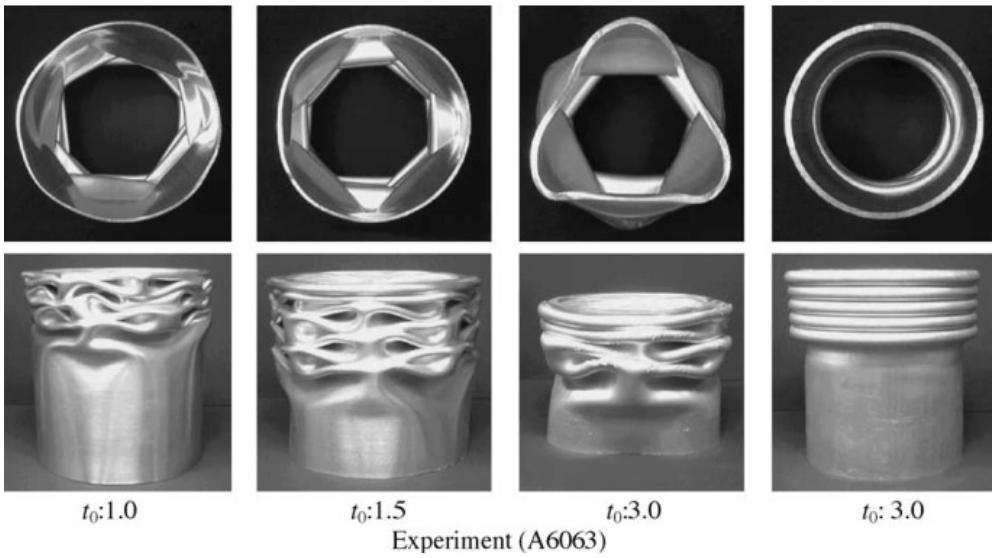

Figure 4. *Folding behavior of A6063 aluminum circular tubes with different thicknesses [109]. With the thickness of 3.0 mm, both diamond (on the left) and accordion mode (on the right) are generated indicating that the folding behavior may be depended on the loading conditions or imperfections.*

When elements for high-speed energy absorption are designed, strain rates and **strain rate sensitivity** must be considered. For example, in car crashes the strain rates are high, typically 100–300 s^{-1}, and the strain rate sensitivity must be taken into account [63]. One consequence of the strain rate sensitivity is that a material which performs well in quasi-static loading, might not be the best choice for the dynamic loading. In quasi-static and dynamic crush tests done by Talonen and Hänninen, *EN 1.4301 absorbed more energy in quasi-static loading than EN 1.4318, but in dynamic loading the situation was the opposite*. EN 1.4301, which performed better in quasi-static energy absorption, has higher 0.2-proof strength but lower strain rate sensitivity than the EN 1.4318. High strain rate sensitivity gives the EN 1.4318 high work hardening with high strain rates, and thus the energy absorption is good in dynamic loading – even better than with the EN 1.4301 which performed better in quasi-static loading. [63] Higher strain hardening rate leads to

more even distribution of the plastic deformation and thus a larger volume is taking part to the energy absorption [63, see 1]. High strength steels often have lower strain rate sensitivity than ordinary steels, and in dynamic loading high strength steels might give unsatisfactory energy absorption results if only quasi-static dimensioning is considered [63, see 5,6].

DiPaolo and Tom studied quasi-static crush of carbon steel ASTM A36 and A513 and austenitic stainless steel AISI 304 and 316 square hollow tubes. In these tests, all the tubes had same kind of folding behavior regardless of the material and different **material properties** such as strength, as shown in Figure 5. [64] Aluminum square hollow tubes were reported to have fractures in the corners in quasi-static crushing due to the localized severe deformation [109], but stainless steel has not been reported to have similar fractures in folding [63, 64, 72]. From this point of view, the excellent ductility of stainless steel gives it an advantage over aluminum as no fractures are present with the stainless steels, but on the other hand, the excellent ductility of the stainless steel is not fully utilized.

Temperature can have a significant impact in the energy absorption properties. In the same study mentioned above, with two different carbon and stainless steels, increasing the temperature from 22 °C to 93 °C lowered the maximum load, mean load and energy absorption. Cycle mean load, which is the mean load during one folding cycle and is an indicative of the energy absorption, decreased 10–14% with this temperature increase. Lowering the temperature from 22 °C to -46 °C increased the maximum load, mean load and energy absorption. Cycle mean load, after the initial first fold in the secondary folding phase, increased 13–20% with this temperature decrease. [64] These results show that the *energy absorption properties of carbon and stainless steels can vary up to 20% with a 70 °C temperature variation*.

Crush initiators are one way to lower the peak crushing load formed in the initial state. With crush initiators, the tube can be made to fold in a controlled manner from specific locations. In a study performed by Eren et al. (2009), new rib-styled crush initiators in steel tubes were tested in an explicit nonlinear finite element analysis. The benefit of this rib initiator is that it is not affecting the corners of the tube and thus the tube can still take loads effectively in different directions (shear, bending). Using FEA, the stress concentration areas of an unmodified tube were first located. These are the locations where the folding naturally occurs. Then the rib-type crush initiators were placed in these locations as shown in Figure 6. Both concave and convex ribs and different pattern variations of them were used to obtain the best result. Based on the simulation results from the energy absorption of the first 100 mm crush, the best energy absorption was reached when all the ribs were pointing outwards. *Compared to a tube without initiators, 25% improvement in absorbed energy and over 50% decrease in peak load were obtained simultaneously by using crush initiators*. For an unmodified tube and the tube with the best energy absorption, the peak loads were 129.5 kN and 59.1 kN, respectively, so the initial crush force was reduced by more than 50% while the energy absorption was increased. The energy

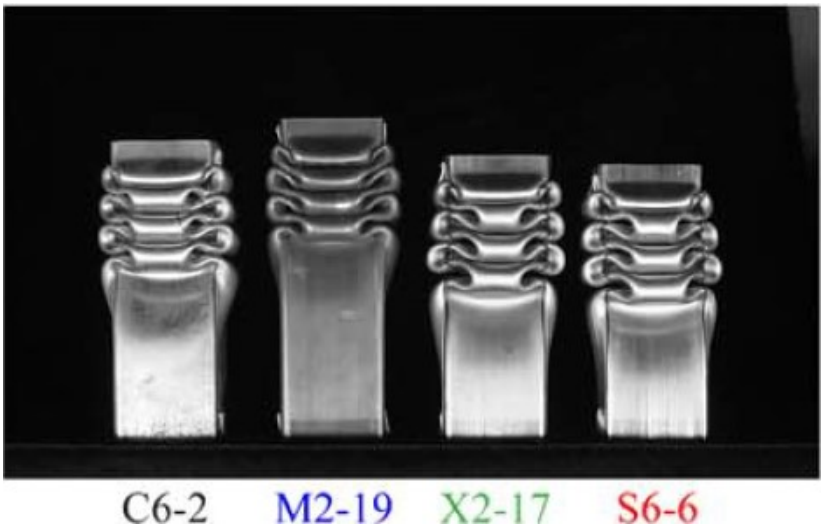

Figure 5. *Quasi-static folding behavior of ASTM A36, ASTM A513, AISI 316 and AISI 304 square hollow tubes, respectively, in room temperature [64]. All the tubes have same kind of folding behavior.*

absorption for the same tubes were 3513 J and 4408 J, respectively, giving a 25% improvement. These results with three other configurations are given in Table 2. [110] *These simulation results suggest that the different initiator configurations give remarkably different energy absorptions while the peak load remains almost constant.*

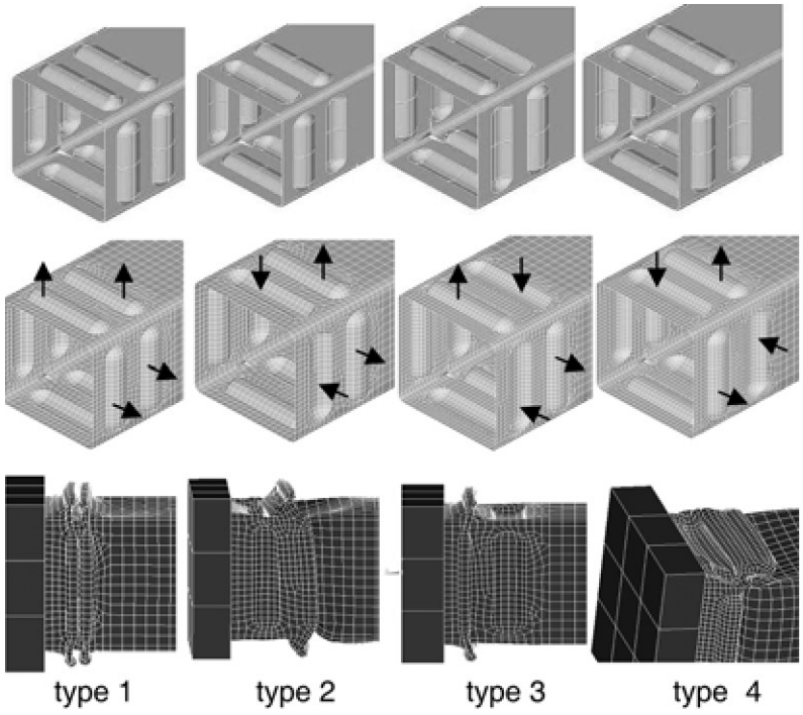

Figure 6. *Rib-style crush initiators [110].*

Table 2. *Crush test simulation results from [110] with different rib arrangements. Tube without initiators is given for reference. Initiator types are presented Figure 6.*

	Peak load (kN)	Difference (%)	Energy absorption (J)	Difference (%)
Tube without initiators	129.5	-	3513	-
Convex initiators (type 1)	59.1	-54	4408	+25
Concave and convex initiators (type 2)	58.5	-54	4096	+16
Concave and convex ribs on adjacent sides (type 3)	56.9	-56	2934	-16
Concave and convex ribs on adjacent sides (type 4)	57.7	-55	3278	-7

3.3 Bitubular structures

To increase the effective use of material in crush applications, **bitubular structures** can be used. Vinayagar and Kumar tested AISI 304 (EN 1.4301) double tubes with different quasi-static test configurations: circle outer tube with constant diameter was crushed together with different sized triangle, square and hexagon inner tubes. Considering the system mass, *multiple double tube configurations reached higher specific energy absorption values (energy absorption per mass) than bare outer tubes indicating better energy absorption*. The force fluctuation in force-displacement response was also lower with bitubes than with single tubes. Increasing the size of the inner tube increased the interaction between the inner and outer tubes leading to better energy absorption. As it might be expected based on the test results of [109] on the effect of the number of polygon corners, increasing the number of corners of the inner tube led to better energy absorption. For example, with inner tube maximum outer dimension of 60 mm and the circular tube diameter of 90 mm, the specific energy absorption increased from 4.917 kJ/kg to 6.346 kJ/kg when the inner tube was changed from triangle to hexagon. With larger inner tubes, maximum dimension of 80 mm, the difference was smaller though the specific energy absorption was better: with triangle and hexagonal tubes the values were 6.291 kJ/kg and 6.722 kJ/kg, respectively. It was proposed that increasing the number of corners increased the number of plastic hinges and folds and thus also the energy absorption was enhanced, as the energy was used for the increased plastic deformation. Increasing the number of sides of the inner polygon tube increases the number of the folds and decreases the fold length, and the changes inner tube behavior may also change the folding behavior of the outer tube. [59]

Haghi et al. (2009) performed quasi-static crush tests and simulation with LS-DYNA software for bitubular aluminum square tubes with different tube lengths and different orientations of the tubes relative to each other. The tubes were placed in two different

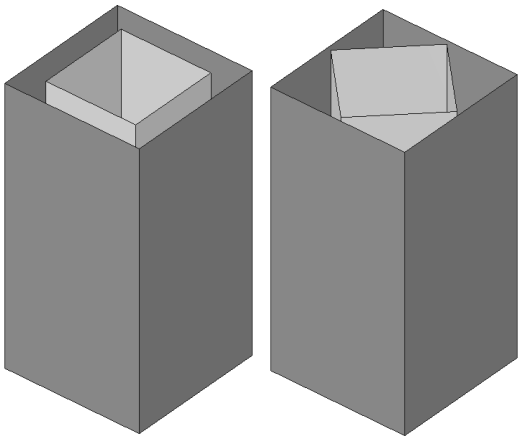

Figure 7. *Illustration figure for the bitubular specimen arrangement used in [111]. On the left the parallel and on the right the diamond arrangement. Specimen dimensions were 40x40x2 and 60x60x2 for the inner and outer tubes, respectively.*

orientations: in parallel and in diamond arrangements, where the tubes had the same orientation and a 45° angle, respectively, as demonstrated in Figure 7. *In general diamond arrangement gave better results than parallel arrangement*. Parallel tubes with the same length of 120 mm had an 8% increase in the energy absorption compared to the combined energy absorption of the inner and outer tubes crushed separately. In diamond arrangement, the interaction between the tubes increased, and the energy absorption of diamond arrangement 120 mm tubes was 36% higher than energy absorption of separately crushed tubes. Despite the better energy absorption, using two tubes with the same length had an undesirable property: the initial crush force, which should be as low as possible, was the sum of the inner and outer tube initial crush forces and thus high. To overcome this problem, unequal lengths in bitubes were tested. It was found, that in both parallel and diamond arrangements, *when the inner tube was shorter and had an appropriate length, the maximum crush force came from the outer tube initial crush force only*, and the crush force remained below that also when the inner tube started to fold. On the other hand, using shorter outer tubes and longer inner tubes leaded to higher peak crush forces than observed with single outer tube, and the folding behavior was in general ununiform, which is not desired property in this application. [111]

Table 3. *Some results from [111]. Bitubes were in diamond arrangement. The best energy absorption was obtained with 110 mm inner and 120 mm outer tubes while the peak load remained at the level of a single outer tube initial crush.*

Outer/inner tube length (mm)	Energy absorption (J)	Peak load (kN)	Mean load (kN)	Load efficiency factor (-)
120 outer tube only	681	33.9	9.5	0.28
120/120 (separately)	1291	56.8	17.6	0.31
120/120 (bitubular)	1752	56.8	25.0	0.44
110/120 (bitubular)	1856	33.9	26.5	0.78
100/120 (bitubular)	1770	44.9	25.2	0.56

The best arrangement of bitubes in simulations of [111] was found to be a diamond orientation with 120 mm outer and 110 mm inner tube. In that arrangement, the energy absorption was even higher than with two equal length bitubes. Some results are given in Table 3 for comparison. The combined energy absorption for the 120 mm inner and outer tubes crushed separately was 1291 J, whereas bitubes in diamond configuration with inner/outer tube lengths of 110/120 had the best energy absorption with 1752 J. The enhanced energy absorption can be explained with better interaction between the tubes and changed outer tube folding behavior. At the same time, the peak force for this bitubular structure was only the peak force of the single outer tube (initial crush force). The **load efficiency factor**, the peak load divided by the mean load, was clearly the best for the 110/120 bitubular configuration: for 110/120 bitubular structure it was 0.78 whereas for the outer tube crushed individually it was only 0.28 – *a 178% increase in load efficiency factor was obtained with bitubular structure*. For a steady compression with low force fluctuations, a high load efficiency factor is desirable. It is worth noticing that in diamond configuration, a wrongly sized inner tube can lead to a situation where the maximum peak force of a bitubular structure is not obtained from the initial crush of the outer tube but from the point where the inner tube starts to fold. This can appear when the beginning of a secondary outer tube fold and the initial crush force of the inner tube occur simultaneously. For instance, the peak load of a single outer tube and 100/120 mm inner/outer bitubes were 33.9 kN and 44.9 kN, respectively. [111]

3.4 Other ways of improving energy absorption

Taherishargh et al. (2016) studied crashworthiness properties of **stainless steel tubes filled with aluminum foam** in axial compression and bending. AISI 304 (approximately equivalent to EN 1.4301) circular tubes had an outer diameter of 25.4 mm and thickness of 0.9 mm or 1.2 mm. The inner surfaces of the tubes were ground using 400 grit sandpaper and then the tubes were washed and dried. With an *in situ* infiltration process described in the study, aluminum foam filled tubes were produced. 40 mm long specimen were tested in quasi-static compression tests, and 140 mm long specimen were used in quasi-static and dynamic 3-point pending experiments. [67]

In compression tests, two types of folding behavior were observed for the circular tubes: axisymmetric concertina mode and mixed mode. In the latter the deformation started at the upper or lower end of the tube and leaded to two non-axisymmetric folds. By increasing the ratio of the thickness to diameter, the folding behavior of the empty AISI 304 tubes chanced from concertina mode to mixed mode. [67] It was opposite to the findings in [109] for the aluminum tubes where the concertina mode was only observed with thicker CHS cross section. The foam filled tubes had concertina mode folding behavior regardless of the thickness of the tube. Both empty and foam filled tubes were discovered to have the same amount of folds and peaks in force–displacement curve when compressed, but the crushing force of the foam filled tubes remained a lot steadier than of the empty tubes. Foam filled tubes also had 30–50% higher load levels, though they also had

larger cross sectional area because of the foam. It was concluded that *in compression adding aluminum foam increased the specific energy absorption of the 0.9 mm and 1.2 mm thick tubes by 13% and 8%, respectively, whereas increasing the thickness of the empty tube from 0.9 mm to 1.2 mm increased the specific energy absorption by 9%.* [67]

Foam filling also increased the energy absorption efficiency in compression (absorbed energy divided by the ideal maximum absorbed energy). The energy absorption efficiency for all empty and foam filled specimen were around 90% at 2.5–3 mm displacement (of total 25 mm displacement). After that the efficiency of the empty tubes dropped to a level of 50…75% at the displacement of 8 mm whereas the efficiency of the foam filled tubes remained at around 90% until approximately 12.5 mm displacement. Then the efficiency started to decrease almost linearly to a 30% efficiency at 25 mm displacement. Based on these results on specific energy absorption and efficiency, it was concluded that these foam fillings enhanced the crashworthiness performance, because they increased both specific energy absorption and efficiency. [67] It was noted, that for example in [112], aluminum square tubes with aluminum foam filling had worse energy absorption properties than empty aluminum tubes with same outer dimensions and corresponding weight. Also adding polyurethane foam filling into aluminum circular tubes showed negligible effect on load and energy capacity and decreased the specific energy absorption in [113]. [67]

In three point bending tests of [67] quasi-static and dynamic loading conditions were used. The loading speeds were 0.1 mm/s and 284 mm/s, respectively. The differences in the load-displacement curve of the empty and foam filled tubes were very clear. At around 12 mm midspan displacement, the empty tubes in dynamic tests had a peak value of approximately 5 kN and 7 kN for 0.9 mm and 1.2 mm thicknesses, respectively. After the peak value the force slowly decreased to 3 kN and 4.7 kN at displacement of 30 mm. In the quasi-static test, the peak load value for the 0.9 mm thick tube was 4.6 kN and at the 30 mm displacement the forces for the quasi-static and dynamic testing of 0.9 mm thick tubes were coincident. *The reason for the decrease in the force was the local inward fold of the empty tube at the loading point, which caused ovalization of the tube and formation of a plastic hinge.* [67]

The behavior of the foam filled tubes were very different because the foam filling reduced the local denting and ovalization of the tubes. At the midspan the lower part of the foam filled tube experienced larger tensile plastic strains than the empty tube. The density of the foam was locally increased at the loading point as it was compressed. The friction and chemical bonding between the tube and foam filling caused remarkable tensile deformation and cracks on the foam, but the presence of the tube prevented catastrophic failure of the foam filling. The load of the foam filled tubes increased as the displacement increased. This was mainly due to the restricted ovalization and interaction between the tube and the foam filling. In quasi-static bend loading, the force of the 0.9 mm thick foam filled tube increased somewhat linearly to 10 kN force at approximately 3 mm mid-span

displacement. After that the force increased more slowly and at 24 mm displacement the force was around 20 kN. That is remarkably higher than the maximum load of 4.6 kN for the empty 0.9 mm tube in quasi-static loading. Unlike in the case of empty tubes, the thickness of the foam filled tubes had low impact on the load-displacement behavior, and the force at 24 mm displacement for the thicker 1.2 mm foam filled tube was around 21.5 kN which is only 7.5% more than for the 0.9 mm tube. The force of 0.9 mm foam filled tube at 24 mm displacement in dynamic loading was approximately 21 kN, so the effect of dynamic loading with this loading speed was quite small, too. *In quasi-static bending, the specific energy absorption of the foam filled tubes with 0.9 mm tube thickness was 2.12 times the value of the 0.9 mm thick empty tubes, and thus a 112% increase in specific energy absorption was obtained with foam filling in bending.* [67]

3.5 Finite element modelling of axial crush of square hollow section tubes

In this work crashworthiness simulations were performed with ANSYS R19.0 finite element analysis (FEA) software using explicit dynamics ANSYS AUTODYN solver. The aim was to develop finite element models (FEM) that can predict the axial crush behavior of stainless steel square hollow section tubes and use the model for parametric studies if the results correspond to the experimental results. Local imperfections were considered in all models, and they were obtained from linear buckling analysis (LBA) using ANSYS APDL solver. Simulation models were compared against experimental data presented by DiPaolo and Tom (2009) [64] and Kashani et al. (2013) [111].

3.5.1 Simulation model validation, single tube

The simulation model of a single AISI 304 tube was validated against the experimental quasi-static tests done by DiPaolo and Tom (2009). In their experiment, 305 mm long 50×50 AISI 304 tubes with measured average thickness of 1.50 mm were used in axial crush tests. Crush initiators, machined grooves on the full width of the tube, were used on opposite sides. Another set of initiators were used below the first pair on adjacent sides. Test were performed in three temperatures: -46 °C, 22 °C and 93 °C. Mechanical properties were tested in uniaxial tension tests. For AISI 304 the following values were obtained in room temperature: 0.2% proof stress 449 MPa, ultimate strength 706 MPa and ultimate elongation 0.50. Grooved end caps, that restrict the movement in transverse direction to the compression, were used in the experimental axial crush tests. [64] In simulation of this work, fixed support was used at the bottom edges and all degrees of freedom expect y-translation were restricted at the top edges. 200 mm movement downwards in y-direction was set to the top of the tube. Local imperfections were obtained from a linear buckling analysis. First and second buckling modes were tested, and the second buckling mode gave better agreement with the experimental test: both folding shape and

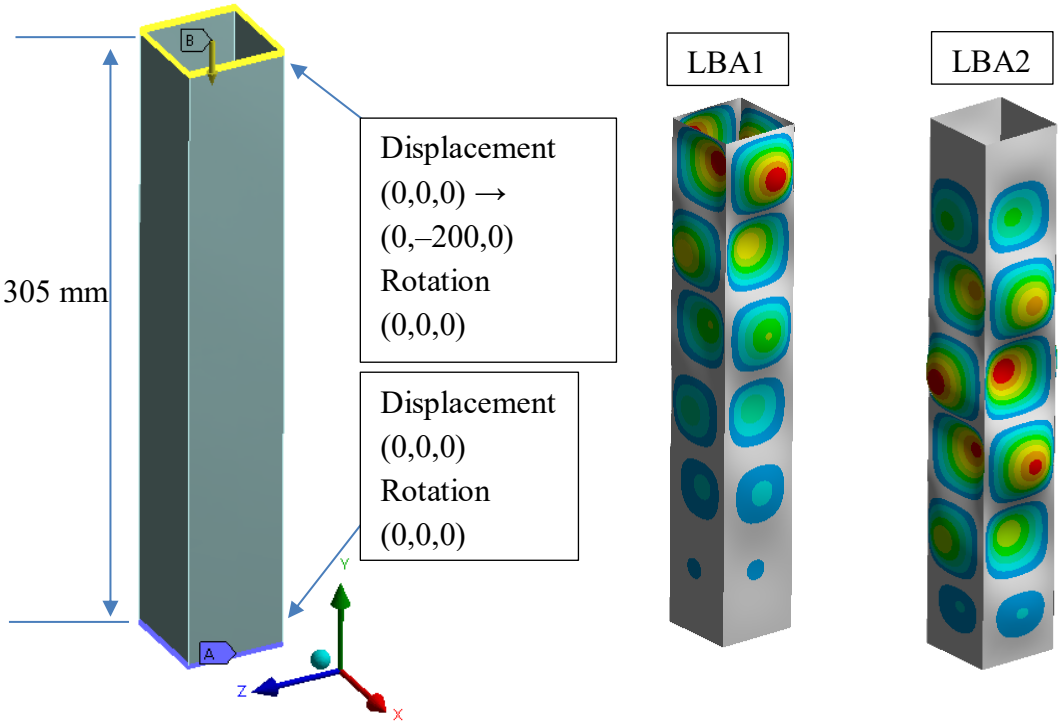

Figure 8. *On the left geometry and constraints of the simulation model. Constraints were scoped to the edges at the top and bottom of the tube. On the right two first modes from linear buckling analysis (LBA).*

force–displacement curve were closer to the experimental data. The amplitude of the imperfection was $b/200$, where b is the width of the tube. The rounding of the corners or the crush initiators were not modelled. Geometry and constraints are shown in Figure 8.

Nonlinear material model was used in the simulation. The material model was constructed using the two-stage Ramberg–Osgood material model presented in Design Manual for Structural Stainless Steel [3]. 0.2% proof strength, ultimate strength and ultimate elongation values were taken from the experimental data of [64], whereas the Yong's modulus E and Ramberg–Osgood coefficient n were obtained from the design manual. True stress–logarithmic strain curve was determined from the engineering stress–engineering strain curve. Multilinear isotropic hardening was chosen in ANSYS to model the plasticity. The true stress–logarithmic strain curve was converted to multilinear true stress–logarithmic plastic strain curve with 10 data points. The material modeling is shown in detail in appendix 1. Effects of cold working on the strength of the corners were not considered. The model was meshed with linear SHELL181 shell elements. According to ANSYS Mechanical manual, SHELL181 is suitable for large strain nonlinear applications [114]. Different mesh sizes were tested, and 2.0 mm element size was chosen for suitable results and efficiency. Frictional contacts with 0.2 friction coefficient and thickness effect were used, and self-contact of bodies were considered. The experiments in [64] were quasi-static with speed of 2.5 mm/min, but the simulation was carried out in 1.0 s analysis time for

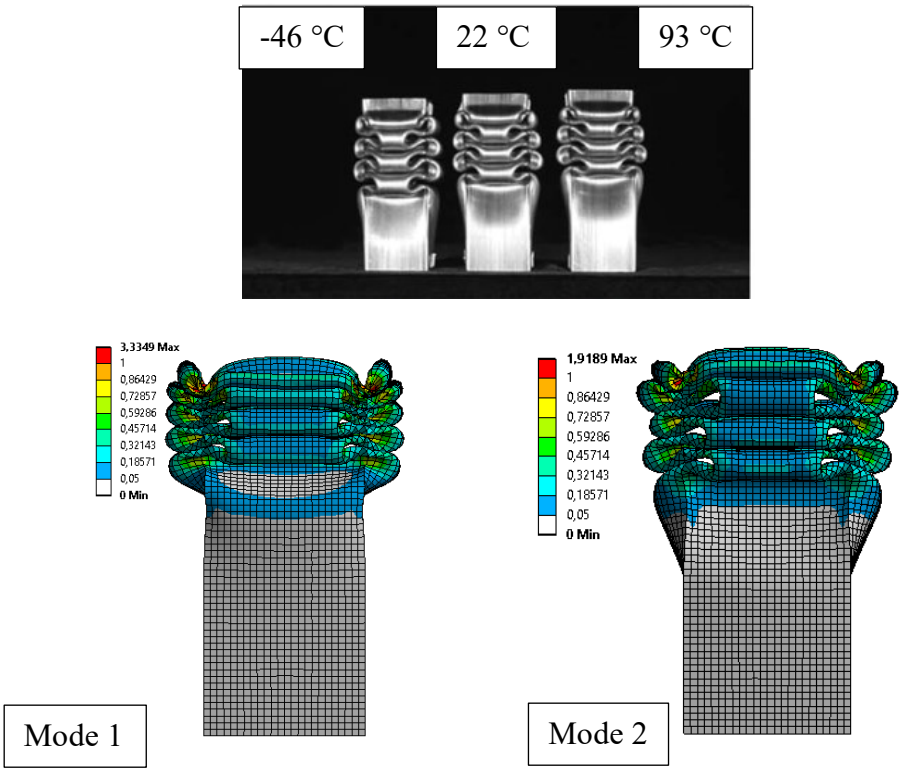

Figure 9. *Axial crush test results for AISI 304 tubes in different temperatures from [64] at the top and simulation results (plastic strain, mm/mm) with first and second buckling mode imperfections at the bottom. 2nd LBA mode imperfection gives better correspondence with the experimental results.*

shorter calculation times. Displacement of 200 mm in that time equals to 200 mm/s. Using linear buckling mode 2 imperfection with *b*/200 amplitude, the ratio of maximum kinetic energy to total energy was only 0.09% and thus the inertial effects are negligible. Mass scaling of elements up to 1000 times the original mass was applied in the analysis settings to shorten the calculation time.

Figure 9 shows the folding behavior of AISI 304 tubes in experiments [64] and in FEA validation model. From the figure can be seen that the folding behavior of both tubes, with 1st and 2nd LBA mode imperfections, corresponded well to the experimental results but the shape of the tube with 2nd LBA mode imperfection was closer to the experimental tests. The difference can be seen at the width of the fold (relative to the width of the tube, seen on the front face in the figure) which was smaller for the 2nd LBA mode. Below the lowest completed folds on the sides new forming folds also behaved more accurately with the 2nd LBA imperfection model. One remarkable difference between the simulation model and experiments was the behavior of the top of the tube: there was a short part of undeformed tube in experiments, but in the simulation the top part of the tube experienced severe plastic deformation and was folded so that at the end of the analysis the top edges of the tube were at the level of the first folds in vertical direction.

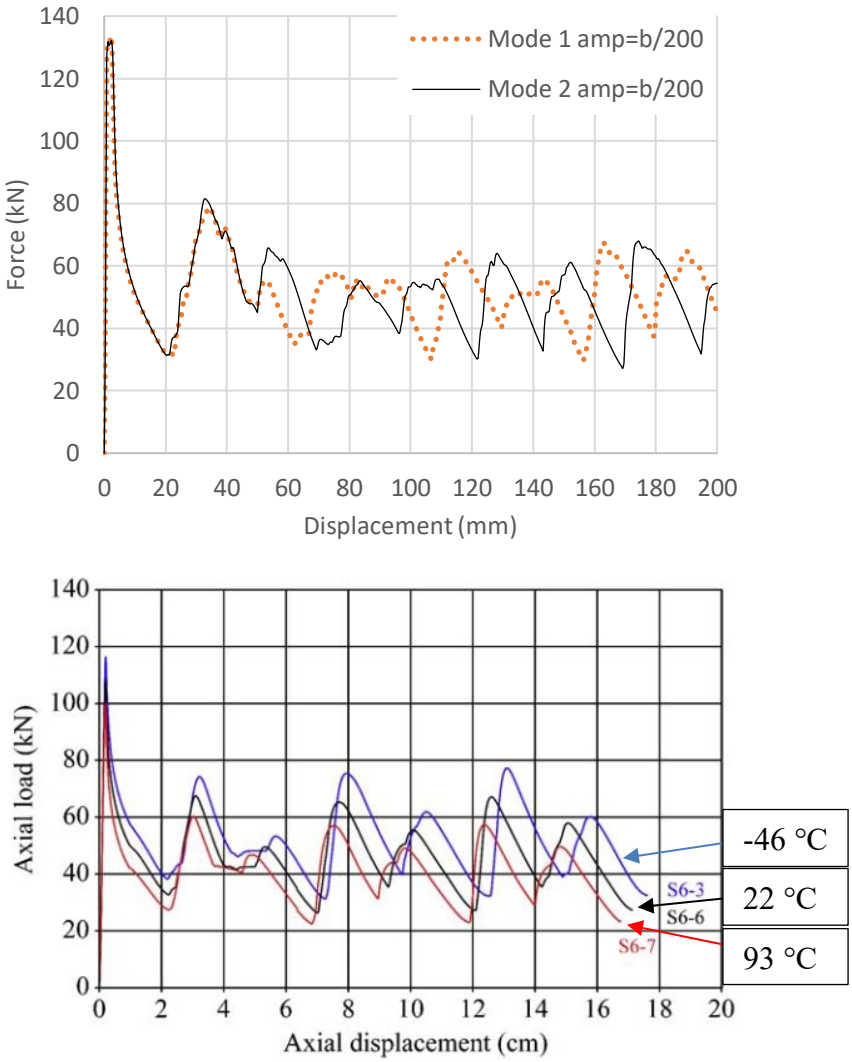

Figure 10. *At the top force–displacement curve from simulation with 1st and 2nd LBA mode imperfections, b/200 imperfection amplitude. Experimental curves in different temperatures below [64]. S6-6 is the room temperature curve.*

Figure 10 presents the force–displacement curves for simulation and axial crush experiments. Both 1st and 2nd LBA mode imperfection models with *b*/200 amplitude are shown. The curve with 2nd LBA mode imperfection (black line) had very good correlation with the experimental curve. The number of force peaks and the displacement which they occur at were quite accurately predicted at the range of 0…170 mm crush distance, which was the experimental data range. The magnitudes of the force peaks were also close to the experimental values. *With the 1st LBA mode imperfection the displacements between the force peaks were shorter than in experimental tests, but with the 2nd LBA imperfection the peak distance was close to the experimental data*. The peak force in experiments was 107.8 kN [64], whereas the first force peak in simulation using 2nd linear buckling mode as imperfection was 132.1 kN, so the simulation model overestimated the initial peak force by 22.5%. The error of peak force with 1st linear buckling mode was 23.8%. It should be noted, that the crush initiators were not modelled and thus it was expected that

the initial force peak was overestimated in simulation. Other load peaks of 1st and 2nd LBA mode imperfection models and tests had a quite good correspondence at around 50–70 kN loads, depending on the peak, though the places and shapes of the peaks were not as good relative to the tests with 1st LBA mode imperfection than with the 2nd LBA mode imperfection.

***Table 4**. Mean crushing forces (F_{mean}) and initial peak forces (F_{peak}) for experiments in [64] and simulation models with 1st and 2nd LBA mode imperfections. The errors of the simulation models are also presented.*

	F_{mean} (kN)	F_{mean} error (%)	F_{peak} (kN)	F_{peak} error (%)
Experiment	46.6	-	107.8	-
FEA, mode 1 imperfection	52.7	13.1	133.5	23.8
FEA, mode 2 imperfection	51.8	11.1	132.1	22.5

In the experiments the initial and secondary folding phase mean loads were 46.6 kN and 46.5 kN, respectively [64]. In the simulation, the mean load for the whole displacement range were 52.7 kN and 51.8 kN for 1st and 2nd LBA mode imperfection models, respectively. These values mean 13.1% and 11.1% overprediction errors for the mean load. Mean and peak loads with corresponding errors are gathered together in Table 4. Based on the folding behavior presented in Figure 9, axial load–displacement curve presented in Figure 10 and force values given in Table 4, the *simulation model with b/200 imperfection amplitude and 2nd LBA mode imperfection shape can give reasonable predictions for this quasi-static axial crush of a single AISI 304 (EN 1.4301) square tube with around 10% error in mean crushing force*.

3.5.2 Simulation model validation, bitubular structures

In order to simulate crashworthiness of bitubular strcutures, it is necessary to validate simulation models also against bitubular axial crush tests. In this work, the validation was done against experimental test carried out by Kashani et al. [111], where bitubular aluminum tubes were tested and simulated with LS-DYNA as already presended in chapter 3.3. The material model for aluminum was modelled with the same two-stage Ramberg–Osgood model which was used for the validation of single stainless steel tube axial crush, because aluminum has also nonlinear stress–strain behavior similar to stainless steels. Yield strength, ultimate strength, Young's modulus and ultimate elongations were obtained from the tensile test data provided in [111]. The developed engineering stress–strain curve had a good agreement with the tensile test data. Material modelling and comparison to the test data is shown in appendix 2.

Engineering stress–strain curve was converted to true stress–logarithmic strain curve and further to 10 point multilinear true stress–logarithmic plastic strain curve to be used in ANSYS. Material model for top and bottom plates were linear elastic and the plates were

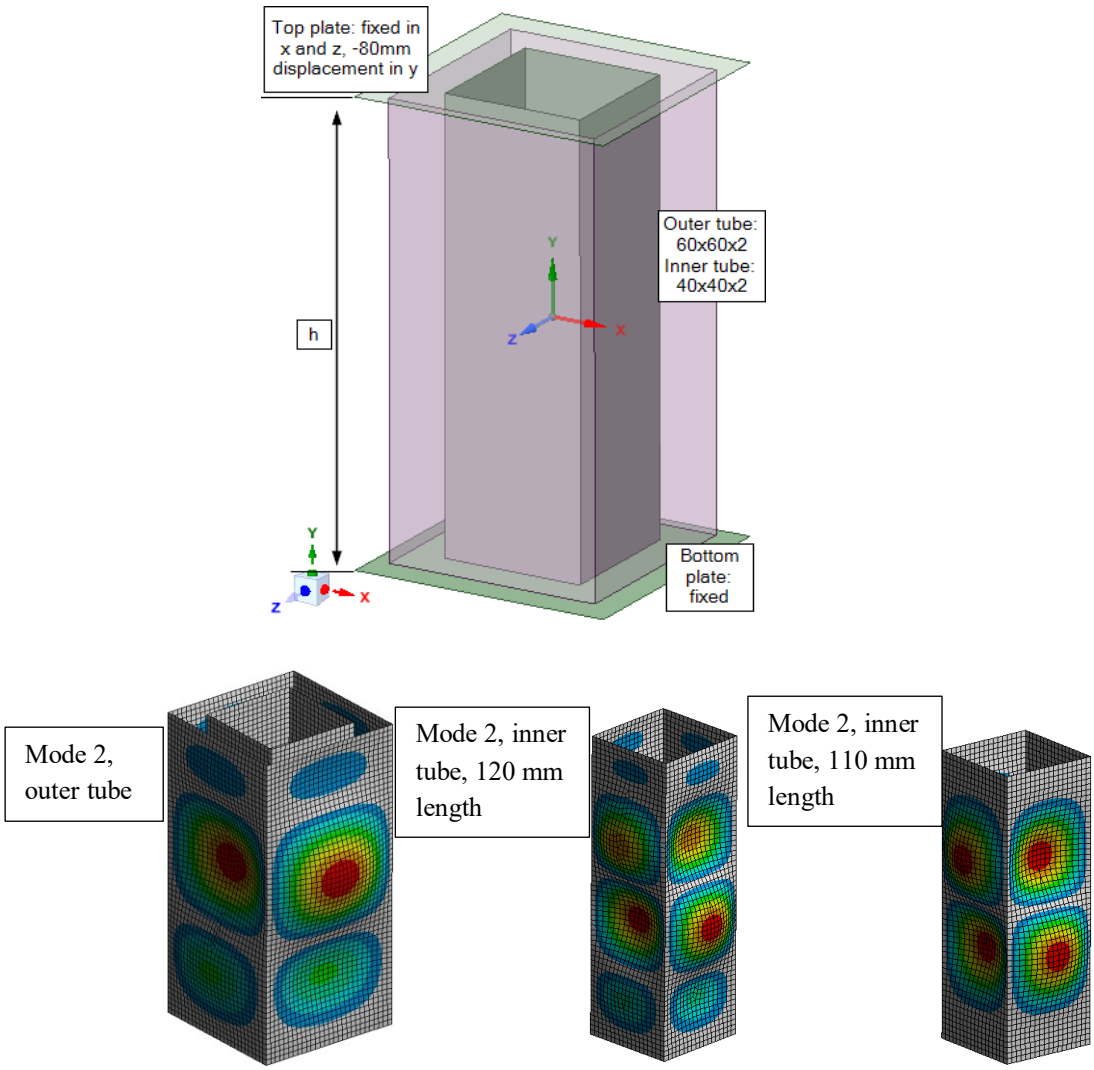

Figure 11. *Simulation model geometry, boundary conditions and imperfection shapes from linear buckling analysis.*

supported from the whole surface so plates had no deformation. Before modelling bitubular structure, the material model was first validated with a single tube axial crush using 60×60×2 tube with 120 mm length. When the energy absoprtion and mean force were compared to the experimental results given in [111] the *single tube simulation model for aluminum overestimated the energy absortpion with 9.7%,* which can be seen as a good result as the error is less than 10%. The peak force of the model was overestimated by 46.7%. Based on the low energy absorption error, the used material model can give suitable predictions on simulation.

Geometry of the bitubular model is shown in Figure 11. Outer and inner tube dimensions were 60×60×2 and 40×40×2, respectively. Height *h* was varied for inner and outer tube. Bottom plate was fixed from the whole surface, and the whole surface of the top plate was forced to a diplacement of -80 mm in y-direction while the x- and z-translations were fixed. Second mode of the linear buckling analysis was used as imperfection for both inner and outer tube. Imperfection amplitude was *b*/200, corresponding to 0.2 mm and

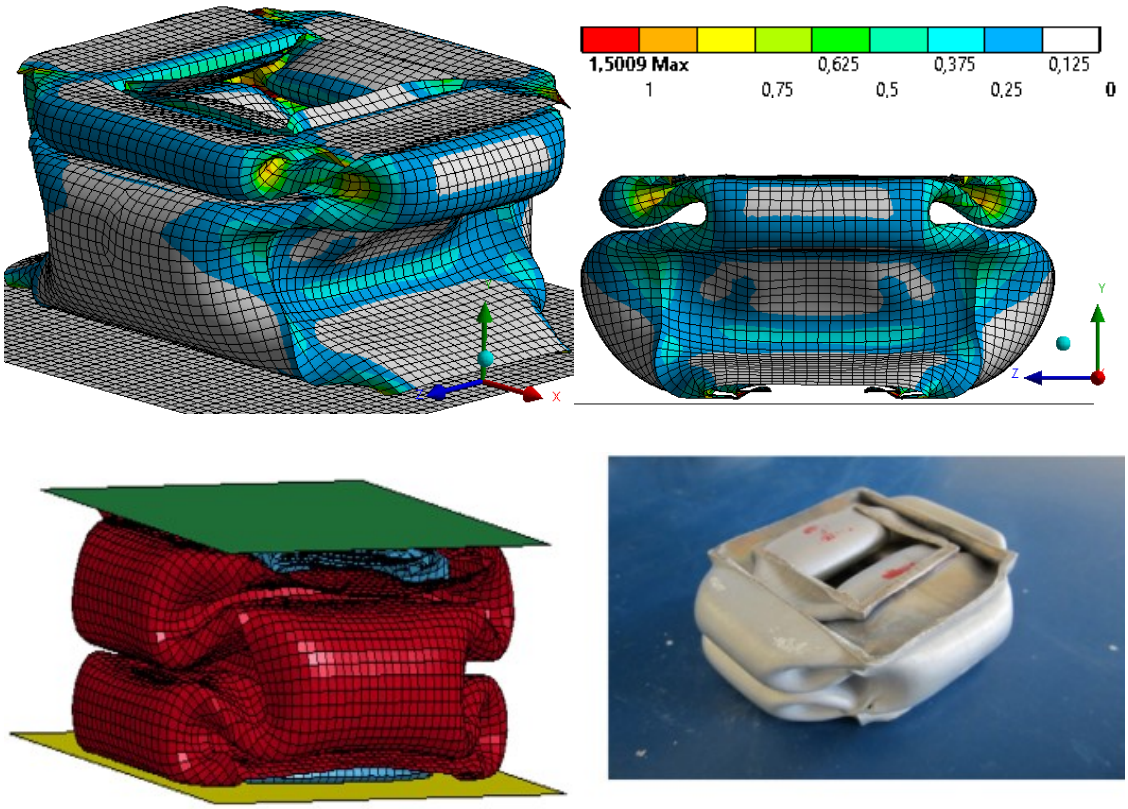

Figure 12. *Above: folding behavior (plastic strain) of parallel 120 mm tubes at 80 mm displacement in simulation of this work. Below: corresponding folding behavior of simulation and experimental results in [111]. In reference study [111] the folds have very similar heights in both experiments and simulation whereas in the simulation of this work the height of the folds are remarkably different.*

0.3 mm amplitudes for inner and outer tube, respectively. In linear buckling analysis the studied tube was fixed from the bottom edges and lateral displacements at the top edges were fixed while a compression was set to the tube.

The axial crush simulation was performed as a quasi-static problem. The 80 mm displacement of the top plate was carried out in 0.8 s leading to 100 mm/s compression speed. The same speed was used also in the numerical simulation in [111], though the speed in experiments was 10 mm/min. Mass scaling of elements up to 1000 times the original mass was allowed in the analysis settings to shorten the calculation time. All contacts were frictional with 0.2 friction coefficient. Thickness effect of the surfaces was taken into account, which means that the contacts were modelled using outer surfaces of the shell elements instead of the midplane.

Figure 12 shows the folding behavior of the parallel 120 mm long bitubular structure at 80 mm top plate displacement in the simulation of this study. Numerical and experimental results from [111] are also shown at the bottom of the figure. The results of the current simulation compared to the experimental and numerical results of [111] were somewhat similar. The main difference between the simulation of this work and both experimental

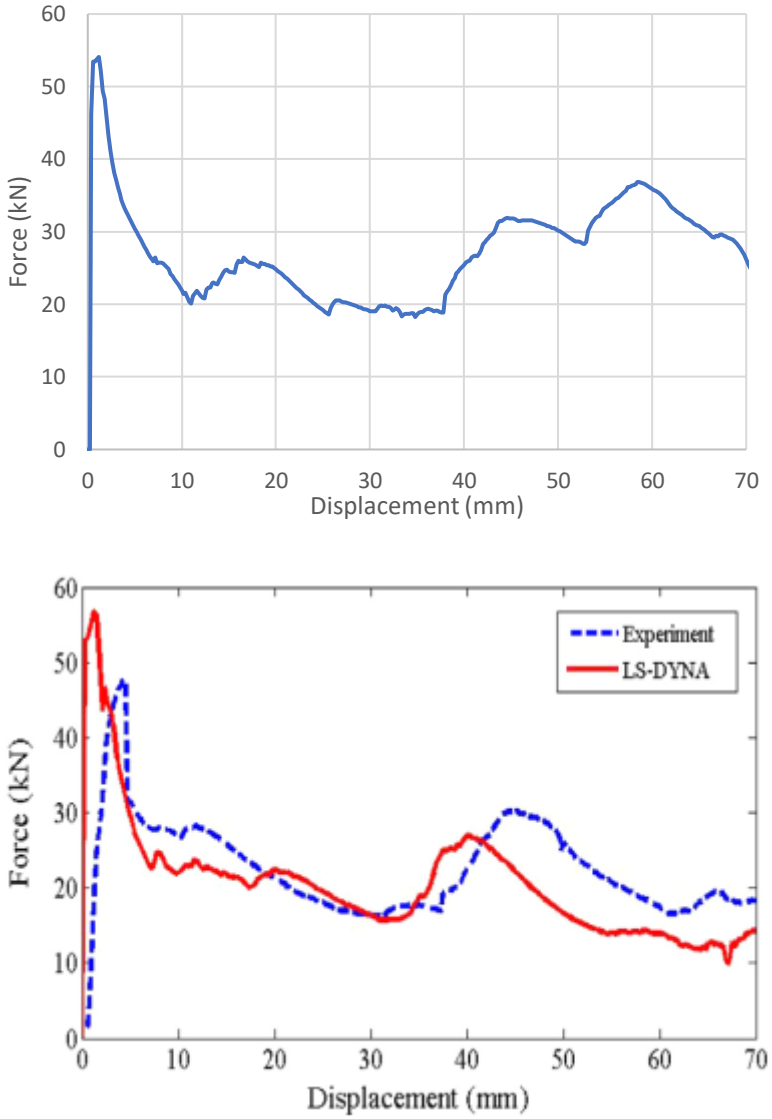

Figure 13. *Force–displacement-curves, simulation from this work above and experimental and simulation results from [111] below. Parallel configuration with 120 mm tubes. Current simulation was close to the experimental and previous simulation results up to approximately 50 mm displacement, which after the current simulation gave larger forces.*

and numerical results in [111] was that the height of the folds (in axial direction) were very similar in the reference study, whereas in this work there was a clear difference in the height of the folds. In the simulation of this study both the top and bottom of the outer tube and the bottom of the inner tube tended to spread outward on the opposite sides. Similar behavior, though to a lesser extent, can be seen on the outer tube of the experimental test.

Force–displacement curves for bitubular axial crush simulation with parallel 120 mm tubes are shown in Figure 13, where the simulation of this work but also experimental and simulation results from [111] are shown. The initial peak in the simulation of this

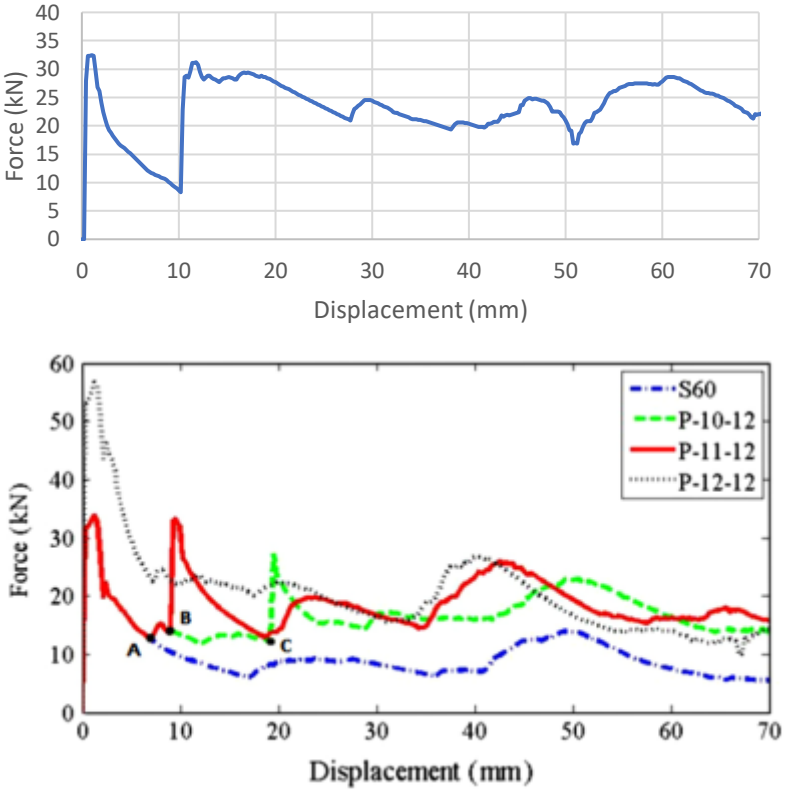

Figure 14. *Force–displacement-curves, simulation from this work above and simulation results from [111] below. Parallel configuration with 110 mm inner and 120 mm outer tubes is shown above, which corresponds to the red P-11-12 curve below. In the simulation of this work the two first force peaks are just over 30 kN like in the simulation of [111], but after that the simulation of this work gave larger forces than the reference simulation.*

work and in the experiment of [111] were 54.1 kN and 47.7 kN, respectively, giving a 13% overprediction for the simulation model. After the initial peak the force–displacement curves were very similar up to axial displacement of approximately 45 mm. In the displacement range up to 45 mm the lowest forces were around 20 kN and at 45 mm displacement the force was close to 30 kN in both experimental results and in the current simulation. After the 45 mm axial displacement the force in the simulation of this work started to grow whereas in experimental and numerical studies of [111] the force started to decrease. Energy absorption in the experiment was 1487 J and in the current simulation it was 1911 J, which means that the *energy absorption in the simulation of this work had a 29% overprediciton error*. Based on the force–displacement graph, the energy error mostly came from the range of 45–70 mm axial displacement, where the force in simulation of this work was higher than in the experiment.

Figure 14 shows the simulation results for bitubular parallel configuration with 110 mm inner tube and 120 mm outer tube in the current work (above) and in [111] (below). The graphs show that the two first force peaks were a little bit over 30 kN in both simulations and the first force peak from the initial crush of the outer tube was slightly higher than

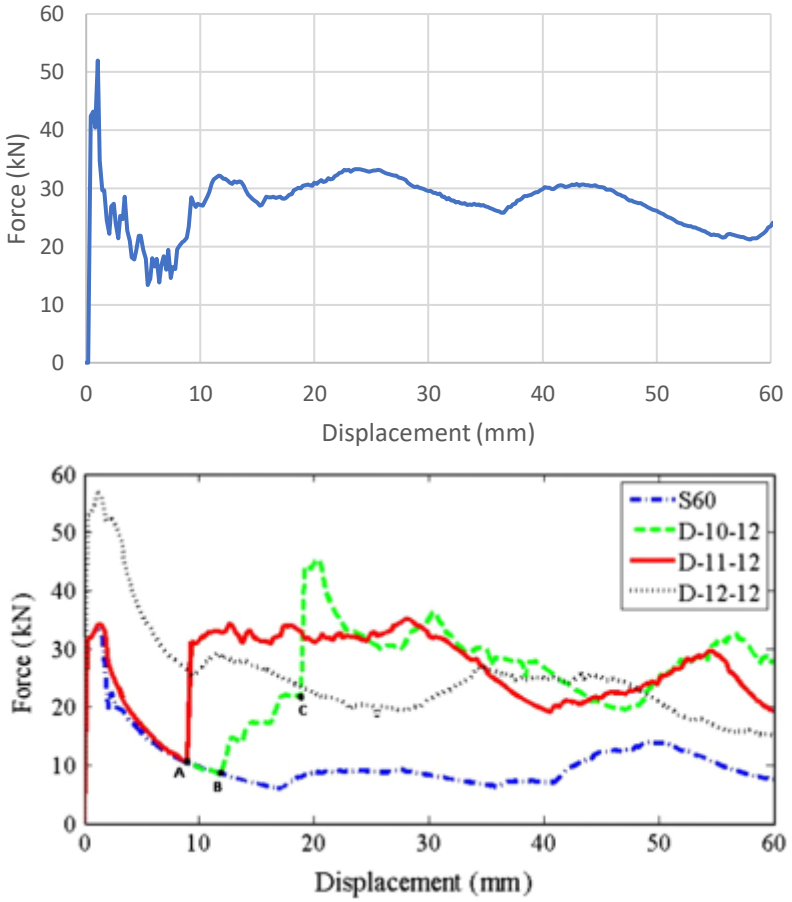

Figure 15. *Force–displacement-curves, simulation from this work above and simulation results from [111] below. The curve above is for diamond configuration with 120 mm tubes, which corresponds to the dotted D-12-12 curve below. After the initial force peaks the force in the simulation of this study remained at higher level than in the reference simulation leading to higher energy absorption predictions.*

the second peak, which was caused by the initial crush of the inner tube and continuous folding of the outer tube. The initial peaks were 32.5 kN and 33.9 kN for the simulation of this work and reference study [111], respectively, giving an 4.1% difference with respect to the reference simulation. After the initial crush of the shorter inner tube (after axial displacement of 10 mm) the force in the simulation of this work remained higher than in the reference simulation. Mean forces for the current and reference study were 23.1 kN and 17.7 kN, respectively, so *a 30.5% difference was found in this work relative to the reference study.* Because the total absorbed energy can be calculated as the mean force multiplied with the overall displacement, the difference in the absorbed energy was also 30.5%.

Force–displacement curves from simulation of bitubular axial crush of 120 mm long tubes in diamond configuration are presented in Figure 15, where the upper curve presents the simulation of this work and lower graph presents three diamond arrangement crush simulations and one single tube crush simulation in [111]. The dotted black line in the

lower graph belongs to the diamond arrangement with 120 mm tubes, which was simulated also in this work. The curves are given in a range of 0…60 mm displacement like in the reference study. The graphs show that the magnitude of the initial force peak was rather similar for both simulations, 52 kN and 56.8 kN for simulations of current and reference study, respectively. It equals to 8.5% difference with respect to the reference study. After the initial peak and short lower magnitude force area, the force fluctuates at around 30 kN up to around 50 mm displacement in the current study whereas in the reference simulation the force fluctuates between 20…30 kN in 10…50 mm displacement range. The mean load values also showed that the load in the current study was higher than in the study of Kashani et al. as the values were 27.5 kN and 25 kN, respectively. Thus *a 10% difference can be seen between the mean crush forces and energy absorptions of these two simulations.*

4. STRUCTURAL FIRE DESIGN WITH STAINLESS STEELS

Fire design is often a part of the normal design procedure in design of load bearing structures. Requirements for the fire design of stainless steels are the same as for carbon steel. The structure must have sufficient load bearing capacity for the given fire situation. Deformation criteria should be used when the fire protection or the design of the separating elements require it to be considered. When the fire design of the separating elements is carried out using standard fire curve, no deformation criteria is necessary. [3] Because the probability of a fire is low, large plastic deformation is acceptable if the overall load bearing capacity of the structure remains at a level where collapse is avoided [47].

4.1 Elevated temperature properties of stainless steel

Stainless steels have good mechanical properties in elevated temperatures. The reduction in the strength of austenitic stainless steels in temperatures above 550 °C is smaller than the corresponding reduction of the strength of carbon steels. All stainless steel grades retain higher stiffness than mild steel in all temperatures. [3, 106] If the structure can be designed without fire protection such as fire-retardant paint, the structure will have some benefits: surface treatments do not restrict the designing, maintenance costs are lower without than with fire protection, structures are easy to clean and they have good wear resistance. [49]

Emissivity of stainless steel ε_m is lower than of carbon steel and is usually taken as 0.4 like in 4th edition of Design Manual for Structural Stainless Steel [3] and EN 1993-1-2 [106], whereas 0.7 for carbon steel is used in EN 1993-1-2 [106]. Convective heat transfer coefficient α_c for stainless steel is usually taken as 25 W/m^{2}K. However, different values for these coefficients has been proposed, and for instance Gardner and Ng proposed values 0.2 and 35 W/m^{2}K for austenitic stainless steel emissivity and convective heat transfer coefficient, respectively [58]. In other study emissivity of the stainless steel Polarit 725 (austenitic EN 1.4301) was measured to be 0.21. Two different surface finishes were used, but they resulted in the same emissivity value. Two similar S355 carbon steel samples were also tested, and resultant emissivity was determined to be 0.51 and 0.56 in the first and second test, respectively. Convective heat transfer coefficient 25 W/m^{2}K was used. It was also noted that *the temperature of the stainless steel increases more slowly than of the carbon steel tube* (both tubes were RHS 80×160×4), and after 15 min standard fire the temperature difference was 90 °C. [55] These results for stainless steel emissivity are

close to the ones obtained in [58] (α_c = 0.2), although the convective heat transfer coefficient was different. In this work the values presented in Design Manual for Structural Stainless Steel [3] and Eurocode [106] (α_c = 25 W/m^{2}K and ε_m = 0.4) were used.

Mechanical properties in elevated temperatures can be obtained from isothermal (steady-state) or anisothermal (transient) testing. In isothermal testing the specimen is in constant temperature and the load is increased until the failure of the specimen. In anisothermal testing a certain load level is applied to the specimen and temperature is then increased until the specimen fails. Anisothermal testing is usually considered to give better results with respect to actual fire situations if the temperature development corresponds to real fire condition. [47, 49] In temperature over 400 °C creep strain becomes more remarkable and thus anisothermal measurements usually give smaller (stricter) reduction factors for strength and modulus of elasticity than isothermal tests. Slower heating in transient tests means more conservative values for reduction factors as the influence of creep increases with slower heating. Temperature in fire-protected carbon steel structures usually increases 5–10 °C/min in fire situation, but stainless steel is often unprotected against fire and thus the temperature rise in stainless steels can be faster than in mild steels: using reduction factors from transient tests with slow heating leads to conservative reduction factors for unprotected stainless steel members. [47] When both carbon steel and stainless steel are unprotected, the temperature rise in stainless steel is lower than in carbon steel [52]. Reduction factors obtained from steady-state and transient test may not be equivalent, which was noted for instance in [50], where stress–strain curves from these two methods were remarkably different for austenitic S30408 stainless steel in temperature range of 600–800 °C, whereas results in lower temperatures were more similar. [50].

In general, austenitic stainless steels have the best fire performance among stainless steels: lowest reductions for modulus of elasticity and strength in elevated temperatures, especially at temperatures over 700 °C, which can be seen from the reduction factors presented in [3]. Fire design of austenitic stainless steels without fire protection is possible, though the reductions in the strength and stiffness can be remarkable in 30 min fire. Depending on the cross section and slenderness of the member, the load levels (the ratio of elevated temperature and room temperature load) for austenitic EN 1.4301 and titanium stabilized EN 1.4571 for 30 min fire are 0.25–0.35 and up to over 0.40, respectively. Thus, the fire design without fire protection for 30 min fire can lead to oversized structures in normal temperatures. [86] Austenitic stainless steels have about 50% larger thermal expansion than mild steels [49] which can cause excessive loads in restrained structural members. On the other hand, the temperature increase in stainless steel sections is slower than in unprotected mild steel cross sections, and the temperature change can be assumed to be lower.

In stabilized ferritic stainless steel grades free interstitial elements are tied to stabile nitrides and carbides with stabilizing elements such as niobium and titanium. Nitrides and carbides prevent dislocation movement and cause grain boundary slipping and growth

enhancing the high temperature strength and creep resistance. The difference of the non-stabilized and stabilized ferritic grades is most significant in the temperature range above 500 °C, where the stabilized grades retain strength properties better than the non-stabilized grades. For non-stabilized ferritic stainless steel grades EN 1.4003 and EN 1.4016 the critical temperature for the steady state creep deformation is 650 °C whereas the corresponding temperature for stabilized grades EN 1.4509, 1.4521 and 1.4621 is 750 °C. When the temperature is over 600 °C, non-stabilized ferritic grades are in steady state creep condition where work hardening does not exist, and the strength rapidly decreases as the temperature increases. Ultimate strength is usually reached earlier in temperatures over 700 °C, even before 10% total strain. [87]

Reduction factors for carbon steels in elevated temperatures are given in EN 1993-1-2 [106] and new proposed reduction factors for strength, stiffness and strain of stainless steels are given in the fourth edition of Design Manual for Structural Stainless Steel [3]. It is expected that these values for stainless steels will be used in the next revision of Eurocode fire design EN 1993-1-2. Reduction factors for carbon steel and for some stainless steels according to these sources are shown in Figure 16. Reduction factor $k_{p0,2,\theta}$ is the 0.2% proof strength at temperature θ relative to the design strength f_y at room temperature and $k_{E,\theta}$ is the modulus of elasticity in temperature θ relative to the modulus of elasticity E at room temperature. [3] The figure shows that among the chosen stainless steels the decrease in strength in 500 °C is lowest for the ferritic EN 1.4003 (ferritic group II) with a reduction factor of 0.75 and carbon steel has corresponding value 0.78. Titanium stabilized austenitic stainless steel EN 1.4571 (austenitic group III) also has a low reduction in strength at 500 °C with a 0.69 reduction factor. At 700 °C the highest factor and the lowest reduction is for EN 1.4571 (AIII) with a reduction factor of 0.59, whereas the factors for carbon steel and ferritic stainless steel group II are 0.23 and 0.16, respectively. *The stiffness reduction is clearly lower for all stainless steels than for carbon steel* especially at 700 °C, where the reduction factor for modulus of elasticity is only 0.13 for carbon steel and 0.54…0.71 for stainless steels. *Overall austenitic stainless steel EN 1.4571 (in group AIII) have the best mechanical properties in elevated temperatures among the chosen grades*.

When the **effect of cold working** on the proof strength is considered, **in elevated temperatures** one should use strength reduction factors specific for the cold-worked strengths. In Design Manual for Structural Stainless Steel (2017) is proposed that the reduction factor $k_{p0,2,\theta,CF}$ for cold-worked material strength is the same as $k_{p0,2,\theta}$ in temperatures under 700 °C and $0.8 \times k_{p0,2,\theta}$ for temperatures over 700 °C [3]. Ala-Outinen (1996) showed in her study that the increased strength from cold working (relative to the base material strength) of an EN 1.4301 RHS tube remained constant up to 600 °C temperature. After that the effect of cold working decreased and completely disappeared at 900 °C. The titanium stabilized EN 1.4571 showed similar behavior with respect to the

ratio between the cold-worked strength and base material strength, though the effect of cold working remains little longer, and disappears at approximately 950 °C. [49]

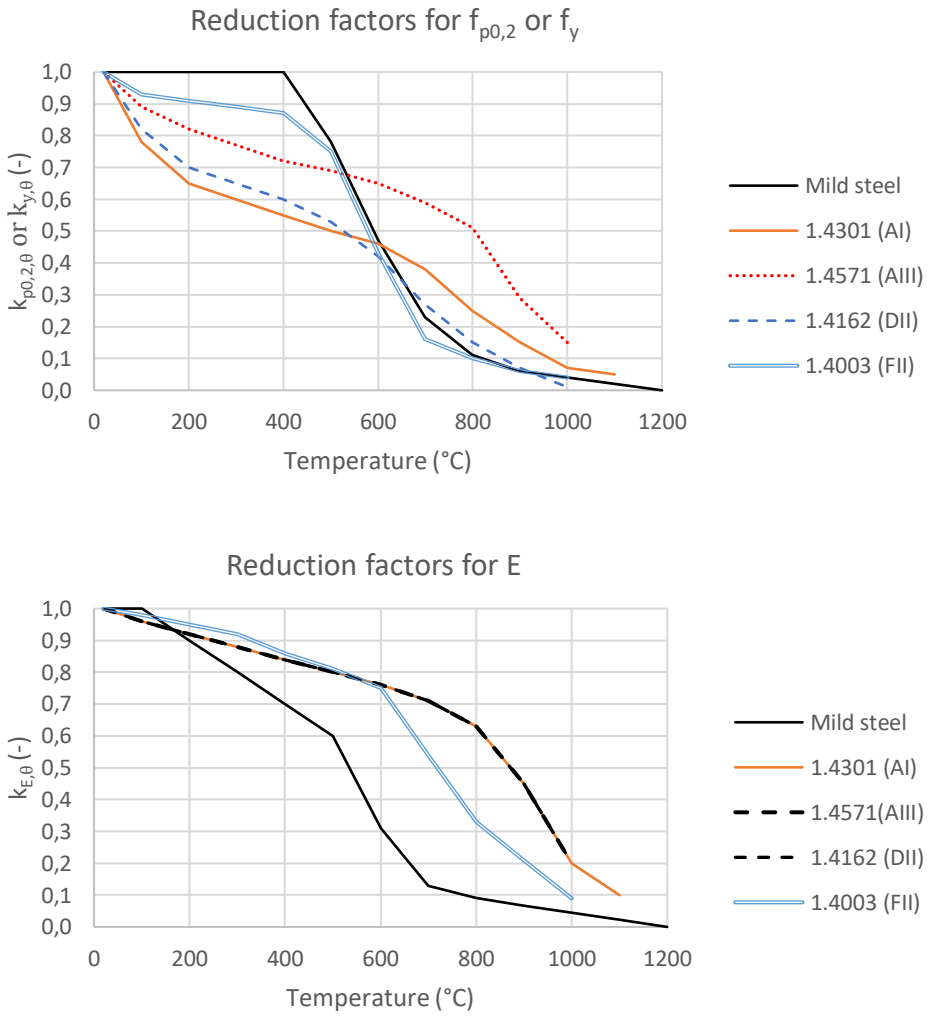

***Figure 16**. Reduction factors for carbon steel according to EN 1993-1-2 [106] and for stainless steel according to Design Manual for Structural Stainless steel [3]. Markings like (AI) for stainless steels means the group they belong in design manual.*

J. Brnic et al (2010) studied the mechanical properties and short-time creep of AISI 304 (closest EN-equivalent is EN 1.4301) in temperature range of 20 °C…700 °C [48]. Alloying element contents and measured 0.2% proof strength, ultimate strength and ultimate elongation in room temperature are given in Table 5. Also corresponding values for EN 1.4301 according to EN 10088:4-2009 [90] are shown (when given in standard). There are some differences in the alloying of the tested sample and EN 1.4301 standard values. The 0.2% proof strength of 540 MPa and 734 MPa ultimate strength satisfy the limits given in EN standard for EN 1.4301, but the 37% ultimate elongation does not fulfill the requirement of minimum 45% elongation at fracture. Because of the differences

in chemical composition and mechanical properties, the examined material does not exactly correspond to EN 1.4301. However, in the study was found that at 700 °C temperature the tensile specimen tended to creep approximately 3% in 60 min even with low stress level, which was 0.43 times the 0.2% proof strength in that temperature. With higher stress levels the creep was significantly faster, and at stress of 0.59 times the 0.2% proof strength 10% strains were reached in under 30 min. At 600 °C, stress of 0.50 times the 0.2% proof strength at 600 °C showed only minimal creep whereas with stress of 0.86 times the proof strength 10% strain was reached in just over 50 min. It was concluded that AISI 304 is not suitable to be used in 700 °C temperatures and that in lower temperatures and in appropriate stress levels the material can be used as a sufficiently creep resistant material. [48] It should be noted that these recommendations consider rather continuous use of AISI 304 in elevated temperatures than short time exposure like fire.

Table 5. *Alloying element contents (mass-%), 0.2% proof strength, ultimate strength and ultimate elongation for AISI 304 test sample used in [48] and values given in EN 10088-4:2009 [90] for EN 1.4301. The tested sample does not exactly fulfill the requirements for EN 1.4301.*

	Ni (m-%)	Mo (m-%)	V (m-%)	Cu (m-%)	Co (m-%)	$f_{0.2}$ (MPa)	f_u (MPa)	ε_t (%)
AISI 304 test sample	6.53	0.39	0.09	0.42	0.17	540	734	37
EN 1.4301 (EN 10088-4:2009)	8.0 – 10.5	-		-		230	540 – 750	45

At elevated temperatures the form of the nonlinear stress–strain curve of stainless steel retains the form of the room temperature curve [47]. To model the mechanical behavior of stainless steel in elevated temperatures, a two-stage stress–strain relation for stainless steels in elevated temperatures is given in EN 1993-1-2 [106]. It is rather complicated and includes factors with no physical meaning. To overcome these issues and to obtain more accurate predictions of the material behavior, Gardner et al. (2010) [47] proposed new stress–strain relation for elevated temperatures. This model is included in Design Manual for Structural Stainless Steel (2017) [3] with little different markings and is presented with equations (6) and (7). In equation (7) the material behavior between the 0.2% stress and ultimate stress is described with 0.2% and 2% strain, corresponding strengths and modulus of elasticity up to 0.2% strain. Another option for describing the stress–strain curve between the 0.2% and ultimate strengths is given in equation (8) where 0.2% and tensile stress are used. These equations are equivalent to the room temperature material model presented in the design manual [3].

$$\varepsilon = \frac{\sigma}{E_\theta} + 0.002\left[\frac{\sigma}{f_{p0,2,\theta}}\right]^{n_\theta} \text{ for } \sigma \leq f_{p0,2,\theta} \tag{6}$$

$$\varepsilon = \frac{\sigma - f_{p,0,2,\theta}}{E_{p,0,2,\theta}} + \left(0.02 - \varepsilon_{p0,2,\theta} - \frac{f_{2,\theta} - f_{p0,2,\theta}}{E_{p0,2,\theta}}\right) \times \left[\frac{\sigma - f_{p0,2,\theta}}{f_{2,\theta} - f_{p0,2,\theta}}\right]^{m_{\theta,2}} + \varepsilon_{p0,2,\theta} \quad \text{for } f_{p0,2,\theta} \leq \sigma \leq f_{u,\theta} \tag{7}$$

$$\varepsilon = \frac{\sigma - f_{p,0,2,\theta}}{E_{p,0,2,\theta}} + \varepsilon_{u,\theta} \left[\frac{\sigma - f_{p0,2,\theta}}{f_{u,\theta} - f_{p0,2,\theta}}\right]^{m_\theta} + \varepsilon_{p0,2,\theta} \quad \text{for } f_{p0,2,\theta} \leq \sigma \leq f_{u,\theta}, \tag{8}$$

where σ is engineering stress, ε engineering strain, E_θ modulus of elasticity at temperature θ, $f_{p0,2,\theta}$ stress at 0.2% total strain at temperature θ, $f_{2,\theta}$ stress at 2% total strain at temperature θ, $\varepsilon_{p0,2,\theta}$ total strain corresponding to $f_{p0,2,\theta}$, $E_{p0,2,\theta}$ tangent modulus at $f_{p0,2,\theta}$, $\varepsilon_{u,\theta}$ ultimate elongation at temperature θ and n_θ, m_θ and $m_{\theta,2}$ are exponents defining the material nonlinearity at temperature θ.

After-fire properties of austenitic EN 1.4301 stainless steel were studied by Wang et al. (2014). The effect of fire exposure on the after-fire mechanical properties of circular tubes and flat portions of square tubes was limited, and the room-temperature properties were discovered after up to approximately 500 °C fire. In over 500 °C fire exposure the after-fire yield strength began to decrease, and after exposing to 1000 °C fire the after-fire strength was about 80–90% from the original strength. The influence of fire on after-fire ultimate strength was insignificant (2.1% decrease after 1000 °C fire). On the other hand, fire exposure without mechanical loading had a remarkable impact on strain-hardened corners of square tubes. The post-fire yield strength of the corner area material decreased as the temperature of the fire exposure increased. After a 1000 °C fire, strain hardening effects had disappeared because dislocations had been able to recover, and martensite had transformed back to austenite. The shape of the post-fire and normal room temperature stress–strain curves were almost the same. *Compared to carbon steel, the after-fire properties of austenitic stainless steels were significantly better: the reductions in yield strength and ultimate strength were 11.0% and 2.1% for stainless steel and 21.4% and 9.8% for carbon steel, respectively.* [56]

After-fire properties of ferritic EN 1.4003 differ remarkably from the austenitic grades. The after-fire modulus of elasticity remains almost unchanged up to 1000 °C fire exposure. Yield strength experiences only slight changes when the fire temperature is below 400 °C. After 500–700 °C fire, yield strength decreases to minimum level of around 65% from the initial room temperature strength, and after higher temperature fire it rapidly increases up to level of over 160%. Post-fire ultimate strength is almost constant up to 700 °C temperature and then it quickly grows. After 850–1000 °C fire the ultimate strength is twice the initial room temperature strength. The reason for the remarkable strength increase in elevated temperatures is the formation of hard and brittle martensite. In temperature range under 400 °C after-fire ultimate elongation first decreases to 80% of the initial elongation and then increases so that at 700 °C ultimate elongation is almost 40% higher than initially. In higher temperatures formation of brittle martensite decreases the after-fire ultimate elongation to around 20% of the initial elongation. The speed of

cooling showed no significant effect on modulus of elasticity or strengths, but the after-fire ultimate elongation changes in 600–800 °C fire exposure depending on the cooling rate. The faster the cooling process is, the higher the ultimate elongation is after fire. The Ramberg–Osgood parameter also changes with respect to cooling rate in temperature range 600–700 °C. [54]

Han et al. (2013) studied the **concrete filled stainless steel tubes** (CFSST) in elevated temperatures in their paper. Full-scale compression experiments in elevated temperatures were carried out for S30408 (EN 1.4301 or AISI 304) austenitic stainless steel square and circle tubes which were filled with concrete. Square specimens were 315×315×5 with load levels (fire load–room temperature load radio) of 0.15 and 0.30, 630×630×10 with load level of 0.30 and circular specimens were 300×5 with load levels of 0.30 and 0.45. The compression load was applied to the specimen 30 min before increasing temperature. Failure criteria were maximum 0.01×H axial shortening or 0.003×H/min deformation rate, where H is the height of the specimen. The square specimen with 0.15 load level survived the maximum test time of 4 hours in fire but other specimens failed before the maximum time. In the same study a finite element model of the concrete filled column was constructed using ABAQUS software and verified against experimental data with a reasonable correspondence. The verified FE-model was used to describe the structural behavior, such as stress and strain, in detail. [79]

Three stages were recognized in the CFSST compression test in elevated temperatures. In the first stage, the stainless steel tube warmed faster than the concrete. Because of the large temperature difference between the tube and the concrete core, the stainless steel shell expanded faster than the concrete core and thus carried most of the load of the column. Because of the excess load and lengthening of the tube, the tube yielded prematurely, and tension formed into the concrete core. The concrete core gave support to the tube and to some extent maintained the load bearing capacity after the local buckling of the tube. In the second stage, the concrete core started to take most of the load as the temperature increased and steel tube started to fail. Temperature at the outer layers of the concrete was higher than in the middle, so the outer part of the concrete experienced higher elongation and higher compressive stresses and crushed first. Failure of the steel and outer part of the concrete lowered the support of the core and thus lowered its capacity. In the final stage the concrete was not able to carry the load which had been transferred from the tube to the concrete and the column failed. The results showed that there was a clear load transfer between the tube and concrete core. [79]

The study also compared finite element models of circular concrete filled carbon steel tubes (CFST) and CFSST columns with 300×5 mm cross section, 3 m length, 0.30 load level and pinned boundary conditions. *The fire resistance time for the carbon steel and stainless steel columns were 48 min and 82 min, respectively, so using unprotected stainless steel instead of unprotected carbon steel gives remarkable benefit*. The difference can be explained with that the strength and stiffness of the carbon steel decreases a lot

faster than that of the stainless steel as the temperature increases at the end stages of the fire. This led to rapid decrease in the load bearing capacity and flexural stiffness of the CFST. The temperature of the concrete also increased faster in the carbon steel than in the stainless steel column. [79] In the study austenitic EN 1.4301 equivalent stainless steel was used, but stabilized grades, especially EN 1.4571, had better mechanical properties in elevated temperatures. With such stabilized grades the fire resistance time can be expected to be even better than 82 min with non-stabilized grade.

Tao and Ghannam (2013) carried out finite element analysis with FE-software ABAQUS considering the heat transfer in concrete filled carbon and stainless steel tubes. Their FE-model was calibrated with experimental data from several different researches, with in total 107 CFST and 14 CFSST column tests. Circle and square tubes were found in both CFST and CFSST tests and also rectangular sections were used with carbon steel tubes. This study showed that *the temperatures in both concrete and steel were lower in the concrete filled stainless steel columns than in the corresponding carbon steel columns*. The reason was proposed to be the lower emissivity of the stainless steel and remarkably lower thermal conductivity in temperatures under 800 °C, when compared to mild steel. [82]

Tao et al. (2016) executed fire tests with 4 square (200×200×4) and 8 circular (200×3) concrete filled stainless steel tubes with austenitic AISI 304 steel (approximately equivalent to EN 1.4301). Both in fire and after fire properties were studied. The effects of cross section type, load level (in a range of 0.28–0.48), steel reinforcement and test type (fire resistance test and post-fire test with the initial load) were considered. In fire resistance tests, the load was first applied to the pinned-end column and then the column was heated by increasing the furnace temperature at average 40 °C/min. The temperature was kept constant until the failure of the column after reaching 800 °C furnace temperature. In case of post-fire tests with initial load, after reaching 800 °C temperature, the temperature was kept constant for approximately half of the fire resistance time of its reference column. The column was cooled by natural convection, and then axially loaded until a failure. It was noted that the results were affected by that the target temperature of 800 °C was not exactly reached with all specimen and initial measured imperfections were different for each specimen. Also, ISO 834 standard fire curve was not used in this study. A finite element model was created and verified against the experimental data. [78]

In the same study the specimen achieved high fire resistance times ranging from 122 min to 197 min where SHS columns had values of 154 min and 155 min. Fire resistance time was measured from the beginning of the heating. Columns showed same kind of failure modes in both fire resistance and post-fire tests. Local buckling was discovered at almost full length of the column in SHS cross sections after 15 minutes in fire. Global buckling was also evident. CHS columns instead experienced local buckling only at the mid-range of the column and failed by global buckling. Local buckling of CHS columns was noticed after 20 minutes in fire. [78] Fire tests with EN 1.4301 CFSST columns performed by

Ghannam et al. (2013) also showed, that *square hollow sections were more prone to local buckling than the circular hollow section columns*. All 6 columns with fire load levels 0.3 and 0.45 studied achieved fire resistance time over 2 hours. [80]

The post-fire test specimen in study of Tao et al. had a lateral residual deflection of about 1–3 mm at middle height of the column after fire, but local buckling of the tube in general was more apparent. When the post-fire test specimens were loaded after the fire, new local buckling was not developed but the ones created in fire became more severe, and lateral deflection rapidly increased after reaching the maximum load. The measured circular column capacity decreased under 4% when compared to the results of a verified FE-model in room temperature. Good post-fire properties for circular concrete filled stainless steel tubes can be explained with small local buckling in fire exposure, and thus with the support the tube gives to the concrete core after fire. The two rectangular post-fire columns, however, experienced 29% and 36% loss in capacity when compared to the room temperature strength predicted by the FE-model. Severe local buckling along the entire length of the tube decreased the strength of the tube and also decreased the support which the steel casing gave to the concrete core. [78] *According to these results it would be favorable to use circular tubes when fire situation is considered.*

4.2 Design of compressed carbon and stainless steel members

In this work mass and cost comparisons of carbon and stainless steel compressed members were carried out. The design of stainless steel members in room temperature and fire was done according to Design Manual for Structural Stainless Steel (2017) [3]. Eurocode was used for carbon steel design. The design equations used in chapters 4.3 and 4.4 are presented herein. Members from cross section classes 1, 2 and 3 are included.

4.2.1 Room temperature design of compressed carbon steel members

Room temperature design of compressed carbon steel members was done according to EN 1993-1-1 [115]. First, cross section classification of the carbon steel members in room temperature is done with equations (9).

$$\begin{aligned} &Class\ 1\ if\ \frac{c}{t} \leq 33\varepsilon \\ &Class\ 2\ if\ 33 < \frac{c}{t} \leq 38\varepsilon \\ &lass\ 3\ if\ 38 < \frac{c}{t} \leq 42\varepsilon, \end{aligned} \tag{9}$$

where c is taken as the length of the inner edge of the side (without corner fillets) and t is the thickness of the section. Factor ε is defined as $\varepsilon = \sqrt{235MPa/f_y}$. Cross section outside these classes belong to cross section class 4.

Critical load according to theory of elasticity N_{cr} (Euler buckling), is defined as

$$N_{cr} = \frac{\pi^2 EI}{L_{cr}^2}, \tag{10}$$

where E is modulus of elasticity, I is the second moment of the area and L_{cr} is critical buckling length. For members of cross section class 1, 2 and 3, slenderness $\bar{\lambda}$ is defined with equation (11).

$$\bar{\lambda} = \sqrt{\frac{Af_y}{N_{cr}}}, \tag{11}$$

where A and f_y are cross sectional area and yield strength of the member, respectively. Factor Φ is defined as

$$\Phi = 0.5\left[1 + \alpha\left(\bar{\lambda} - 0.2\right) + \bar{\lambda}^2\right], \tag{12}$$

where α is the factor of inaccuracy, and it is 0.49 for buckling curve c. Reduction factor χ is calculated as

$$\chi = \frac{1}{\Phi + \sqrt{\Phi^2 - \bar{\lambda}^2}} \leq 1. \tag{13}$$

Buckling resistance $N_{b,Rd}$ for class 1,2 and 3 members is defined as

$$N_{b,Rd} = \frac{\chi A f_y}{\gamma_{M1}}, \tag{14}$$

where partial safety factor γ_{M1} is 1.0 for carbon steel. It is ensured that the compressive design load N_{Ed} is not greater than the compression resistance of the member.

$$\frac{N_{Ed}}{N_{b,Rd}} \leq 1.0, \tag{15}$$

4.2.2 Fire design of compressed carbon steel members

Fire design of compressed carbon steel members was carried out according to EN 1993-1-2 [106]. Reduction factors for carbon steel are obtained from Table 3.1 in the aforementioned Eurocode part. Cross section classification is done in the same way as in room temperature design with equations (9), but the limits are modified:

$$\varepsilon = 0.85\sqrt{235MPa/f_y}. \tag{16}$$

Factor α is defined in fire design as

$$\alpha = 0.65\sqrt{\frac{235MPa}{f_y}}. \tag{17}$$

The non-dimensional slenderness $\bar{\lambda}_\theta$ at member temperature θ_a is obtained from

$$\bar{\lambda}_\theta = \bar{\lambda}\sqrt{\frac{k_{y,\theta}}{k_{E,\theta}}}, \tag{18}$$

where $\bar{\lambda}$ is the slenderness in room temperature, equation (11). Factors $k_{y,\theta}$ and $k_{E,\theta}$ are reduction factors for yield strength and modulus of elasticity at member temperature θ_a. Factor φ_θ is used to determine the reduction factor for flexural buckling in the fire situation, χ_{fi}.

$$\varphi_\theta = \frac{1}{2}\left[1 + \alpha\bar{\lambda}_\theta + \bar{\lambda}_\theta^2\right] \tag{19}$$

$$\chi_{fi} = \frac{1}{\varphi_\theta + \sqrt{\varphi_\theta^2 - \bar{\lambda}_\theta^2}} \tag{20}$$

The design buckling resistance at time *t* and with uniform cross section temperature θ_a is obtained from the equation below.

$$N_{b,fi,t,Rd} = \frac{\chi_{fi}Ak_{y,\theta}f_y}{\gamma_{M,fi}}. \tag{21}$$

where $k_{y,\theta}$ is the reduction factor for the yield strength at temperature θ_a. Safety factor $\gamma_{M,fi}$ is taken as 1.0 as recommended in EN 1993-1-2 [106]. Now the fire design load $N_{fi,Ed}$ can be compared to the buckling resistance.

$$\frac{N_{fi,Ed}}{N_{b,fi,t,Rd}} \leq 1.0, \tag{22}$$

Standard temperature–time curve is defined in EN 1991-1-2 [116]:

$$\theta_g = 20 + 345\log_{10}(8t + 1), \tag{23}$$

where t is time in minutes and θ_g gas temperature in degrees Celsius. Net heat flux $\dot{h}_{net}$ on the fire exposed surfaces (given in EN 1991-1-2 [116]) is calculated with equation (24).

$$\dot{h}_{net} = \dot{h}_{net,c} + \dot{h}_{net,r}\ , \tag{24}$$

where $\dot{h}_{net,c}$ is net convective heat flux and $\dot{h}_{net,r}$ net radiative heat flux, equations (25) and (26).

$$\dot{h}_{net,c} = \alpha_c(\theta_g - \theta_m), \tag{25}$$

where α_c is convection coefficient (taken as 25 W/m^{2}K), θ_g gas temperature and θ_m surface temperature of the member.

$$\dot{h}_{net,r} = \Phi\varepsilon_m\varepsilon_f\sigma[(\theta_r + 273)^4 - (\theta_m + 273)^4], \tag{26}$$

where Φ is configuration factor (taken as 1.0), ε_m is surface emissivity of the steel (taken as 0.70 for carbon steel), ε_f is emissivity of the fire (taken as 1.0), σ is Stephan–Boltzmann constant (5.67×10^{-8} W/m^{2}K^4), θ_r is effective temperature of the environment and can be taken as the gas temperature θ_g in case of fully fire engulfed members, θ_m is member surface temperature. Temperatures are given in °C units.

Specific heat of the steel c_a is computed as follows:

$$\begin{aligned}
c_a &= 425 + 0.773\theta_a - 1.69\times10^{-3}\theta_a^2 \\
&\quad + 2.22\times10^{-6}\theta_a^3 \quad for\ \ 20\,°C \leq \theta_a \leq 600\,°C \\
c_a &= 666 + \frac{13002}{738 - \theta_a} \quad for\ 600\,°C < \theta_a \leq 735\,°C \\
c_a &= 545 + \frac{17820}{\theta_a - 731} \quad for\ 735\,°C < \theta_a \leq 900\,°C \\
c_a &= 650 \quad for\ 900\,°C < \theta_a \leq 1200\,°C
\end{aligned} \tag{27}$$

where θ_a is the steel temperature.

The uniform temperature rise of the cross section $\Delta\theta_{a,t}$ is defined with equation (28).

$$\Delta\theta_{a,t} = k_{sh}\frac{A_m/V}{c_a\rho_a}\dot{h}_{net}\Delta t, \tag{28}$$

where k_{sh} is correction factor for the shadow effect and is taken here as 1.0 for SHS tubes, ρ_a is density of the steel and taken as 7850 kg/m^3 as recommended. A_m is the area exposed to fire and V volume of the member.

4.2.3 Room temperature design of compressed stainless steel members

Room temperature design of the axially compressed stainless steel members was done according to Design Manual for Structural Stainless Steel [3], where new, more accurate design rules are presented. Manual uses similar cross section classification than in Eurocode, but the limits are different.

$$\begin{aligned} &Class\ 1\ if\ \frac{c}{t} \leq 33\varepsilon \\ &Class\ 2\ if\ 33 < \frac{c}{t} \leq 35\varepsilon \\ &Class\ 3\ if\ 35 < \frac{c}{t} \leq 37\varepsilon, \end{aligned} \tag{29}$$

Parameter c is defined as $c = (h - 3t)$ or $c = (b - 3t)$, where h, b and t are the height, width and thickness of the cross section for RHS profiles. Factor ε is defined as

$$\varepsilon = \sqrt{\frac{235MPa}{f_y}\frac{E}{210GPa}}, \tag{30}$$

where f_y is the design strength (0.2% proof strength in compression). Critical load N_{cr} according to theory of elasticity is calculated as before in equation (10). Non-dimensional slenderness $\bar{\lambda}$ is also defined as in case of carbon steel in Eurocode, equation (11). Factor Φ is defined as

$$\phi = 0.5\left[1 + \alpha\left(\bar{\lambda} - \bar{\lambda}_0\right) + \bar{\lambda}^2\right], \tag{31}$$

where $\bar{\lambda}_0$ and α are obtained for cold formed rectangular hollow section from Table 6.1 in [3]. Limiting non-dimensional slenderness $\bar{\lambda}_0$ is 0.3 for austenitic and duplex RHS and 0.2 for ferritic RHS members, and α is 0.49 for all stainless steel cold formed rectangular hollow sections. Reduction factor for buckling χ is defined as

$$\chi = \frac{1}{\phi + \sqrt{\phi^2 - \bar{\lambda}^2}} \leq 1. \tag{32}$$

Buckling resistance for class 1,2 and 3 members are defined like for the carbon steel members in equation (14). Safety factor γ_{M1} is 1.1 for stainless steels in [3] and it is straightly adopted from the EN 1993-1-4 [94].

4.2.4 Fire design of compressed stainless steel members

Fire design of compressed stainless steel members is done according to [3]. Reduction factors for design strength and modulus of elasticity of stainless steel are taken from Table 8.1 in [3], where 7 reduction factor groups are presented. Cross section classification is done according to equation (33).

$$\begin{aligned} &Class\ 1\ if\ \frac{c}{t} \leq 33\varepsilon_\theta \\ &Class\ 2\ if\ 33 < \frac{c}{t} \leq 35\varepsilon_\theta \\ &Class\ 3\ if\ 35 < \frac{c}{t} \leq 37\varepsilon_\theta, \end{aligned} \tag{33}$$

where ε_θ is defined with room temperature parameter ε as

$$\varepsilon_\theta = \varepsilon \sqrt{\frac{k_{E,\theta}}{k_{y,\theta}}}. \tag{34}$$

It would be also possible to calculate ε_θ conservatively from $\varepsilon_\theta = 0.85\varepsilon$, but equation (34) is used in this work. The modified non-dimensional slenderness in elevated temperatures is defined as

$$\bar{\lambda}_\theta = \bar{\lambda} \sqrt{\frac{k_{p0.2,\theta}}{k_{E,\theta}}}, \tag{35}$$

where $k_{p0.2,\theta}$ is reduction factor for 0.2% proof strength. Factor ϕ_θ can be obtained from

$$\phi_\theta = 0.5\left[1 + \alpha\left(\bar{\lambda}_\theta - \bar{\lambda}_0\right) + \bar{\lambda}_\theta^2\right], \tag{36}$$

where α and $\bar{\lambda}_0$ are the same room temperature buckling coefficients than in room temperature design. Now the reduction factor for buckling in fire χ_{fi} can be calculated.

$$\chi_{fi} = \frac{1}{\phi_\theta + \sqrt{{\phi_\theta}^2 - {\bar{\lambda}_\theta}^2}} \leq 1 \tag{37}$$

The design buckling resistance $N_{b,fi,t,Rd}$ at time t and at uniform member temperature θ is given by equation (38).

$$N_{b,fi,t,Rd} = \frac{\chi_{fi} A k_{p0.2,\theta} f_y}{\gamma_{M,fi}}, \tag{38}$$

where $\gamma_{M,fi}$ is partial material safety factor and can be taken as 1.0 as recommended in EN 1993-1-2 [106].

The same standard temperature–time curve, defined in EN 1991-1-2 [116] and presented herein as equation (23), is used in the design manual [3]. Also, the net heat flux $\dot{h}_{net,d}$, is the same as with carbon steels in equation (24), though it is marked as $\dot{h}_{net}$ in the case of carbon steel. The net convective and radiative heat fluxes are also the same as in Eurocode for carbon steels, but design manual [3] uses θ for member temperature instead of θ_m used in Eurocode for carbon steel. The design manual [3] has only resultant emissivity ε_{res} instead of separate emissivity for fire and steel, and it can be taken as the emissivity of the steel, 0.4. This leads to the same design emissivity as proposed in EN 1993-1-2 [106] for stainless steel. It should be noted, that the design emissivity of the stainless steel (0.4) differs from the design emissivity of the carbon steel (0.7).

Specific heat c of the stainless steel is defined as

$$\begin{aligned} c &= 450 + 0.28 \times \theta - 2.91 \times 10^{-4}\theta^2 \\ &\quad + 1.34 \times 10^{-7}\theta^3 \qquad for\ austenic\ and\ duplex \\ c &= 430 + 0.26 \times \theta \qquad for\ ferritic, \end{aligned} \tag{39}$$

where θ is the uniform temperature of the steel member. The uniform temperature increase in member, $\Delta\theta_t$ is calculated for stainless steel similarly than for the carbon steel. The correction factor k_{sh} is neglected and notations for specific heat and density are different than of the carbon steel, so the form of the equation for the temperature increase $\Delta\theta_{a,t}$ in member is

$$\Delta\theta_a = \frac{A_m/V}{c\rho} \dot{h}_{net,d} \Delta t, \tag{40}$$

where the density ρ is considered to be temperature independent and can be obtained from Table 2.7 in [3] for different stainless steel grades.

4.3 Mass comparison of axially loaded members in fire design

A comparative study of unprotected carbon steel and stainless steel axially loaded members is presented in this chapter. It was assumed that the members had pinned end supports, so buckling length was the length of the member. Any loads from restricted elongation due to fire and supports are not considered. Room temperature design and fire design of carbon steel were calculated according to EN 1993-1-1 [115] and EN 1993-1-2 [106] and stainless steel according to Design Manual for Structural Stainless Steel [3],

which presents newer data for stainless steels in fire than the Eurocode. The strength values for stainless steels are obtained from strength of cold rolled strips, presented in design manual Table 2.2 [3]. These values are adopted from EN 10088-4 [90], and in case of ferritic stainless steels which have different properties in longitudinal and transverse directions, lower values from longitudinal direction are used. The calculation rules are presented in chapters 4.2.1 to 4.2.4. In total 59 commonly available (carbon steel) square hollow section profiles shown in appendix 3 were calculated with carbon steel and stainless steel and the lightest profile with utilization rates of maximum 1.0 in room temperature and fire was chosen for each material. Stalatube offers tubes with freely selectable width, height and thickness of the profile giving the stainless steel an advantage, but in this study only the general square hollow sections were used. Profiles with cross section class 4 were not taken into account. Stainless steel densities are given in table 2.7 of [3], where 7900 kg/m^3 and 8000 kg/m^3 were given for austenitic, 7700 kg/m^3 and 7800 kg/m^3 for duplex and 7700 kg/m^3 for ferritic stainless steels, depending on the grade [3]. The maximum suggested values were used for each group.

Fire reduction factor η_{fi} is defined as a ratio of the fire situation loads and room temperature ultimate limit state load, as shown in equation (41) [106]

$$\eta_{fi} = \frac{G_k + \psi_{fi} Q_{k,1}}{\gamma_G G_k + \gamma_{Q,1} Q_{k,1}}, \tag{41}$$

where values ψ_{fi} =0.30, $\gamma_G = 1.35$, $\gamma_{Q,1} = 1.50$ are used. G_k is permanent load and $Q_{k,1}$ characteristic leading variable action. For variable action factor ψ_{fi} can be either $\psi_{1,1}$ or $\psi_{2,1}$ and $\psi_{2,1}$ is recommended in EN 1991-1-2 [116]. Factor ψ_{fi}=0.30 corresponds to $\psi_{2,1}$ for imposed loads of domestic or office areas. Here three different load cases are calculated using equation (41). Load cases are shown in Table 6. Total design load was kept at 100 kN but the ratio of live load and dead load was varied so that the ratio Q_k/G_k obtained values 2.33, 1.00 and 0.43 leading to fire reduction factor values 0.35, 0.46 and 0.57, respectively. One can see that as Q_k/G_kratio increased the fire reduction parameter η_{fi} decreased. Also, if factor ψ_{fi} has larger value, the fire design load will increase while the room temperature load remains the same, and thus increasing ψ_{fi} can lead to larger sections in fire design and lower utilization rates in room temperature design.

Table 6. *Three different load cases (LC) for fire design comparison. Permanent load (G_k), variable load (Q_k), room temperature ultimate limit state (ULS) load, fire situation load and fire reduction factors are shown.*

	G_k (kN)	Q_k (kN)	ULS load (kN)	Fire load (kN)	η_{fi} (-)
LC1	30	70	145.5	51	0.35
LC2	50	50	142.5	65	0.46
LC3	70	30	139.5	79	0.57

Table 7 shows calculation results for compressed square hollow section tubes in room temperature and in 15 min standard fire. Critical buckling length was 3000 mm and load case 1 shown above (room temperature load 145.5 kN, η_{fi} = 0.35) was used. In this case stainless steels members were 21–32% lighter than S355 mild steel members. *The lightest member was achieved with ferritic EN 1.4509 (group F1) which had a mass of 8.8 kg/m whereas the mass of the mild steel member was 13.0 kg/m and thus a 32% reduction in weight was achieved when compared to S355.* Also, all the members from austenitic and duplex grades achieved masses 9.1 kg/m and 9.2 kg/m, respectively. Only for ferritic EN 1.4003 and carbon steel the fire situation was more severe than the room temperature loading, and for all other grades the utilization rate in room temperature loading was greater than in fire. It should be noted that the profile sizes have discrete dimensions, and if profile dimensions were freely selectable, utilization rates would be higher and mass would be lower for all profiles. The difference would be naturally largest for those profiles which now have the smallest utilization rates.

Table 7. *Cross sections with the lowest masses for compressive load case 1 (room temperature load 145.5 kN, η_{fi} = 0.35) in 15 min standard-curve fire. Critical buckling length was 3000 mm. Room temperature design strength f_y (0.2% proof strength for stainless steels, yield strength for carbon steel), member mass, member end temperature and utilization rates (UR) for room temperature (RT) and fire design are shown. Relative member mass with respect to S355 member mass is presented in last column. Ferritic group I steel EN 1.4509 and all austenitic and duplex stainless steels had approximately the same mass, whereas ferritic group II steel EN 1.4003 and S355 had higher mass.*

	f_y (MPa)	Cross section (mm)	Mass (kg/m)	Temperature (°C)	UR, RT (%)	UR, fire (%)	m/m_{S355} (-)
A1 (1.4301)	230	100×100×3	9.1	712.8	90	64	0.70
A2 (1.4404)	240	100×100×3	9.1	712.8	88	50	0.70
A3 (1.4571)	240	100×100×3	9.1	712.8	88	45	0.70
F1 (1.4509)	230	100×100×3	8.8	710.7	94	74	0.68
F2 (1.4003)	280	90×90×4	10.3	691.6	82	94	0.79
D1 (1.4062)	530	80×80×4	9.2	696.5	89	76	0.71
D2 (1.4162)	530	80×80×4	9.2	696.5	89	53	0.71
S355	355	110×110×4	13.0	700.1	42	96	1.00

Results for compressed columns in room temperature and 15 min standard fire with load case 2 mentioned earlier (room temperature load 142.5 kN, η_{fi} = 0.46) are shown in Table 8. It can be seen that for austenitic grades and duplex EN 1.4162 (DII group) the room temperature loading was determining, and fire design was not critical for these members. For other stainless steel grades, the difference between room temperature and fire design utilization rates ranged from 2 to 10 percentage points, but for structural mild steel the difference was even 51 percentage points – only about a third of the room temperature capacity of unprotected mild steel was used when the utilization rate in 15 min fire was 85%. *By using stainless steels, 31–45% mass reductions were obtained in this load configuration when compared to the unprotected S355 mild steel.*

Table 8. *Cross sections with the lowest masses for compressive load case 2 (room temperature load 142.5 kN, η_{fi} = 0.46) in 15 min standard-curve fire. Critical buckling length was 3000 mm. Room temperature design strength f_y (0.2% proof strength for stainless steels, yield strength for carbon steel), member mass, member end temperature and utilization rates (UR) for room temperature (RT) and standard fire loading are shown. Relative member mass with respect to S355 member mass is presented in last column. As the fire load increases the stainless steels perform better compared to mild steel, which can be seen from the cross section mass and utilization rates.*

	f_y (MPa)	Cross section (mm)	Mass (kg/m)	Temperature (°C)	UR, RT (%)	UR, fire (%)	m/m_{S355} (-)
A1 (1.4301)	230	100×100×3	9.1	712.8	88	82	0.57
A2 (1.4404)	240	100×100×3	9.1	712.8	86	64	0.57
A3 (1.4571)	240	100×100×3	9.1	712.8	86	57	0.57
F1 (1.4509)	230	100×100×3	8.8	710.7	92	94	0.55
F2 (1.4003)	280	80×80×5	11.1	667.5	88	94	0.69
D1 (1.4062)	530	80×80×4	9.2	696.5	87	97	0.58
D2 (1.4162)	530	80×80×4	9.2	696.5	87	67	0.58
S355	355	110×110×5	16.0	685.6	34	85	1.00

Table 9 presents calculation results for compressed columns in room temperature and in 15 min standard fire with load case 3 (room temperature load 139.5 kN, η_{fi} = 0.57). *In these loading conditions only stabilized austenitic grades EN 1.4401, EN 1.4571 and duplex EN 1.4162 were designed by room temperature conditions*. Room temperature ultimate limit state utilization rate was only 57% which underlines the good high-temperature mechanical properties of EN 1.4571. The lowest mass, 9.1 kg, was achieved with these two stabilized austenitic grades, but also duplex EN 1.4162 had a low mass, 9.2 kg. However, as the duplex EN 1.4162 is more expensive than austenitic grades, austenitic grades are preferable. The mass of mild steel column was 17.6 kg, and by using unprotected stainless steels instead of unprotected carbon steel 28–48% mass reduction was achieved.

Calculation results for load case 2 (room temperature load 142.5 kN, fire reduction factor η_{fi} 0.46) in room temperature and in 30 min standard fire are presented in Table 10. Room temperature dimensioning was critical only for stabilized austenitic EN 1.4571 whose utilization rates for room temperature load and fire load were 86% and 74%, respectively. The stabilized austenitic EN 1.4401 showed also good fire performance. When the mass is considered, austenitic grades and duplex EN 1.4162 (group D2) had reasonable fire resistance when unprotected. In case of duplex the reduction factor for strength is 0.15 at 800 °C temperature, and the fire performance is mainly caused by the high 0.2% proof strength. This also leads to noticeable over dimensioning in room temperature service, which can be seen from the utilization rates: 63% and 93% in room temperature and fire, respectively. The same behavior can be seen with non-stabilized austenitic EN 1.4301. Considering the high cost of austenitic and especially duplex steel, overdesign in room temperature is not desirable. Ferritic stainless steel members at these loading conditions

did not have noteworthy difference in mass compared to structural steel members, because at 800 °C the reduction factors for strength are about the same for both ferritic stainless steels and mild steel (0.10 and 0.11), but some difference can be seen in the reduction factors for modulus of elasticity which are 0.33 and 0.09, respectively. *With austenitic stainless steels 55–63% mass reductions can be obtained when compared to the S355 mild steel. As can be seen from the results, using unprotected carbon steel, ferritic stainless steel or group I duplex grades in 30 min fire is not reasonable, but stabilized austenitic grades showed good mechanical properties also in fire.*

Table 9. *Cross sections with the lowest masses for compressive load case 3 (room temperature load 139.5 kN, η_{fi} = 0.57) in 15 min standard-curve fire. Critical buckling length was 3000 mm. Room temperature design strength f_y (0.2% proof strength for stainless steels, yield strength for carbon steel), member mass, member end temperature and utilization rates for room temperature and standard fire loading are shown. Relative member mass with respect to S355 member mass is presented in last column. Only stabilized austenitic grades EN 1.4401, EN 1.4571 and duplex EN 1.4162 were designed with room temperature load. Structural steel was clearly the heaviest member.*

	f_y (MPa)	Cross section (mm)	Mass (kg/m)	Temperature (°C)	UR, RT (%)	UR, fire (%)	m/m_{S355} (-)
A1 (1.4301)	230	100×100×3	9.1	712.8	86	100	0.54
A2 (1.4404)	240	100×100×3	9.1	712.8	84	78	0.54
A3 (1.4571)	240	100×100×3	9.1	712.8	84	69	0.54
F1 (1.4509)	230	90×90×4	10.3	691.6	86	96	0.61
F2 (1.4003)	280	90×90×5	12.6	666.6	65	92	0.74
D1 (1.4062)	530	90×90×4	10.4	696.1	61	96	0.61
D2 (1.4162)	530	80×80×4	9.2	696.5	85	82	0.54
S355	355	100×100×6	17.0	667.8	35	95	1.00

Table 10. *Lowest mass cross sections for compressive load, case 2 (room temperature load 142.5 kN, fire reduction factor 0.46), in 30 min standard-curve fire. Critical buckling was length 3000 mm. Room temperature design strength f_y (0.2% proof strength for stainless steels, yield strength for carbon steel), member mass, member end temperature and utilization rates for room temperature and standard fire loading are shown. Relative member mass with respect to S355 member mass is presented in last column. Room temperature design was critical only for EN 1.4571 member.*

	f_y (MPa)	Cross section (mm)	Mass (kg/m)	Temperature (°C)	UR, RT (%)	UR, fire (%)	m/m_{S355} (-)
A1 (1.4301)	230	100×100×4	12.0	831.2	68	98	0.49
A2 (1.4404)	240	100×100×3	9.1	834.1	86	87	0.37
A3 (1.4571)	240	100×100×3	9.1	834.1	86	74	0.37
F1 (1.4509)	230	120×120×8	25.9	809.6	28	99	1.06
F2 (1.4003)	280	150×150×5	21.8	825.9	25	98	0.89
D1 (1.4062)	530	100×100×6	16.9	825.0	34	97	0.69
D2 (1.4162)	530	90×90×4	10.4	831.6	63	93	0.42
S355	355	140×140×6	24.5	823.0	18	98	1.00

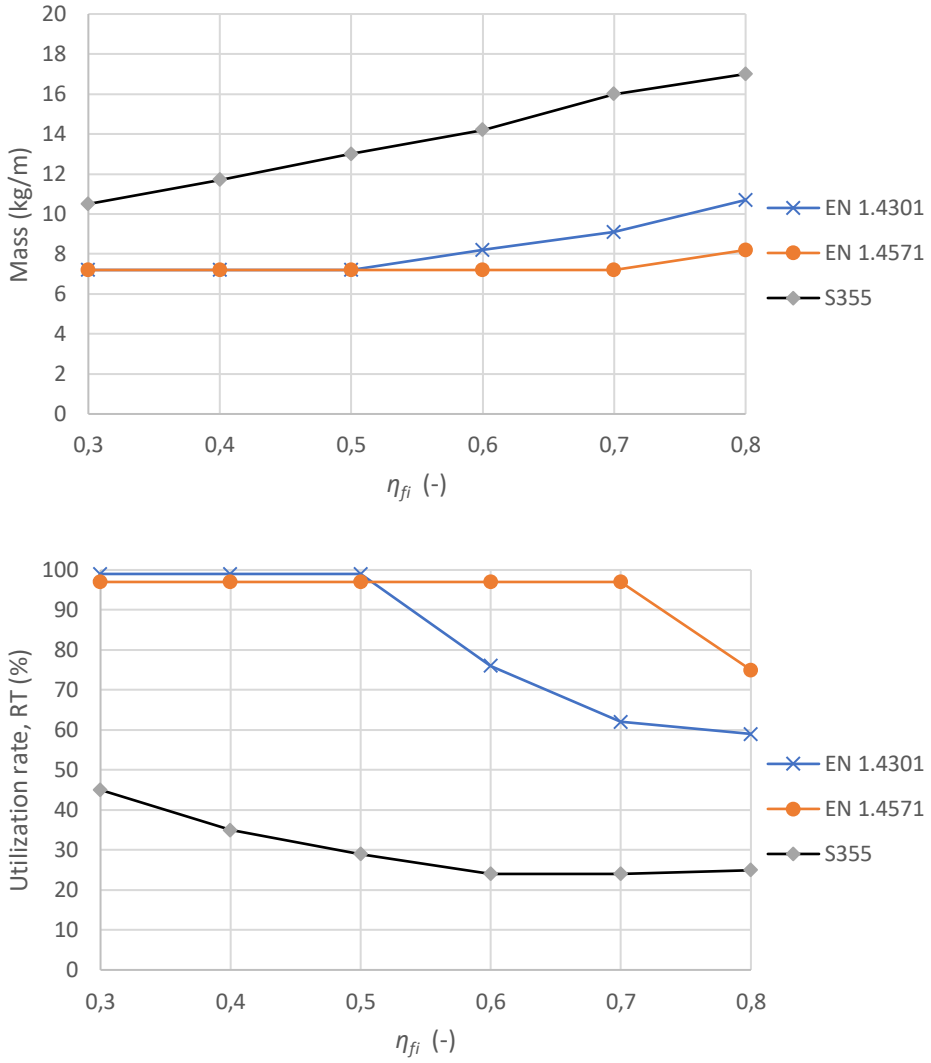

η_{fi} (ψ_{fi} = 0.3)	0.3	0.4	0.5	0.6	0.7
Q_k/G_k	3.967	1.533	0.722	0.317	0.073

Figure 17. *Mass and room temperature utilization rate as a function of fire reduction factor η_{fi}. 15 min standard fire. Fire reduction factor and corresponding live load–dead-load ratios with ψ_{fi} = 0.3 are also shown. Both mass curve and room temperature utilization curve shows that the fire design was critical for carbon steel with all fire reduction factors whereas for EN 1.4571 fire design was critical only with η_{fi} greater than 0.7. For EN 1.4301 room temperature design was critical up to fire reduction factor 0.5.*

The fire reduction factor η_{fi}, which is the ratio of total load in fire and normal room temperature ultimate limit load, is a key parameter affecting the fire design. Next a study with different fire reduction factors for axially loaded members is presented. Values 0.3, 0.4, 0.5, 0.6, 0.7, 0.8 were given for the fire reduction factor while the room temperature axial ULS load for the member was kept at 100 kN. Thus, the fire situation load was $\eta_{fi} \times$ 100 kN, ranging from 30 kN to 80 kN. The buckling length was 3000 mm, and the profile selection was the same as in previous comparisons, listed in appendix 3. Columns

were calculated in both room temperature and fire, and the profile with minimum mass with cross section class 1–3 was chosen. Austenitic basic stainless steel EN 1.4301, stabilized austenitic EN 1.4571 and mild steel S355 were chosen for this comparison. Design was accomplished according to EN 1993-1-1 [115] and EN 1993-1-2 [106] for carbon steel and according to Design Manual for Structural Stainless Steel [3] for stainless steel. Appendix 4 shows calculation assumptions and results, such as utilization rates in room temperature and fire design, in more detail.

Figure 17 shows the results for the calculation as mass and room temperature utilization rate with respect to the fire reduction factor in 15 min standard fire. The graphs show that already with $\eta_{fi} = 0.3$ mild steel was strongly dimensioned trough the fire design: the room temperature utilization ratio for the best unprotected profile in fire was only 45% and the mass was significantly higher than the mass of the austenitic stainless steel grades. It can be noted that the non-stabilized EN 1.4301 had the same mass and room temperature utilization rates with fire reduction factor values 0.3, 0.4 and 0.5 which means that *not until $\eta_{fi} = 0.6$ the fire resistance was determining the cross section of the EN 1.4301 column. In the case of stabilized EN 1.4571 the mass started to increase and room temperature utilization rate to decrease when fire reduction factor reached value 0.8, which clearly showed the good fire resistance properties of EN 1.4571.*

Similar study about the effects of the fire reduction factor on the mass and load ratio was carried out in 30 min standard fire. The results are shown in Figure 18 and appendix 5 shows the study in more detail. Austenitic EN 1.4301 and EN 1.4571 and carbon steel S355 were used also in this study. It is noted, that using unprotected structural carbon steel in 30 min fire is not common in structural design, but it is presented here as a reference for comparing the differences of carbon and stainless steels. At fire reduction factor 0.3 both EN 1.4301 and EN 1.4571 were dimensioned through room temperature ultimate limit state design. With fire reduction factors 0.354 and 0.555 the utilization rates in room temperature and fire design were the same for EN 1.4301 and EN 1.4571 members, respectively. Those values correspond to load ratios 2.26 and 0.471 (variable load–permanent load) when $\psi_{fi} = 0.3$ is used for elevated temperature load combination. It means that *in this example, EN 1.4301 and EN 1.4571 austenitic stainless steels can be used unprotected in 30 min fire without any over dimensioning in the room temperature design when the fire reduction factors are under 0.354 and 0.555* (or load ratios greater than 2.26 and 0.471 with $\psi_{fi} = 0.3$), respectively. Beyond these ranges fire design is dominant and room temperature utilization rate will decrease.

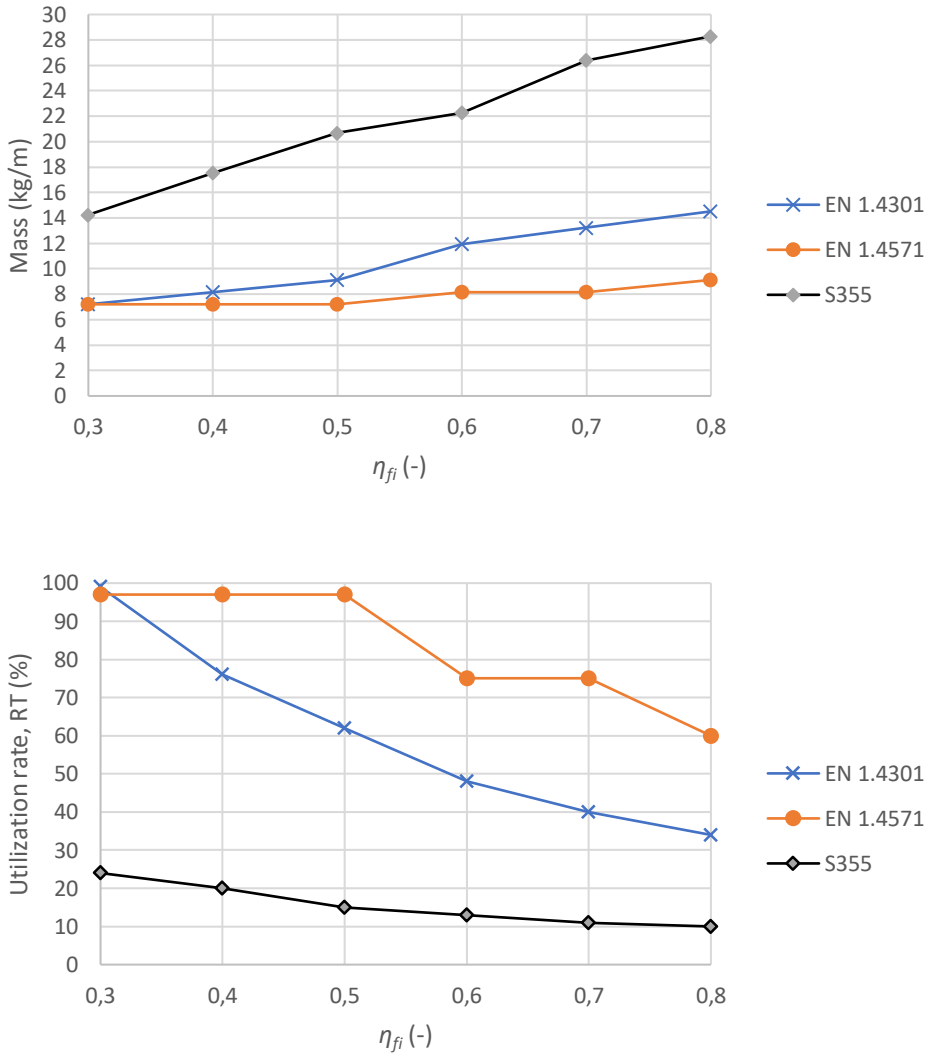

η_{fi} (ψ_{fi} = 0.3)	0.3	0.4	0.5	0.6	0.7
Q_k/G_k	3.967	1.533	0.722	0.317	0.073

Figure 18. *Lowest mass and room temperature utilization rate as a function of fire reduction factor η_{fi}. 30 min standard fire. Fire reduction factor and corresponding live load–deadload ratios with ψ_{fi} = 0.3 are also shown. Both mass curve and room temperature utilization curve shows that for EN 1.4571 fire design is critical with η_{fi} greater than 0.5. For EN 1.4301 room temperature design is critical with fire reduction factor 0.3. Structural steel would not be designed for 30 min fire without fire protection, but it is still shown here as a reference.*

4.4 Cost comparison of axially loaded members in fire design

When axially loaded stainless steel and unprotected mild steel members in fire were compared with respect to mass, stainless steels – especially austenitic grades – showed excellent fire performance. However, in practical use also the costs of the different options are usually considered. In case of mild steel, fire protection painting is often used at least in

30 min or longer fire to obtain better performance, lower mass and lower costs. In this chapter comparison of fire protected mild steel and unprotected stainless steels in 15 min and 30 min standard fire concerning total manufacturing and protection costs are shown. It was assumed in this study, that the buckling length equals to the member length, which means pinned end members. The same cross sections that were used in mass comparison, shown in appendix 3, were used also herein. S355 was chosen for the mild steel whereas austenitic EN 1.4301 and EN 1.4571 and duplex EN 1.4162 were chosen to represent stainless steels. Mild steel was designed with Eurocode [106, 115] (and fire-retardant paint data sheets) and stainless steels with Design Manual for Structural Stainless Steel [3] like in mass comparison before.

Precise information about the fire protection prices, including cleaning of the member, paint work and finishing, is difficult to obtain. Also, the price of stainless steel fluctuates and is remarkably depended on the unsteady nickel price. The volume of the steel order affects the price of the tube too, and ordering larger quantities usually lowers the price for both stainless steel and mild steel tubes. These matters affect the precision of the cost calculations. However, these comparisons are made with good faith that these values can give generic, suggestive prices and relations between unprotected stainless steel and protected mild steel prices. The exact prices are always depended on the current prices of steels, paints and labor concerning the given application. Life cycle costs including fire protection repairs are not considered, but it would give an advantage for the stainless steels as they do not need any paint repairs. Lower mass of the stainless steel is also beneficial in transportation and installation of the members, where lower weight decreases the costs. It is not considered in this work, either. Austenitic stainless steels have high value as scrap metal, so at the end of the life cycle a part of the initial costs are retrieved.

Prices 1.00 €/kg, 3.20 €/kg, 4.50 €/kg and 5.00 €/kg were used for S355, EN 1.4301, EN 1.4571 and EN 1.4162, respectively. These prices are approximated long term average market prices and they will vary by time and product type. Nullifire S707-60 intumescent coating [117] was used as a fire-retardant paint. The price of the paint was taken as 13.42 €/kg [118]. It needs a primer paint, and PM021 epoxy primer [119], recommended in S707-60 technical data sheet [117], with 170 µm wet film thickness (allowed range 100 – 300 µm) was chosen. The price of the primer in a 20 L can was 14.3 €/L (converted from 12.6 £/L) [119]. Dry paint layer is thinner than a wet paint layer, and it was taken into account in the calculations. For the Nullifire S707-60 the portion of dry elements is 72% and it is expected that this value represents the ratio of dry layer and wet layer. Loss of paint, caused by the spray missing the tube while painting, is given in [120] to be 15–40% with careful painting. In this work the loss of paints was assumed to be 25% and was considered in total costs. Necessary fire-retardant paint thickness was obtained from certified product declaration for the S707-60 paint, published by Finnish Constructional Steelwork Association [121].

Labor cost were obtained from [120], where cost structure for 30 min standard fire is given as shown in Table 11. In [120] is presented that the paints cover 60–70% of the total fire protection costs, but in this study with paint and labor costs given in Table 11 the portion of paints in total costs were 32–53%. In this work the three labor sections – cleaning and materials, paint work, finishing and protection – were assumed to have costs of 3.50 €/m^2, 9.25 €/m^2, and 4.25 €/m^2, respectively.

Table 11. *30 min fire protection cost structure according to [120] and values used in calculation examples in this work.*

	Portion of total costs (%)	Used portion of total costs (%)	Costs for 50 €/m^2 total costs (€/m^2)
Cleaning and materials	2–10	7.0	3.50
Paints	60–70	66.0	33.00
Paint work	15–20	18.5	9.25
Finishing and protection	5–10	8.5	4.25

First the results for a comparison of compressed tubes in 15 min standard fire are shown in Table 12. Critical buckling length was 3.0 m, room temperature load 100 kN and fire situation load 55 kN ($\eta_{fi} = 0.55$). Unprotected S355 with overdimensioning for elevated temperatures was also calculated. For this study, costs of one layer of primer paint for unprotected members were considered to approximate the costs of normal paint or paint against corrosion. Two cross sections were calculated for S355 members with fire protection: one with the lowest mass (80×80×3) and one with bigger section thickness and thus higher critical temperature, lower cross section factor A_m/V and thinner required paint thickness (70×70×4). In cross section factor, term A_m is the surface area subjected to fire and V is the volume of the steel. Stainless steel profiles with the lowest mass (and thus the lowest price) were chosen.

The results show that S355 with thicker cross section and fire protection had the lowest overall costs with 54.6 € and the fire-protected mild steel tube with the lightest cross section had costs very close to the most affordable one with 56.9 €. Unprotected oversized mild steel member (with one layer of primer paint) was 79% heavier and 29% more expensive than the cheapest member. *EN 1.4301 member was the cheapest among the stainless steel members with 78.4 € costs, which is 44% higher than the most economical mild steel tube but only 11.5% more expensive than the unprotected S355 member, which would be a likely option for a R15 fire design*. A second EN 1.4301 column is also shown in the results: it had an elevated temperature utilization rate just over 100% with 100.2%. With that tube the cost would have been 69.2 € and the difference to the cheapest mild steel column would be 27%.

Stabilized austenitic EN 1.4571 has excellent mechanical properties in elevated temperatures, and as the results show, the room temperature design was more severe than the fire

design meaning that all the good mechanical properties in fire were not utilized. Because of the high price of the EN 1.4571, it was not as competitive as non-stabilized EN 1.4301 when the costs were compared. The highest cost with 105.4 € was obtained from duplex EN 1.4162, which has utilization rates of 78% and 77% in fire and room temperature, respectively: room temperature and elevated temperature utilization rates were almost the same. The reduction in elevated temperatures for modulus of elasticity is the same for duplex and austenitic stainless steels, but after 700 °C temperature the reduction in 0.2% proof strength is higher for EN 1.4162 duplex (group DII) than for EN 1.4301 (group AI). High strength of EN 1.4162 makes it competitive with austenitic steels when the mass is considered but the high cost of material leads to more expensive duplex members.

Table 12. *Cost comparison of mild steel and stainless steel members in 15 min standard fire with 100 kN ULS load and 0.55 fire reduction factor. Room temperature design strength f_y (yield strength or 0.2% proof strength), cross section, utilization rates (UR) in room temperature (RT) and fire, critical temperature, required thickness of fire-retardant paint and total costs are presented. Cost of bare carbon steel tube without any paints or labor is presented in brackets. Relative cost is the member cost with respect to cost of the most affordable member. Protected S355 column with thicker cross section had the lowest costs. EN 1.4301 costs are similar to unprotected S355 column but stabilized austenitic EN 1.4571 and duplex EN 1.4062 had remarkably higher costs.*

	f_y (MPa)	Cross section (mm)	UR, RT (%)	UR, fire (%)	T_{crit} (°C)	t_{paint} (µm)	Cost (€), total/ (tube)	Relative cost (–)
S355 un-protected	355	120×120×4	24	85	-	-	70.3 (42.7)	1.29
S355 with Nullifire	355	70×70×4	86	-	546	300	54.6 (23.9)	1.00
S355 with Nullifire	355	80×80×3	77	-	565	300	56.9 (21.2)	1.04
EN 1.4301 (1)	230	90×90×3	76	82	-	-	78.4	1.44
EN 1.4301 (2)	230	80×80×3	99	100.2	-	-	69.2	1.26
EN 1.4571	240	80×80×3	97	75	-	-	97.3	1.78
EN 1.4162	530	80×80×3	78	77	-	-	105.4	1.93

Next comparison with same materials (S355 with Nullifire S707-60 fire retardant paint, unprotected EN 1.4301, EN 1.4571 and EN 1.4162) was made for compressed SHS tubes in 30 min standard fire. Critical buckling length was 3.0 m, room temperature load 100 kN and fire situation load 55 kN (η_{fi} = 0.55). The results in Table 13 show that mild steel with fire-retardant paint was again the cheapest member with 67.1 € total costs. It should be noted that if the mild steel member was first designed in room temperature design to the (mass optimum) cross section 80×80×3, the overall costs for protected member was 91.8 €. That was 37% higher than for the thicker 70×70×4 mild steel tube with

the lowest overall costs and which had 9 percentage points lower utilization rate in room temperature design.

In 30 min standard fire non-stabilized EN 1.4301 was dimensioned through fire design, and the utilization rate in normal temperature ultimate limit state was 59% meaning remarkable overdesigning in room temperature loading. The costs for EN 1.4301 member were 102.5 € which was 53% higher or 35.4 € more than for the protected mild steel tube with lowest costs. *Stabilized EN 1.4571 with better elevated temperature performance had almost equal utilization rates in room temperature and fire design with values 97% and 96%, respectively, and it was the most affordable among the chosen stainless steels.* Hence the whole mechanical load bearing capacity of EN 1.4571 was utilized in both designs. The costs for the EN 1.4571 member were 97.3 €, which was 45% higher or 30.2 € more than the mild steel tube with lowest overall costs, but only 6% higher than the overall costs of the mild steel tube with lowest mass. It means that if the mild steel tube was first purely designed in room temperature and then the necessary fire-retardant paint protection was determined for that cross section, the overall initial costs of EN 1.4571 member would be almost the same as for the protected mild steel tube. EN 1.4162 duplex member had the highest costs, 137.5 €, which was caused by the high cost of material but also by the overdesign in room temperature as the utilization rates for room temperature was only 61% whereas it was 97% for elevated temperature. If only the mass of the structure was considered, duplex member with 27.5 kg weight would be comparable with the cheapest mild steel member with 23.9 kg (without paints).

Table 13. *Cost comparison of mild steel and stainless steel members in 30 min standard fire, fire reduction factor was 0.55 and room temperature normal load 100 kN. Room temperature design strength (yield strength or 0.2% proof strength), cross section, utilization rates (UR) in room temperature (RT) and fire, critical temperature, required thickness of fire-retardant paint and total costs are presented. Cost of bare carbon steel tube without any paints or labor is presented in brackets. Relative cost is the member cost with respect to cost of the most affordable member. In 30 min fire stabilized EN 1.4571 was the most affordable stainless steel with 97.3 € costs, but S355 with fire protection with 67.1 € costs had the lowest total costs.*

	f_y (MPa)	Cross section (mm)	UR, RT (%)	UR, fire (%)	T_{crit} (°C)	t_{paint} (µm)	Cost (€), total/ (tube)	Relative cost (–)
S355 with Nullifire	355	70×70×4	86	-	546	800	67.1 (23.9)	1.00
S355 with Nullifire	355	80×80×3	77	-	565	1200	91.8 (21.2)	1.37
EN 1.4301	230	90×90×4	59	97	-	-	102.5	1.53
EN 1.4571	240	80×80×3	97	96	-	-	97.3	1.45
EN 1.4162	530	80×80×4	61	97	-	-	137.5	2.05

Table 14 presents results for members in 30 min standard fire with 3.0 m critical length but with higher 500 kN room temperature load and 275 kN elevated temperature load while keeping the fire reduction factor the same as in the two previous studies (η_{fi} = 0.55). The purpose of increasing load but keeping the load ratio the same as before was to see the effect of larger and thicker cross sections and lower cross section factors (A_m/V) to the total costs. Again, the profile with lowest mass was used for the stainless steels and hence the most affordable cross section was chosen. With this load the outer dimensions of the two different mild steel sections were the same and only the thickness was different, because smaller 110×110×6 section did not have the necessary capacity for the room temperature load. The results show that even when the outer dimensions of the mild steel tube were the same, using 1 mm thicker tube and lowering the room temperature utilization rate by 14 percentage points, the total costs were almost exactly the same with only half percent difference. Overall costs for the cheapest S355 column were 119.0 € using 120×120×5 cross section.

Table 14. *Cost comparison of mild steel and stainless steel members in 30 min standard fire, η_{fi} = 0.55 and room temperature normal load 500 kN. Room temperature design strength f_y (yield strength or 0.2% proof strength), cross section, utilization rates (UR) in room temperature (RT) and fire, critical temperature, required thickness of fire-retardant paint and total costs are presented. Cost of bare carbon steel tube without any paints or labor is presented in brackets. Relative cost is the member cost with respect to cost of the most affordable member. If only the initial costs are considered, stainless steel is remarkably more expensive than mild steel with fire protection in these example conditions.*

	f_y (MPa)	Cross section (mm)	UR, RT (%)	UR, fire (%)	T_{crit} (°C)	t_{paint} (µm)	Cost (€), total/ (tube)	Relative cost (–)
S355 with Nullifire	355	120×120×6	85	-	558	400	119.5 (62.2)	1.00
S355 with Nullifire	355	120×120×5	99	-	529	600	119.0 (52.6)	1.00
EN 1.4301	230	150×150×10	54	92	-	-	403.7	3.39
EN 1.4571	240	140×140×6	89	93	-	-	337.3	2.83
EN 1.4162	530	120×120×10	52	99	-	-	474.6	3.99

In the case of EN 1.4301 the increased load led to 150×150×10 cross section and 403.7 € costs which was 239% or 284.7 € more than for the mild steel. Room temperature and elevated temperature utilization rates were 54% and 92%, respectively. Especially the increased thickness rapidly increased the mass and the costs of the column. *EN 1.4571 costs were 337.3 € which was the lowest among stainless steels but still 183% or 218.3 € more than the total costs for the protected mild steel.* Utilization rates were about the same, 89% and 93% for room temperature and elevated temperatures, respectively. Duplex column (EN 1.4162) had the highest costs, 474.6 €, which was almost four times the

costs of the mild steel column with fire protection. Low utilization rate in room temperature means that fire design was critical and was increasing cross section dimensions, especially thickness. High material costs combined with the large 10 mm thickness and large mass were the main reasons for the high costs of duplex column. *Overall with large loads and cross sections, and with these steel, paint and labor prices, the total costs of stainless steel columns were remarkably higher than the costs of mild steel columns with fire protection.*

Table 15. *Cost comparison of mild steel and stainless steel members in 30 min standard fire with 0.40 fire reduction factor and 100 kN room temperature normal load. Room temperature design strength f_y (yield strength or 0.2% proof strength), cross section, utilization rates (UR) in room temperature (RT) and fire, critical temperature, required thickness of fire-retardant paint and total costs are presented. Cost of bare carbon steel tube without any paints or labor is presented in brackets. Relative cost is the member cost with respect to cost of the most affordable member. Austenitic EN 1.4301 was the most affordable among stainless steels with 78.4 € cost, which is only 26% more expensive than the cheapest mild steel tube and little cheaper than the mild steel tube with lowest mass.*

	f_y (MPa)	Cross section (mm)	UR, RT (%)	UR, fire (%)	T_{crit} (°C)	t_{paint} (µm)	Cost (€), total/ (tube)	Relative cost (–)
S355 with Nullifire	355	70×70×4	86	-	592	600	62.1 (23.9)	1.00
S355 with Nullifire	355	80×80×3	77	-	610	800	80.1 (21.2)	1.29
EN 1.4301	230	90×90×3	76	93	-	-	78.4	1.26
EN 1.4571	240	80×80×3	97	70	-	-	97.3	1.57
EN 1.4162	530	80×80×3	78	92	-	-	105.4	1.70

A comparison between carbon steel with fire protection and unprotected stainless steel was carried out in 30 min standard fire with lower fire reduction factor than before: 100 kN room temperature and 40 kN elevated temperature loads which led to 0.40 reduction factor. Critical buckling length remained the same, 3.0 m. Table 15 shows the results. S355 tube with fire protection and thicker cross section was the cheapest column with 62.1 € total costs. *EN 1.4301 member had cost of 78.4 € which was 26% or 16.3 € more than the total costs of the most affordable mild steel member*. It can be noted that in this example the mild steel tube with the best room temperature design utilization rate and lowest mass (80.1 €) was a bit more expensive than the EN 1.4301 member. Room temperature design was determinative for the stabilized austenitic EN 1.4571: room and elevated temperature utilization ratios were 97% and 70%, respectively, and all the good elevated temperature properties were not used in this load case. *Smaller cross section and mass were obtained with stabilized EN 1.4571 than with non-stabilized EN 1.4301, but*

the stabilized grade member was still more expensive with total costs of 97.3 €. It was 24% more than the costs of EN 1.4301 and 57% more than the total costs of the cheapest S355 member with fire protection. Duplex tube was the most expensive with cost of 105.4 € which was 70% more than the costs of the cheapest mild steel member.

Effect of buckling length on axially loaded member mass and cost was tested with unprotected S355 (with one layer of regular paint taken into account in costs), austenitic EN 1.4301 and duplex EN 1.4162. As before, structural steel design was carried out according to Eurocode [106, 115] and stainless steel design with Design Manual for Structural Stainless Steel [3] design rules. All members were loaded with 200 kN and 110 kN compression in room temperature and elevated temperature design, respectively. 15 min standard fire was used. Critical lengths of the members were 2.0 m, 3.0 m, 4.0 m, 5.0 m and 6.0 m. Masses and costs are presented per unit length so increasing member length does not increase the total costs due to the longer member, and only the effects of the increased cross section size are shown. Cross sections, masses and prices are shown in appendix 6.

Figure 19 shows masses of the members as a function of buckling length. The graph shows that austenitic EN 1.4301 and duplex EN 1.4162 had very similar masses with all tested buckling lengths, whereas the S355 members were heavier as expected. Especially at longer member lengths the absolute mass difference was more remarkable, though relatively the difference (in percentage) was smaller at longer lengths. At 2.0 m buckling length the S355 member was 86% heavier than the EN 1.4162 and at 6.0 m buckling length the difference was 54%.

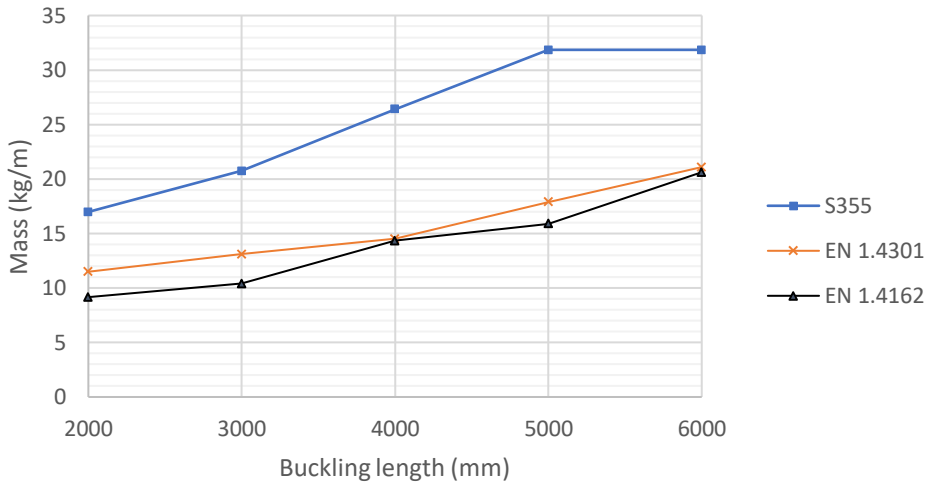

Figure 19. *Masses per unit length of axially loaded members as a function of buckling length. S355 was unprotected. Masses of stainless steel members were around the same whereas the mass of carbon steel member was significantly higher.*

Figure 20 shows the total price of the member per one meter with respect to the buckling length. Although the reduction factors of strength and stiffness were favorable for stainless steel, the costs of stainless steel increased more rapidly than the costs of carbon steel when the buckling length was increased. At 2.0 m buckling length EN 1.4162 member was 87% more expensive than S355 member, and at 6.0 m length the difference was 155%. EN 1.4301 member was 50% and 67% more expensive than the S355 member at 2.0 m and 6.0 m buckling lengths, respectively. These results suggest that as the length of axially loaded members increase while the load is kept constant, the overall costs of stainless steel members increase faster than the overall costs of the carbon steel.

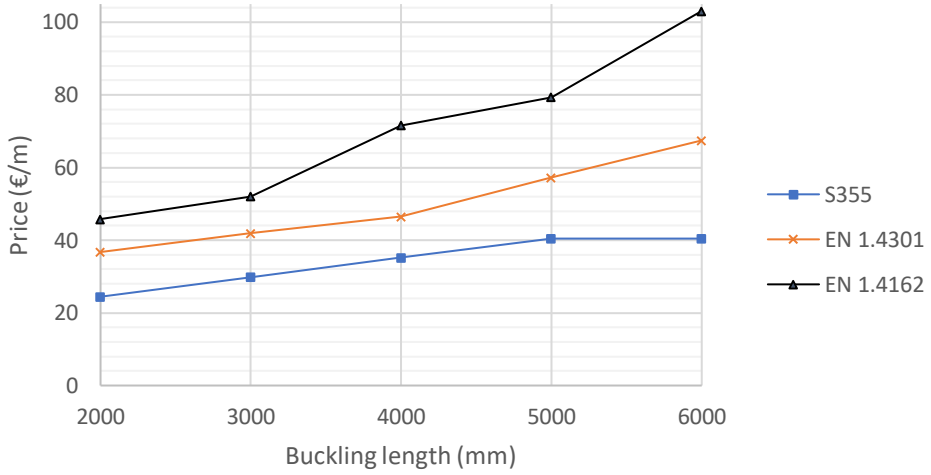

Figure 20. *Prices per unit length of axially loaded members as a function of buckling length. S355 member was unprotected (a layer of ordinary paint was taken into account in cots). Duplex EN 1.4571 with highest material cost was the most expensive and carbon steel member the most affordable.*

5. DISCUSSION

In this work the energy absorption and elevated temperature properties were studied in more detail. Here the reliability of the results and the meaning of these results are discussed.

5.1 Energy absorption

Energy absorption properties of a structural member can be described with parameters like total absorbed energy, mean crush force, peak crush force and specific energy absorption [J/kg]. For a good and smooth deceleration and energy absorption, the ratio of peak force and mean force should be as low as possible. [109] Energy absorption in general can be improved by using proper geometry, and in case of polygon, the more corners the polygon has, the better the energy absorption is. [59, 109] Stronger strain hardening stabilizes the folding behavior of the tube and increases energy absorption [109]. Strain rate sensitivity should also be considered, because materials with high strain rate sensitivity perform relatively better in dynamic loading than in quasi-static loading, compared to materials with low strain rate sensitivity [63]. Using crush initiators lowers the peak force but using different initiators can also lead to different folding behavior and different energy absorption [110]. Using bitubular structures is one way to improve the energy absorption, and if the length of the inner and outer tubes are selected properly, the peak force does not increase compared to the crush of a single outer tube [111].

In this work, finite element models of axial crush of single and bitubular square hollow section structures were set up with ANSYS AUTODYN in chapter 3.5.1. The single tube model for austenitic AISI 304 (close to EN 1.4301) tube axial crush had good agreement with the experimental data presented by DiPaolo and Tom [64]. Simulation model with second buckling mode imperfection gave 11.1% overpredictions for the mean load and thus for the energy absorption, but the initial peak force had a larger error, 25.5% overprediction. It should be noted, that crush initiators were used in the experimental tests but were not modelled in simulations. Modelling crush initiators would have lowered the peak force in the simulation. Overall, the folding behavior was very similar between the simulation model and experiments: the number of folds matched, and the folding shape was quite well predicted in the simulation. The force–displacement curve also had a good agreement with the test data.

Simulation of the axial crush of a bitubular structure was presented in chapter 3.5.2. The validation was done with experimental data gathered by Kashani et al. [111], where aluminum was used. For this reason, the material model of the aluminum was first checked with a single tube axial crush model, which had under 10% error in energy absorption.

After validating the material model with single tube model, the simulation was carried out for bitubular structures. The parallel configuration with 120 mm inner and outer tubes (P-12-12) was compared to the experimental results obtained in [111]. The comparison showed that the simulation model of this work overpredicted the energy absorption by 29% and peak force by 13%. Parallel arrangement with 110 mm and 120 mm inner and outer tubes (P-11-12) and diamond arrangement with 120 mm tubes (D-12-12) were also compared to the simulation results of [111]. The P-11-12 simulation models showed 4.1% and 30.5% differences in the peak force and energy absorption, respectively, whereas the differences between the D-12-12 models were 8.5% and 10% for peak force and energy absorption, respectively. The energy absorption from the results of this study were in all cases higher than the experimental and numerical results in [111].

It was shown that the simulation models for single aluminum or AISI 304 tubes were able to give good predictions about energy absorption in axial crush. The error in absorbed energy was around 10% in both cases. The initial peak forces had a larger difference compared to the experimental data. However, when the bitubular axial crush model was compared to the experimental data, the error in energy absorption was 29%. Because the single tube models gave remarkably better results, the interaction between the two tubes was assumed to be the main source for the excessive error. Different calculation parameters, also some that have no physical meaning, such as static damping which changes the dynamic solution to a relaxation iteration converging to a state of stress equilibrium [114], had a remarkable impact on the results of the quasi-static axial crush simulation. By calculating and varying different calculation parameters, good results from the single tube simulation models were obtained, but similar accuracy was not obtained for the bitubular simulation. It was also unclear how the correct calculation parameters should be determined if the geometry changes, for instance. For these two reasons, the 30% error in bitubular simulation model and uncertainty about the effects of calculation parameters on the results, further parametric studies were not performed as the results could not be considered to be reliable.

5.2 Fire design

Concrete filled stainless steel columns were studied in [78-80, 82]. Comparisons to concrete filled carbon steel columns were made. Austenitic stainless steel CFSST columns showed excellent elevated temperature behavior. Numerical comparison of circular hollow section concrete filled carbon steel and stainless steel columns proposed that changing the steel material from carbon steel to stainless steel without any other changes enhanced the fire resistance time from 48 min to 82 min giving 71% enhancement [79]. In [82] and [79] was found that the temperatures in both concrete and steel were lower when stainless steel tube was used. The reason for the temperature difference was the lower emissivity and thermal conductivity of the stainless steel [82]. Circular hollow sections

outperformed the square hollow sections in fire, and they were less prone to local buckling [78, 80]. Based on the results in literature, using stainless steel in concrete filled columns increases the fire resistance time. At the same time the need of maintenance during the service is significantly reduced, and the aesthetic appearance can be considered more attractive.

A comparative mass study of unprotected axially loaded mild steel and stainless steel members was carried out and presented in chapter 4.3. The study based on room temperature and fire design, EN 1993-1-1 and EN 1993-1-2 [106, 115] for carbon steel and Design Manual for Structural Stainless Steel [3] for stainless steel, showed, that stainless steels have remarkably better elevated temperature properties than mild steels. With 15 min standard fire with reduction factor of 0.35, room temperature design was determinative for all stainless steels except for ferritic EN 1.4003 (group FII) fire. With fire reduction factor of 0.46, the fire design was less severe than the room temperature design for all austenitic stainless steels and EN 1.4162 duplex steel (group DII). Only the two stabilized austenitic stainless steels from reduction factor groups AII and AIII and EN 1.4162 duplex from DII were dimensioned through the room temperature design when the reduction factor η_{fi} was 0.57. At the same time, even with the lowest fire situation load ($\eta_{fi} = 0.35$) in 15 min standard fire, the S355 column had a room temperature utilization rate of only 42% whereas the elevated temperature utilization rate was 96%. In 30 min standard fire with fire reduction factor 0.46, room temperature design was critical only for the stabilized austenitic EN 1.4571 member, which had utilization rates of 86% and 74% in room temperature and fire design, respectively. In practice, unprotected carbon steel is not commonly used for R30 fire resistance criterion, and the utilization rate in room temperature design was only 18% for the carbon steel column.

These results underline that especially the stabilized austenitic stainless steels in groups AII and AIII (EN 1.4401, EN 1.4404, EN 1.4541, EN 1.4571) and DII group duplex steels (EN 1.4462, EN 1.4162, EN 1.4662) have good fire performance compared to the mild steel in case of compressed tubes. The lower the fire design load (or fire reduction factor) is, the better the other stainless steels also perform in elevated temperatures. Based only on the mass of the structure, austenitic stainless steels and group II duplex stainless steels can be very effectively used in R15 fire design, and depending on the fire reduction factor, without any overdesign in room temperature design. With low fire reduction factors also ferritic grades and duplex grades in group DI (EN 1.4362, EN 1.4062, EN 1.4482) can be competitive. In 30 min standard fire the stabilized austenitic stainless steel EN 1.4571 (group AIII) showed excellent performance and showed no overdesign in room temperature conditions when the fire reduction factor was under 0.555 – with larger reduction factor values the fire design was ruling and increased the necessary cross section. It should be noted that the design in fire is also depended on the buckling length, for instance, and different loading and support conditions can lead to different values for critical reduction factor.

Costs of protected and unprotected mild steel and unprotected stainless steel members in fire were calculated and compared in chapter 4.4. Cost information about fire retardant paints and labor related to fire protection are difficult to obtain, but the used values were thought to be valid for a generic suggestive cost comparison. The price of the stainless steel is not stable and can cause variation in costs. Any life cycle costs like paint repairs were not considered, but it would give stainless steels an advantage, as the need for maintenance during the service is minimal. The lower weight of the stainless steel structure would also lead to savings in costs in transport and installation, but these factors are not considered in this work. When the total costs were considered, the influence of the mass of the carbon steel to the total costs was not very significant, but in the case of remarkably more expensive stainless steel any added mass greatly increased the total costs. In 15 min standard fire with 100 kN room temperature load and 0.55 fire reduction factor and buckling length of 3.0 m, S355 column without fire protection but with one layer of regular paint costed 70.3 € whereas the most affordable stainless steel member, made from EN 1.4301, costed 78.4€. If the profile sizes were freely selectable (for example with a 1 mm accuracy), the prices of the unprotected carbon steel and EN 1.4301 stainless steel columns would be even closer to each other. S355 column with increased thickness and fire protection, which had total costs of 54.6 €, was still cheaper than the unprotected mild steel or stainless steel columns. Thus in 15 min standard fire with 0.55 fire reduction factor, the most affordable stainless steel member was 12% and 44% more expensive than the unprotected and fire-protected carbon steel column, respectively.

In the comparison of axially loaded members in 30 min standard fire, unprotected carbon steel members were excluded. With 100 kN room temperature load and 0.55 fire reduction factor the most affordable column was S355 column with increased thickness with total costs of 67.1 €. The cheapest stainless steel column was stabilized EN 1.4571 column with costs of 97.3 €, though basic austenitic EN 1.4301 was not much more expensive, 102.5 €. With these results EN 1.4301 and EN 1.4571 were 45% and 53% more expensive than the S355 with fire retardant paint. Fire design increased the necessary cross section of the expensive duplex EN 1.4162 which had remarkable overdesign in room temperature. That increase was also reflected on the costs, which were 137.5 €.

When a higher 500 kN room temperature load with the same 0.55 fire reduction factor was applied to the axially loaded columns in 30 min fire, the dimensions of the tubes increased remarkably. The room temperature design was still determinative for EN 1.4571, but the low design strength (240 MPa) compared to the mild steel (355 MPa) increased the size of the cross section. Mild steel member with fire protection had total costs of 119.0 € whereas the EN 1.4571 was the most affordable stainless steel with costs of 337.3 €, and EN 1.4571 column was 183% more expensive than the S355 member with fire retardant paint. Increasing cross section size and thickness reduced the cross section factor (A_m/V) value and thus the necessary fire-retardant paint thickness. That lowers the cost of protection (per square meter). Carbon steel was cheaper than stainless steel and

increasing cross section size only moderately increased the total cost, but it had a cost-lowering effect on the fire protection. That was not the case with stainless steel, which had higher material price than carbon steel and thus the increased mass remarkably increased the overall costs.

With a 100 kN room temperature normal load and 0.40 fire reduction factor in 30 min standard fire, the fire protected carbon steel member with thicker cross section had 62.1 € total costs. Austenitic EN 1.4301 member was the most affordable among the chosen stainless steels and costed 78.4 € even though it had some overdesign in room temperature. Titanium stabilized EN 1.4571 had smaller cross section than the EN 1.4301 tube, but the higher material price leaded to larger overall costs (97.3 €). With these loading conditions, EN 1.4301 and EN 1.4571 members were 26% and 57% more expensive than the carbon steel member with fire protection, respectively.

The effect of the buckling length on the mass and the costs of an axially loaded member were also studied by varying the length of the member with pinned end supports. 200 kN room temperature and 110 kN elevated temperature loads were used and austenitic EN 1.4301, duplex EN 1.4261 and unprotected S355 (with a layer of non-protective paint) were chosen. 15 min standard fire curve was used. These results suggest that the cost of the stainless steel members increase faster than that of the mild steel as the buckling length increases. Austenitic EN 1.4301 was more affordable than the duplex EN 1.4162, but it was still 50% and 67% more expensive than the S355 column with 2.0 m and 6.0 m member lengths.

In the fire design study, the mass comparison was quite unequivocal and was done according to the design guidelines given in Eurocode [106, 115] and Design Manual for Structural Stainless Steel [3]. The results can give a realistic illustration about the differences in fire design of unprotected carbon steel and stainless steel, when these design rules are used. However, there was much more uncertainty in cost comparisons, because the prices of stainless steel strongly fluctuate with the price of nickel and exact costs of fire protection for carbon steel were difficult to obtain. Thus, the overall costs of both stainless steel and mild steel columns can vary and have different values in different real-life applications. The prices of the fire protection of the carbon steel columns were chosen so that the maximum values from the range of available cost data were never used to avoid any unfair competitive advantage for stainless steel. It is still believed, that the chosen values can give suggestive but realistic overall costs for carbon steel members with and without fire protection and for unprotected stainless steel members.

Based on the mass and the cost comparisons of the mild steel column with or without fire protection and unprotected stainless steel axially loaded columns, following suggestions are made:

1. When only the mass is considered, stainless steels in general showed better fire performance than carbon steel. Austenitic grades, especially titanium stabilized austenitic EN 1.4571, showed excellent mechanical behavior in elevated temperatures.
2. With large cross sections and high masses, the high material cost of stainless steel can lead to remarkably higher overall costs than with the fire protected carbon steel. Increasing buckling length also increases the cross section size and thus the cost difference between mild steel and stainless steel members.
3. When the overall initial costs are considered, non-stabilized austenitic stainless steel EN 1.4301 performs well in 15 min standard fire. Competitive total costs are also obtained from R30 fire design when the fire reduction factor η_{fi} is low enough, or in other words when the fire design load is low compared to the room temperature design load.
4. Stabilized austenitic EN 1.4571 performs best in 30 min fire and with higher fire reduction factor η_{fi} than that is suitable for EN 1.4301, and when the utilization rates in room temperature and fire are approximately the same for compressed members. With lower fire reduction factors the good elevated temperature mechanical properties of the expensive EN 1.4571 are not fully utilized and higher fire reduction factors lead to overdesign in room temperature. In R30 design with 100 kN fire and 0.55 fire reduction factor ($L_{cr} = 3.0\ m$) the total costs of EN 1.4571 column were 45% higher than for the protected carbon steel column.
5. Increasing the load level or fire reduction factor usually leads to thicker cross sections and lower cross section factors (A_m/V), because the volume increases faster than the surface area exposed to fire. Because stainless steel is more expensive than the mild steel and without fire protection the total costs are directly related to the cost of the steel, high thickness increases the cost of a stainless steel member remarkably. Thus, stainless steel is more competitive with thin cross sections and lower load levels. Mild steel is cheap, and the increased thickness does not have such a remarkable impact on the total costs of the structural member. Increasing only the thickness of a mild steel tube has only minimal effect on the painted area size, but it lowers the overall costs by reducing the need of fire-retardant paint.
6. Because stainless steel is remarkably more expensive than the mild steel, it is important to use the lightest tube possible. In this work the cross sections for both mild steel and stainless steel were chosen from 59 widely available mild steel square hollow section profiles. As Stalatube offers rectangular hollow section stainless steel tubes with freely selectable cross section dimensions, the utilization rates of the stainless steel tubes can be tuned close to 100% utilization rates. For instance, in case of R15 fire design study, the lowest determining utilization rate was 82% for EN 1.4301 which means that remarkable savings in costs could be achieved by choosing a proper cross section outside the common (mild steel) SHS selection. The mass of the member is not as critical for the low-price mild steel as for the more expensive stainless steel.

6. SUMMARY

This work studied the properties of ferritic, austenitic and duplex stainless steels. Stainless steels are corrosion resistant, hygienic and they have nonlinear stress–strain curve [1, 2, 88]. Low maintenance costs, 100% recyclability and good elevated temperature properties are also key factors properties of stainless steels [1]. Ferritic stainless steels are the most affordable among stainless steels but the ductility, formability, weldability and corrosion resistance are no match for the more expensive austenitic grades [88]. The modified face centered cubic grain structure gives to the austenitic stainless steel its mechanical properties: excellent ductility, cold-formability and weldability [43, 88]. Austenitic grades also have high strain hardening [88], but the initial 0.2% proof strength is usually around 220-240 MPa [90]. Duplex stainless steels have a ferritic-austenitic microstructure [88] and the 0.2% proof strength is high, normally around 450-550 MPa [90]. Duplex grades also have good corrosion and stress corrosion cracking resistance [3, 88]. Like ferritic and austenitic grades, the duplex grades cannot be strengthened by thermal treatments but can be strengthened by cold forming [88]. In this work the use of stainless steel in energy absorbing applications and high temperature design was studied in more detail.

Using stainless steel in seismic design was found to be beneficial in [77] and [74]. Using stainless steel in dissipative braces and non-dissipative columns in concentrically braced frames, the overstrength increased by 33% compared to the mild steel structure. Simultaneously the seismic shear demand was lowered up to 40–45%. Using stainless steel in non-dissipative columns and braces of eccentrically braced frames enhanced the overstrength 34% compared to the frame made from only carbon steel. Also, the base shear demand was reduced by 35–40% and up to 50% if all members were made from stainless steel. [77] In [74] a concentrically braced moment resistant frame was studied. Stainless steel was used in hourglass-shaped dissipative pins and replaceable fuse parts. Residual drifts of the proposed structure were up to 80% lower than in buckling resistant braced, concentrically braced frame. [74] In [75] has also been proposed, that the ends of the structural members could be stainless steel while the mid-sections could be mild steel. This way lower cost would be achieved, but the excellent plasticity of stainless steels could be utilized. [75]

Stainless steels have good energy absorbing properties. Austenitic AISI 304 (EN 1.4301) stainless steel was noticed to be an effective material for protecting structures from ballistic impacts, when it was compared to structural low-strength and high-strength steels [66]. In blast shields good energy absorption is necessary, and austenitic and duplex stainless steels are commonly used in corrugated walls [2] in addition to carbon steel [107]. In offshore design, the vessels and platforms are designed to absorb energy in case of collision. In case of collision of two ships, replacing carbon steel with stainless steel in inner

and outer shells of a ship, the energy absorption increased 220% compared to a ship with carbon steel shells [65]. Similarly ship collisions to offshore structures must be considered and structures designed to withstand the collision forces. In these cases energy absorbing properties of stainless steel might be beneficial also in offshore structures such as oil platforms. In marine environment the corrosion resistance of the stainless steel is also beneficial.

There are several features that affect the energy absorbing capabilities of hollow tubes in axial crush. When geometry is considered, the more corners a polygon section has, the better the energy absorption is [59, 109]. Axisymmetric folding behavior was discovered with tubes with at least 6 sides or polygon corners. Strong strain hardening stabilizes the folding behavior and can change the diamond shape folding into symmetric accordion mode. [109] Conflicting results were obtained about the effect of the thickness on the energy absorption of CHS tubes in [109] (aluminum) and [67] (AISI 304), as in the first study increasing the thickness increased the probability of the symmetric accordion mode folding, whereas in the second study increasing the thickness chanced the accordion mode to the diamond mode. [67, 109] Crashworthiness can also be enhanced with crush initiators. Using proper crush initiators lowered the peak crushing force of a SHS tube by over 50% while the total energy absorption was increased by 25% [110].

Similar effect can be achieved by using bitubular structures, which can also increase the energy absorption, while the peak force remains at the level of the outer tube peak force. Best results with SHS tubes were obtained when the outer tube was longer than the inner tube, and the tubes were placed in a diamond configuration in a 45° angle. [111] Using (aluminum) foam filling in stainless steel CHS tubes increased the crashworthiness properties in axial crush to some extent. The difference was more significant in bend loading, where the foam prevented local buckling and ovalization of a CHS tube leading to over 100% improvement in energy absorption in quasi-static bending. In material properties not only the strength and ductility should be considered in dynamic loading, but also strain rate sensitivity should be taken into account: good energy absorption in low strain rates does not ensure good properties with high strain rates. [63] Temperature can also have a remarkable effect on the energy absorption, and a 70 °C temperature change caused up to 20% change in energy absorption of carbon and stainless steels in [64].

In this work a finite element model of axial crush of SHS tubes was developed. The predictions of the single tube model was compared to the experimental results given in literature. The model was validated against AISI 304 tube crush results in [111] and results with aluminum in [64]. Both models showed rather good agreement with the experimental data when folding shape, force–displacement curve and energy absorption were considered. Approximately 10% difference in mean crush force and energy absorption was obtained for both simulations, while the error in peak force was larger. When results from a bitubular FE-model with aluminum material model was compared to the experimental data in [111], the difference in energy absorption and mean crush force was about 30%.

The increased error is assumed to be largely from the interaction behavior of the two tubes, because the single tube model had significantly better accuracy. Because of the increased difference in predictions of bitubular model compared to the experimental results and uncertainty about the effects of calculation parameters such as static damping on the results, further parametric study was not carried out.

In fire design stainless steels have some advantages compared to the mild steels. In design the emissivity of the stainless steels can be taken as 0.40 [3, 106] whereas it is 0.70 for carbon steels [106]. The reductions of the mechanical properties, strength and modulus of elasticity, in elevated temperatures are in general lower for stainless steel than for carbon steel [3, 106]. Because of these facts, stainless steels can be effectively used in fire design without fire protection. The results for axially loaded members in chapter 4 showed, that even in 30 min standard fire it is possible to use some austenitic stainless steels without any fire protection and without any overdesign in room temperature design. In cost comparison, when the life-cycle costs were not considered, the austenitic stainless steel EN 1.4301 was under 30% more expensive than the mild steel column with fire protection in conditions favorable for EN 1.4301. Titanium stabilized EN 1.4571 was about 45% more expensive than the fire protected mild steel column in conditions favorable for the concerned stainless steel. With larger loads and thicker cross sections the cost difference between the stainless steel and mild steel members with fire protection increased, and the costs of stainless steel members were remarkably higher if only the initial costs were taken into account. Stainless steels with thick cross sections were up to 200%–300% more expensive than the carbon steel. If the life-cycle costs were considered, it would benefit stainless steels, which need significantly less maintenance during the service. Lower mass of members would also lower the costs in transportation and installation.

Using stainless steel in concrete filled columns increased the load bearing capacity in both room temperature and elevated temperatures. In room temperature, the axial load resistance increased up to around 20% when stainless steel was used instead of carbon steel mainly due to the higher strain hardening of stainless steel [84]. When concrete filled carbon steel and stainless steel columns were exposed to fire, the fire resistance time of the stainless steel columns were remarkably higher. Fire resistance time of the concrete filled carbon steel and the stainless steel columns were 48 min and 82 min, respectively. [79] Temperatures were found to be lower in both concrete and steel when stainless steel was used instead of carbon steel in concrete filled columns [79, 82]. This was due to the lower emissivity and thermal conductivity of the stainless steel [82].

After-fire properties of stainless steels are good. When austenitic stainless steel EN 1.4301 was first exposed to fire without mechanical loading and then the mechanical properties were tested in room temperature, mechanical properties were almost unchanged after fire exposure up to 500 °C. After over 500 °C fire the 0.2% proof strength started to decrease and after 1000 °C fire exposure it was 80–90% from the original

strength. The influence of the fire on ultimate strength was minimal. Reductions in after-fire strength and stiffness of stainless steel were found to be around 50% and 80% lower than that of the carbon steel, respectively. [56] Ferritic EN 1.4003 had very different behavior. Up to 400 °C fire exposure, the after-fire yield strength had only slight changes. After 500–800 °C fire exposure, the yield strength was at the minimum level of around 65% from the original value. After higher temperature exposure, the yield strength increased up to over 160% from the original yield strength. Ductility of the ferritic EN 1.4003 decreased as the fire exposure temperature increased. [54]

REFERENCES

[1] K.A. Cashell, N.R. Baddoo, Ferritic stainless steels in structural applications, THIN-WALLED STRUCTURES, Vol. 83, 2014, pp. 169-181. DOI: 10.1016/j.tws.2014.03.014.

[2] N.R. Baddoo, Stainless steel in construction: A review of research, applications, challenges and opportunities, Journal of Constructional Steel Research, Vol. 64, Iss. 11, 2008, pp. 1199-1206. DOI: 10.1016/j.jcsr.2008.07.011.

[3] Design Manual for Structural Stainless Steel, 4th ed. Steel Construction Institute, 2017, ISBN: 13: 978-1-85942-226-7.

[4] B. Young, W. Lui, Behavior of Cold-Formed High Strength Stainless Steel Sections, Journal of Structural Engineering, Vol. 131, Iss. 11, 2005, pp. 1738-1745. DOI: 11(1738).

[5] J.A. Lichtenfeld, C.J. Van Tyne, M.C. Mataya, Effect of strain rate on stress-strain behavior of alloy 309 and 304L austenitic stainless steel, Metallurgical and Materials Transactions A, Vol. 37, Iss. 1, 2006, pp. 147-161. DOI: 10.1007/s11661-006-0160-5.

[6] J. Talonen, H. Hänninen, P. Nenonen, G. Pape, Effect of strain rate on the strain-induced $\gamma \rightarrow \alpha'$-martensite transformation and mechanical properties of austenitic stainless steels, Metallurgical and Materials Transactions A, Vol. 36, Iss. 2, 2005, pp. 421-432. DOI: 10.1007/s11661-005-0313-y.

[7] Effects of Strain Rate and Plastic Work on Martensitic Transformation Kinetics of Austenitic Stainless Steel 304, Journal of Iron and Steel Research, International, 2015, pp. 931-936.

[8] S. Afshan, L. Gardner, Experimental Study of Cold-Formed Ferritic Stainless Steel Hollow Sections, Journal of Structural Engineering, Vol. 139, Iss. 5, 2013, pp. 717-728. DOI: 10.1061/(ASCE)ST.1943-541X.0000580.

[9] Y.Q. Wang, T. Chang, Y.J. Shi, H.X. Yuan, L. Yang, D.F. Liao, Experimental study on the constitutive relation of austenitic stainless steel S31608 under monotonic and cyclic loading, Thin-Walled Structures, Vol. 83, 2014, pp. 19. DOI: 10.1016/j.tws.2014.01.028.

[10] H. Sieurin, R. Sandström, E.M. Westin, Fracture toughness of the lean duplex stainless steel LDX 2101, Metallurgical and Materials Transactions A, Vol. 37, Iss. 10, 2006, pp. 2975-2981. DOI: 10.1007/s11661-006-0179-7.

[11] H. LI, Z. JIANG, Z. ZHANG, B. XU, F. LIU, Mechanical Properties of Nickel Free High Nitrogen Austenitic Stainless Steels, Journal of Iron and Steel Research, International, Vol. 14, Iss. 5, Supplement 1, 2007, pp. 330-334. DOI: //doi-org.libproxy.tut.fi/10.1016/S1006-706X(08)60105-3.

[12] E. Mirambell, E. Real, On the calculation of deflections in structural stainless steel beams: an experimental and numerical investigation, Journal of Constructional Steel Research, Vol. 54, Iss. 1, 2000, pp. 109-133. DOI: //doi.org/10.1016/S0143-974X(99)00051-6.

[13] W.M. Quach, J.G. Teng, K.F. Chung, Residual stresses in press-braked stainless steel sections, I: Coiling and uncoiling of sheets, Journal of Constructional Steel Research, Vol. 65, Iss. 8, 2009, pp. 1803-1815. DOI: 10.1016/j.jcsr.2009.04.007.

[14] M. Ashraf, L. Gardner, D.A. Nethercot, Strength enhancement of the corner regions of stainless steel cross-sections, Journal of Constructional Steel Research, Vol. 61, Iss. 1, 2005, pp. 37-52. DOI: 10.1016/j.jcsr.2004.06.001.

[15] S. Afshan, B. Rossi, L. Gardner, Strength enhancements in cold-formed structural sections — Part I: Material testing, Journal of Constructional Steel Research, Vol. 83, 2013, pp. 177-188. DOI: 10.1016/j.jcsr.2012.12.008.

[16] B. Rossi, S. Afshan, L. Gardner, Strength enhancements in cold-formed structural sections — Part II: Predictive models, Journal of Constructional Steel Research, Vol. 83, 2013, pp. 189-196. DOI: 10.1016/j.jcsr.2012.12.007.

[17] R.B. Cruise, L. Gardner, Strength enhancements induced during cold forming of stainless steel sections, Journal of Constructional Steel Research, Vol. 64, Iss. 11, 2008, pp. 1310-1316. DOI: 10.1016/j.jcsr.2008.04.014.

[18] L. Gardner, M. Ashraf, Structural design for non-linear metallic materials, Engineering Structures, Vol. 28, Iss. 6, 2006, pp. 926-934. DOI: 10.1016/j.engstruct.2005.11.001.

[19] M. Milad, N. Zreiba, F. Elhalouani, C. Baradai, The effect of cold work on structure and properties of AISI 304 stainless steel, Journal of Materials Processing Tech, Vol. 203, Iss. 1, 2008, pp. 80-85. DOI: 10.1016/j.jmatprotec.2007.09.080.

[20] W.M. Quach, J.G. Teng, K.F. Chung, Three-Stage Full-Range Stress-Strain Model for Stainless Steels, Journal of Structural Engineering, Vol. 134, Iss. 9, 2008, pp. 1518-1527. DOI: 9(1518).

[21] L. Gardner, D.A. Nethercot, Experiments on stainless steel hollow sections—Part 1: Material and cross-sectional behaviour, Journal of Constructional Steel Research, Vol. 60, Iss. 9, 2004, pp. 1291-1318. DOI: 10.1016/j.jcsr.2003.11.006.

[22] K.J.R. Rasmussen, Full-range stress-strain curves for stainless steel alloys, Journal of Constructional Steel Research, Vol. 59, Iss. 1, 2003, pp. 47-61. DOI: //doi.org/10.1016/S0143-974X(02)00018-4.

[23] J. Becque, K.J.R. Rasmussen, A numerical investigation of local–overall interaction buckling of stainless steel lipped channel columns, Journal of Constructional Steel Research, Vol. 65, Iss. 8, 2009, pp. 1685-1693. DOI: 10.1016/j.jcsr.2009.04.027.

[24] O. Zhao, L. Gardner, B. Young, Buckling of ferritic stainless steel members under combined axial compression and bending, Journal of Constructional Steel Research, Vol. 117, 2016, pp. 35-48. DOI: 10.1016/j.jcsr.2015.10.003.

[25] H. Li, B. Young, Cold-formed ferritic stainless steel tubular structural members subjected to concentrated bearing loads, Engineering Structures, Vol. 145, 2017, pp. 392-405. DOI: 10.1016/j.engstruct.2017.05.022.

[26] F. Zhou, B. Young, Cold-Formed High-Strength Stainless Steel Tubular Sections Subjected to Web Crippling, Journal of Structural Engineering, Vol. 133, Iss. 3, 2007, pp. 368-377. DOI: 3(368).

[27] F. Zhou, B. Young, Cold-Formed Stainless Steel Sections Subjected to Web Crippling, Journal of Structural Engineering, Vol. 132, Iss. 1, 2006, pp. 134-144. DOI: 1(134).

[28] N. Saliba, L. Gardner, Cross-section stability of lean duplex stainless steel welded I-sections, Journal of Constructional Steel Research, Vol. 80, 2013, pp. 1-14. DOI: 10.1016/j.jcsr.2012.09.007.

[29] S.K. Paul, S. Sivaprasad, S. Dhar, S. Tarafder, Cyclic plastic deformation and cyclic hardening/softening behavior in 304LN stainless steel, Theoretical and Applied Fracture Mechanics, Vol. 54, Iss. 1, 2010, pp. 63-70. DOI: 10.1016/j.tafmec.2010.06.016.

[30] K.H. Nip, L. Gardner, A.Y. Elghazouli, Cyclic testing and numerical modelling of carbon steel and stainless steel tubular bracing members, Engineering Structures, Vol. 32, Iss. 2, 2010, pp. 424-441. DOI: 10.1016/j.engstruct.2009.10.005.

[31] F. Zhou, B. Young, Experimental and numerical investigations of cold-formed stainless steel tubular sections subjected to concentrated bearing load, Journal of Constructional Steel Research, Vol. 63, Iss. 11, 2007, pp. 1452-1466. DOI: 10.1016/j.jcsr.2006.12.007.

[32] M. Theofanous, L. Gardner, Experimental and numerical studies of lean duplex stainless steel beams, Journal of Constructional Steel Research, Vol. 66, Iss. 6, 2010, pp. 816-825. DOI: 10.1016/j.jcsr.2010.01.012.

[33] J. Becque, K.J.R. Rasmussen, Experimental investigation of local-overall interaction buckling of stainless steel lipped channel columns, Journal of Constructional Steel Research, Vol. 65, Iss. 8, 2009, pp. 1677-1684. DOI: 10.1016/j.jcsr.2009.04.025.

[34] F. Zhou, L. Li, Experimental study on hysteretic behavior of structural stainless steels under cyclic loading, Journal of Constructional Steel Research, Vol. 122, 2016, pp. 94-109. DOI: 10.1016/j.jcsr.2016.03.006.

[35] K.H. Nip, L. Gardner, C.M. Davies, A.Y. Elghazouli, Extremely low cycle fatigue tests on structural carbon steel and stainless steel, Journal of Constructional Steel Research, Vol. 66, Iss. 1, 2010, pp. 96-110. DOI: 10.1016/j.jcsr.2009.08.004.

[36] L. Yang, M. Zhao, T. Chan, F. Shang, D. Xu, Flexural buckling of welded austenitic and duplex stainless steel I-section columns, Journal of Constructional Steel Research, Vol. 122, 2016, pp. 339-353. DOI: 10.1016/j.jcsr.2016.04.007.

[37] I. Arrayago, K.J.R. Rasmussen, E. Real, Full slenderness range DSM approach for stainless steel hollow cross-sections, Journal of Constructional Steel Research, Vol. 133, 2017, pp. 156-166. DOI: //doi.org/10.1016/j.jcsr.2017.02.002.

[38] R. Greiner, M. Kettler, Interaction of bending and axial compression of stainless steel members, Journal of Constructional Steel Research, Vol. 64, Iss. 11, 2008, pp. 1217-1224. DOI: 10.1016/j.jcsr.2008.05.008.

[39] H.X. Yuan, Y.Q. Wang, L. Gardner, X.X. Du, Y.J. Shi, Local-overall interactive buckling behaviour of welded stainless steel I-section columns, Journal of Constructional Steel Research, Vol. 111, 2015, pp. 75-87. DOI: 10.1016/j.jcsr.2015.04.003.

[40] S. Ahmed, M. Ashraf, Numerical investigation on buckling resistance of stainless steel hollow members, Journal of Constructional Steel Research, Vol. 136, 2017, pp. 193-203. DOI: 10.1016/j.jcsr.2017.05.017.

[41] E. Ellobody, B. Young, Structural performance of cold-formed high strength stainless steel columns, Journal of Constructional Steel Research, Vol. 61, Iss. 12, 2005, pp. 1631-1649. DOI: 10.1016/j.jcsr.2005.05.001.

[42] M. Bock, I. Arrayago, E. Real, Experiments on cold-formed ferritic stainless steel slender sections, Journal of Constructional Steel Research, Vol. 109, 2015, pp. 13-23. DOI: 10.1016/j.jcsr.2015.02.005.

[43] M. Lecce, K.J.R. Rasmussen, Distortional Buckling of Cold-Formed Stainless Steel Sections: Experimental Investigation, Journal of Structural Engineering, Vol. 132, Iss. 4, 2006, pp. 497-504. DOI: 4(497).

[44] A. Bouchaïr, J. Averseng, A. Abidelah, Analysis of the behaviour of stainless steel bolted connections, Journal of Constructional Steel Research, Vol. 64, Iss. 11, 2008, pp. 1264-1274. DOI: 10.1016/j.jcsr.2008.07.009.

[45] E.L. Salih, L. Gardner, D.A. Nethercot, Numerical investigation of net section failure in stainless steel bolted connections, Journal of Constructional Steel Research, Vol. 66, Iss. 12, 2010, pp. 1455-1466. DOI: 10.1016/j.jcsr.2010.05.012.

[46] Y. Cai, B. Young, High temperature tests of cold-formed stainless steel double shear bolted connections, Journal of Constructional Steel Research, Vol. 104, 2015, pp. 49-63. DOI: 10.1016/j.jcsr.2014.09.015.

[47] L. Gardner, A. Insausti, K.T. Ng, M. Ashraf, Elevated temperature material properties of stainless steel alloys, Journal of Constructional Steel Research, Vol. 66, Iss. 5, 2010, pp. 634-647. DOI: 10.1016/j.jcsr.2009.12.016.

[48] Josip Brnic Ji-tai Niu Goran Turkal Marko Canadija Domagoj Lanc, Experimental determination of mechanical properties and short-time creep of AISI 304 stainless steel

at elevated temperatures, 矿物冶金与材料学报：英文版, Vol. 17, Iss. 1, 2010, pp. 39-45. DOI: 10.1007/s12613-010-0107-0.

[49] T. Ala-Outinen, Fire resistance of austenitic stainless steels. Polarit 725 (EN 1.4301) and Polarit 761 (EN 1.4571), VTT, 1996, Available (accessed 9.10.2017): http://www.vtt.fi/inf/pdf/tiedotteet/1996/T1760.pdf.

[50] S. Fan, B. He, X. Xia, H. Gui, M. Liu, Fire resistance of stainless steel beams with rectangular hollow section: Experimental investigation, Fire Safety Journal, Vol. 81, 2016, pp. 17-31. DOI: 10.1016/j.firesaf.2016.01.013.

[51] S. Fan, G. Chen, X. Xia, Z. Ding, M. Liu, Fire resistance of stainless steel beams with rectangular hollow section: Numerical investigation and design, Fire Safety Journal, Vol. 79, 2016, pp. 69-90. DOI: 10.1016/j.firesaf.2015.11.006.

[52] L. Gardner, N.R. Baddoo, Fire testing and design of stainless steel structures, Journal of Constructional Steel Research, Vol. 62, Iss. 6, 2006, pp. 532-543. DOI: 10.1016/j.jcsr.2005.09.009.

[53] E.C. To, B. Young, Performance of cold-formed stainless steel tubular columns at elevated temperatures, Engineering Structures, Vol. 30, Iss. 7, 2008, pp. 2012-2021. DOI: 10.1016/j.engstruct.2007.12.015.

[54] Y. Huang, B. Young, Post-fire behaviour of ferritic stainless steel material, Construction and Building Materials, Vol. 157, 2017, pp. 654. DOI: 10.1016/j.conbuildmat.2017.09.082.

[55] Ruostumaton teräs tulipalolle altistetuissa rakenteissa. (Stainless steel structures exposed to fire), VTT Research Notes 2112, Technical Research Centre of Finland (VTT), Espoo, 2011.

[56] X. Wang, Z. Tao, T. Song, L. Han, Stress-strain model of austenitic stainless steel after exposure to elevated temperatures, Journal of Constructional Steel Research, Vol. 99, 2014, pp. 129-139. DOI: 10.1016/j.jcsr.2014.04.020.

[57] Y. Huang, B. Young, Stress–strain relationship of cold-formed lean duplex stainless steel at elevated temperatures, Journal of Constructional Steel Research, Vol. 92, 2014, pp. 103-113. DOI: 10.1016/j.jcsr.2013.09.007.

[58] L. Gardner, K.T. Ng, Temperature development in structural stainless steel sections exposed to fire, Fire Safety Journal, Vol. 41, Iss. 3, 2006, pp. 185-203. DOI: 10.1016/j.firesaf.2005.11.009.

[59] K. Vinayagar, A. Senthil Kumar, Crashworthiness analysis of double section bitubular thin-walled structures, Thin-Walled Structures, Vol. 112, 2017, pp. 184-193. DOI: 10.1016/j.tws.2016.12.008.

[60] G.S. Langdon, G.K. Schleyer, Deformation and failure of profiled stainless steel blast wall panels. Part III: finite element simulations and overall summary, International

Journal of Impact Engineering, Vol. 32, Iss. 6, 2006, pp. 988-1012. DOI: 10.1016/j.ijimpeng.2004.08.002.

[61] L.A. Louca, J.W. Boh, Y.S. Choo, Design and analysis of stainless steel profiled blast barriers, Journal of Constructional Steel Research, Vol. 60, Iss. 12, 2004, pp. 1699-1723. DOI: //doi.org/10.1016/j.jcsr.2004.04.005.

[62] B. Bhav Singh, K. Sivakumar, T. Balakrishna Bhat, Effect of cold rolling on mechanical properties and ballistic performance of nitrogen-alloyed austenitic steels, International Journal of Impact Engineering, Vol. 36, Iss. 4, 2009, pp. 611-620. DOI: 10.1016/j.ijimpeng.2008.07.082.

[63] J. Talonen, H. Hänninen, Effect of tensile properties on the energy-absorbing capacity of weld-bonded austenitic stainless steel profiles, International Journal of Crashworthiness, Vol. 11, Iss. 4, 2006, pp. 371-378. DOI: 10.1533/ijcr.2005.0112.

[64] B.P. DiPaolo, J.G. Tom, Effects of ambient temperature on a quasi-static axial-crush configuration response of thin-wall, steel box components, Thin-Walled Structures, Vol. 47, Iss. 8, 2009, pp. 984-997. DOI: 10.1016/j.tws.2009.01.007.

[65] E. Lehmann, J. Peschmann, Energy absorption by the steel structure of ships in the event of collisions, Marine Structures, Vol. 15, Iss. 4, 2002, pp. 429-441. DOI: //doi.org/10.1016/S0951-8339(02)00011-4.

[66] J.A. Rodríguez-Martínez, A. Rusinek, R. Pesci, Experimental survey on the behaviour of AISI 304 steel sheets subjected to perforation, Thin-Walled Structures, Vol. 48, Iss. 12, 2010, pp. 966-978. DOI: 10.1016/j.tws.2010.07.005.

[67] M. Taherishargh, M. Vesenjak, I.V. Belova, L. Krstulović-Opara, G.E. Murch, T. Fiedler, In situ manufacturing and mechanical properties of syntactic foam filled tubes, Materials & Design, Vol. 99, 2016, pp. 356-368. DOI: 10.1016/j.matdes.2016.03.077.

[68] G.S. Langdon, G.K. Schleyer, Inelastic deformation and failure of profiled stainless steel blast wall panels. Part I: experimental investigations, International Journal of Impact Engineering, Vol. 31, Iss. 4, 2005, pp. 341-369. DOI: //doi.org/10.1016/j.ijimpeng.2003.12.002.

[69] G.S. Langdon, G.K. Schleyer, Inelastic deformation and failure of profiled stainless steel blast wall panels. Part II: analytical modelling considerations, International Journal of Impact Engineering, Vol. 31, Iss. 4, 2005, pp. 371-399. DOI: //doi.org/10.1016/j.ijimpeng.2003.12.011.

[70] H. Berns, S. Riedner, V. Gavriljuk, Y. Petrov, A. Weihrauch, Microstructural changes in high interstitial stainless austenitic steels due to ballistic impact, Materials Science & Engineering A, Vol. 528, Iss. 13, 2011, pp. 4669-4675. DOI: 10.1016/j.msea.2011.02.062.

[71] S.S. Hsu, N. Jones, Quasi-static and dynamic axial crushing of thin-walled circular stainless steel, mild steel and aluminium alloy tubes, International Journal of Crashworthiness, Vol. 9, Iss. 2, 2004, pp. 195-217. DOI: 10.1533/ijcr.2004.0282.

[72] B.P. DiPaolo, P.J.M. Monteiro, R. Gronsky, Quasi-static axial crush response of a thin-wall, stainless steel box component, International Journal of Solids and Structures, Vol. 41, Iss. 14, 2004, pp. 3707-3733. DOI: 10.1016/j.ijsolstr.2004.02.031.

[73] A.M. Remennikov, S.Y. Kong, B. Uy, Response of Foam- and Concrete-Filled Square Steel Tubes under Low-Velocity Impact Loading, Journal of Performance of Constructed Facilities, Vol. 25, Iss. 5, 2011, pp. 373-381. DOI: 10.1061/(ASCE)CF.1943-5509.0000175.

[74] M. Baiguera, G. Vasdravellis, T.L. Karavasilis, Dual seismic-resistant steel frame with high post-yield stiffness energy-dissipative braces for residual drift reduction, Journal of Constructional Steel Research, Vol. 122, 2016, pp. 198-212. DOI: 10.1016/j.jcsr.2016.03.019.

[75] A.J. Toset, Seismic design of stainless steel structures, Universitat Politècnica de Catalunya, 2014, Available (accessed 7.9.2017): http://upcommons.upc.edu/bitstream/handle/2099.1/23599/TESINA.pdf?sequence=1.

[76] L. Di Sarno, A.S. Elnashai, D.A. Nethercot, Seismic performance assessment of stainless steel frames, Journal of Constructional Steel Research, Vol. 59, Iss. 10, 2003, pp. 1289-1319. DOI: 10.1016/S0143-974X(03)00067-1.

[77] L. DiSarno, A.S. Elnashai, D.A. Nethercot, Seismic response of stainless steel braced frames, Journal of Constructional Steel Research, Vol. 64, Iss. 7, 2008, pp. 914-925. DOI: 10.1016/j.jcsr.2008.01.027.

[78] Z. Tao, M. Ghannam, T. Song, L. Han, Experimental and numerical investigation of concrete-filled stainless steel columns exposed to fire, Journal of Constructional Steel Research, Vol. 118, 2016, pp. 120-134. DOI: 10.1016/j.jcsr.2015.11.003.

[79] L. Han, F. Chen, F. Liao, Z. Tao, B. Uy, Fire performance of concrete filled stainless steel tubular columns, Engineering Structures, Vol. 56, 2013, pp. 165-181. DOI: 10.1016/j.engstruct.2013.05.005.

[80] M. Ghannam, Z. Tao, T.Y. Song, Fire Resistance Tests of Concrete-Filled Stainless Steel Tubular Columns, Composite Construction in Steel and Concrete VII - Proceedings of the 2013 International Conference on Composite Construction in Steel and Concrete, pp. 468-478.

[81] Y. Chen, K. Wang, L. Wang, R. Feng, K. He, Flexural behaviour of concrete-filled stainless steel CHS subjected to static loading, Journal of Constructional Steel Research, Vol. 139, 2017, pp. 30-43. DOI: 10.1016/j.jcsr.2017.09.009.

[82] Z. Tao, M. Ghannam, Heat transfer in concrete-filled carbon and stainless steel tubes exposed to fire, Fire Safety Journal, Vol. 61, 2013, pp. 1-11. DOI: 10.1016/j.firesaf.2013.07.004.

[83] V.I. Patel, Q.Q. Liang, M.N.S. Hadi, Nonlinear analysis of axially loaded circular concrete-filled stainless steel tubular short columns, Journal of Constructional Steel Research, Vol. 101, 2014, pp. 9-18. DOI: //doi.org/10.1016/j.jcsr.2014.04.036.

[84] Z. Tao, B. Uy, F. Liao, L. Han, Nonlinear analysis of concrete-filled square stainless steel stub columns under axial compression, Journal of Constructional Steel Research, Vol. 67, Iss. 11, 2011, pp. 1719-1732. DOI: 10.1016/j.jcsr.2011.04.012.

[85] M. Yousuf, B. Uy, Z. Tao, A. Remennikov, J.Y.R. Liew, Transverse impact resistance of hollow and concrete filled stainless steel columns, Journal of Constructional Steel Research, Vol. 82, 2013, pp. 177-189. DOI: //doi.org/10.1016/j.jcsr.2013.01.005.

[86] J. Kouhi, A. Talja, P. Salmi, T. Ala-Outinen, Current R&D work on the use of stainless steel in construction in Finland, Journal of Constructional Steel Research, Vol. 54, Iss. 1, 2000, pp. 31-50. DOI: 10.1016/S0143-974X(99)00054-1.

[87] Structural Applications of Ferritic Stainless Steels SAFSS (final report), European comission, 2013, Available (accessed 25.10.2017): http://www.steel-stainless.org/media/1221/safss-finalreport.pdf.

[88] N.R. Baddoo, B.A. Burgan, Structural Design of Stainless Steel, The Steel Construction Institute, Ascot, Berkshire, 2001, ISBN: 1 85942 116 4.

[89] G. Gedge, Structural uses of stainless steel — buildings and civil engineering, Journal of Constructional Steel Research, Vol. 64, Iss. 11, 2008, pp. 1194-1198. DOI: 10.1016/j.jcsr.2008.05.006.

[90] Stainless steels. Part 4: Technical delivery conditions for sheet/plate and strip of corrosion resisting steels for construction purposes. (EN 10088-4:2009), Finnish Standards Association SFS, 2009, https://www.sfs.fi/.

[91] Outokumpu Core range, Outokumpu, web page. Available (accessed 11.1.2018): http://www.outokumpu.com/en/products-properties/outokumpu-classic-family/core-range/Pages/default.aspx.

[92] Outokumpu Forta range, Outokumpu, web page. Available (accessed 15.3.2018): http://www.outokumpu.com/en/products-properties/outokumpu-pro-family/forta-range/Pages/default.aspx.

[93] P. Pohjanne, L. Carpén, T. Hakkarainen, P. Kinnunen, A method to predict pitting corrosion of stainless steels in evaporative conditions, Journal of Constructional Steel Research, Vol. 64, Iss. 11, 2008, pp. 1325-1331. DOI: 10.1016/j.jcsr.2008.07.001.

[94] Eurocode 3. Design of steel structures. Part 1-4: General rules. Supplementary rules for stainless steels, Finnish Standards Association SFS, 2006, www.sfs.fi.

[95] E. Real, E. Mirambell, Discussion of "Full-range stress-strain curves for stainless steel alloys" [Journal of Constructional Steel Research 2003;59:47-61], Journal of Constructional Steel Research, Vol. 59, Iss. 10, 2003, pp. 1321-1323. DOI: //doi.org/10.1016/S0143-974X(03)00081-6.

[96] K.J.R. Rasmussen, Reply to: Discussion of Full-range stress-strain curves for stainless steel alloys [Journal of Constructional Steel Research 2003;59:47-61], Journal of

Constructional Steel Research, Vol. 59, Iss. 10, 2003, pp. 1325-1326. DOI: 10.1016/S0143-974X(03)00082-8.

[97] K.J.R. Rasmussen, T. Burns, P. Bezkorovainy, M.R. Bambach, Numerical modelling of stainless steel plates in compression, Journal of Constructional Steel Research, Vol. 59, Iss. 11, 2003, pp. 1345-1362. DOI: 10.1016/S0143-974X(03)00086-5.

[98] M. Ashraf, L. Gardner, D.A. Nethercot, Finite element modelling of structural stainless steel cross-sections, Thin-Walled Structures, Vol. 44, Iss. 10, 2007, pp. 1048-1062. DOI: 10.1016/j.tws.2006.10.010.

[99] Specification for the design of cold-formed stainless steel structural members, SEI/ASCE-8. American Society of Civil Engineers (ASCE), Reston (VA), 2002.

[100] Cold-formed stainless steel structures, AS/NZS4673, Standards Australia, Sydney, 2001.

[101] M. Sarkari Khorrami, M.A. Mostafaei, H. Pouraliakbar, A.H. Kokabi, Study on microstructure and mechanical characteristics of low-carbon steel and ferritic stainless steel joints, Materials Science & Engineering A, Vol. 608, 2014, pp. 35-45. DOI: 10.1016/j.msea.2014.04.065.

[102] M.A. Hadianfard, R. Razani, Effects of semi-rigid behavior of connections in the reliability of steel frames, Structural Safety, Vol. 25, Iss. 2, 2003, pp. 123-138. DOI: //doi.org/10.1016/S0167-4730(02)00046-2.

[103] K. Abdella, R.A. Thannon, A.I. Mehri, F.A. Alshaikh, Inversion of three-stage stress-strain relation for stainless steel in tension and compression, Journal of Constructional Steel Research, Vol. 67, Iss. 5, 2011, pp. 826-832. DOI: //doi.org/10.1016/j.jcsr.2010.12.011.

[104] Eurocode 4: Design of composite steel and concrete structures. Part 1-1: General rules and rules for buildings, Finnish Standards Association SFS, www.sfs.fi.

[105] Q.Q. Liang, S. Fragomeni, Nonlinear analysis of circular concrete-filled steel tubular short columns under axial loading, Journal of Constructional Steel Research, Vol. 65, Iss. 12, 2009, pp. 2186-2196. DOI: //doi.org/10.1016/j.jcsr.2009.06.015.

[106] Eurocode 3: Design of steel structures. Part 1-2: Structural fire design, Finnish Standards Association (SFS), 2005, https://www.sfs.fi/.

[107] Steel Structures In Offshore Applications (presentation), Hämeenlinna University of Applied Sciences, 2018.

[108] M. Storheim, J. Amdahl, Design of offshore structures against accidental ship collisions, Marine Structures, Vol. 37, 2014, pp. 135-172. DOI: //doi.org/10.1016/j.marstruc.2014.03.002.

[109] M. Yamashita, M. Gotoh, Y. Sawairi, Axial crush of hollow cylindrical structures with various polygonal cross-sections: Numerical simulation and experiment, Journal of

Materials Processing Technology, Vol. 140, Iss. 1-3, 2003, pp. 59-64. DOI: 10.1016/S0924-0136(03)00821-5.

[110] I. Eren, Y. Gür, Z. Aksoy, Finite element analysis of collapse of front side rails with new types of crush initiators, International Journal of Automotive Technology, Vol. 10, Iss. 4, 2009, pp. 451-457. DOI: 10.1007/s12239-009-0051-z.

[111] M. Haghi Kashani, H. Shahsavari Alavijeh, H. Akbarshahi, M. Shakeri, Bitubular square tubes with different arrangements under quasi-static axial compression loading, Materials & Design, Vol. 51, 2013, pp. 1095-1103. DOI: 10.1016/j.matdes.2013.04.084.

[112] A. Reyes, O.S. Hopperstad, M. Langseth, Aluminum foam-filled extrusions subjected to oblique loading: experimental and numerical study, International Journal of Solids and Structures, Vol. 41, Iss. 5, 2004, pp. 1645-1675. DOI: //doi.org/10.1016/j.ijsolstr.2003.09.053.

[113] A. Ghamarian, M. Tahaye Abadi, Axial crushing analysis of end-capped circular tubes, Thin-Walled Structures, Vol. 49, Iss. 6, 2011, pp. 743-752. DOI: //doi.org/10.1016/j.tws.2011.01.006.

[114] ANSYS Workbench 19.0 Manual, ANSYS Inc., web page. Available (accessed 23.5.2018): https://ansyshelp.ansys.com/account/secured?returnurl=/Views/Secured/corp/v190/wb2_help/wb2h_getstarted.html.

[115] Eurocode 3: Design of steel structures. Part 1-1: General rules and rules for buildings, Finnis Standards Association SFS, 2005, https://www.sfs.fi/.

[116] Eurocode 1: Actions on structures. Part 1-2: General actions. Actions on structures exposed to fire, Finnish Standards Association SFS, 2003, https://www.sfs.fi/.

[117] Nullifire S707-60HF, tremco illbruck, web page. Available (accessed 15.5.2018): https://www.nullifire.com/en_GB/products/product-finder/product/s707-water-based-intumescent-basecoat-60/.

[118] J. Johansson, Teräsrakenteiden palosuojausmenetelmien kustannusvertailu, Metropolia University of Applied Sciences, 2013.

[119] Nullifire PM021 General Purpose Epoxy Primer, Tremco illbruck, web page. Available (accessed 16.5.2018): https://www.rawlinspaints.com/home/metal-paints/metal-primers-and-undercoats/2242-nullifire-pm021-general-purpose-epoxy-primer.html.

[120] J. Salokangas, A. Roininen, Teräsrakentamisen kustannukset (Costs of steel construction), course material, 2010.

[121] NULLIFIRE S707-60-palosuojamaali putki- ja I-profiilien sekä WQ-palkkien alalaipan palosuojaamiseen (NULLIFIRE S707-60 fire-retardant paint for protecting tube and I-profiles and lower flange of WQ-beams), certified product declaration, Helsinki, Finland, Finnish Constructional Steelwork Association, 2012.

APPENDIX 1: MATERIAL MODEL IN SIMULATION MODEL VALIDATION, AISI 304 / EN 1.4301

Modelling of material behaviour, Design manual for stainless steel, 4th edition [3]

Material properties from the test

$f_y := 449MPa$ $f_u := 706MPa$ Yield (0.2 % proof) and ultimate strengths

$\varepsilon_u := 0.5$ Young's modulus and ultimate elongation

$n := 7$ Table 6.4, n=7 for austenitic stainless steels

$E := 200GPa$

$$E_y := \frac{E}{1 + 0.002 \cdot n \cdot \frac{E}{f_y}}$$

$$m\_ := 1 + 2.8 \cdot \frac{f_y}{f_u}$$

$$\varepsilon(\sigma) := \begin{cases} \frac{\sigma}{E} + 0.002\left(\frac{\sigma}{f_y}\right)^n & \text{if } \sigma \le f_y \\ 0.005 + \frac{f_y}{E} + \frac{\sigma - f_y}{E_y} + \varepsilon_u \cdot \left(\frac{\sigma - f_y}{f_u - f_y}\right)^{m\_} & \text{otherwise} \end{cases}$$

True Cauchy stress and logarithmic strain

$\sigma_{true}(\sigma) := \sigma \cdot (1 + \varepsilon(\sigma))$

$\varepsilon_{log}(\sigma) := \ln(1 + \varepsilon(\sigma))$

ANSYS accepts multilinear (true)stress-(log)plastic strain curves

$$\varepsilon_{pl} = \varepsilon - \frac{f_y}{E} \qquad \text{(C.14)}$$

$$\varepsilon_{pl}(\sigma) := \varepsilon_{log}(\sigma) - \frac{f_y}{E}$$

1) Modelled engineering stress–strain curve for comparison with the reference study.

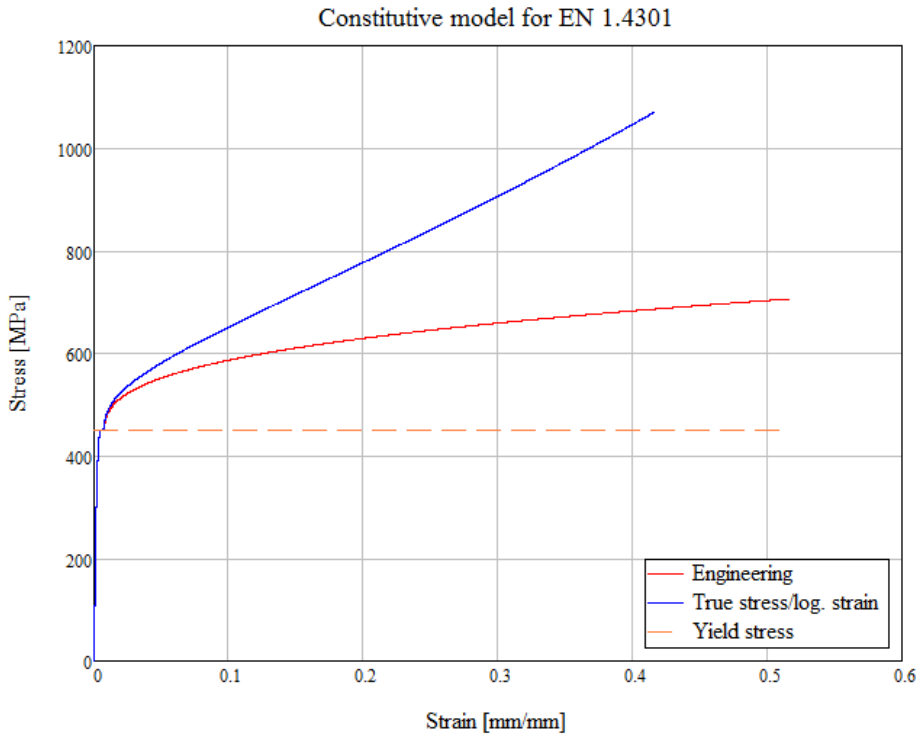

2) Engineering stress–strain relationship from the reference study [64]. S6-5 is the room temperature curve.

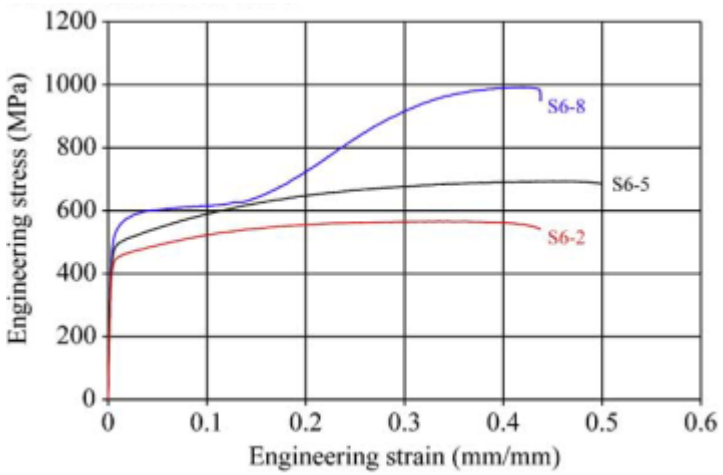

APPENDIX 2: MATERIAL MODEL IN SIMULATION MODEL VALIDATION, ALUMINUM

The material model for aluminum is modelled with the two-stage Ramberg–Osgood model, which is used for stainless steels.

Modelling of material behaviour, Design manual for stainless steel, 4th edition [3]

Material properties from the test for aluminum

$E := 68GPa$ $\varepsilon_u := 0.27$ Young's modulus and ultimate elongation

$f_y := 68MPa$ $f_u := 97MPa$ Yield (0.2 % proof) and ultimate strengths

$n := 7$

$$E_y := \frac{E}{1 + 0.002 \cdot n \cdot \frac{E}{f_y}}$$

$$m\_ := 1 + 2.8 \cdot \frac{f_y}{f_u}$$

$$\varepsilon(\sigma) := \begin{cases} \frac{\sigma}{E} + 0.002\left(\frac{\sigma}{f_y}\right)^n & \text{if } \sigma \le f_y \\ 0.005 + \frac{f_y}{E} + \frac{\sigma - f_y}{E_y} + \varepsilon_u \cdot \left(\frac{\sigma - f_y}{f_u - f_y}\right)^{m\_} & \text{otherwise} \end{cases}$$

True Cauchy stress and logarithmic strain

$\sigma_{true}(\sigma) := \sigma \cdot (1 + \varepsilon(\sigma))$

$\varepsilon_{log}(\sigma) := \ln(1 + \varepsilon(\sigma))$

ANSYS accepts multilinear (true)stress-(log)plastic strain curves

$$\varepsilon_{pl} = \varepsilon - \frac{f_y}{E} \qquad (C.14)$$

$$\varepsilon_{pl}(\sigma) := \varepsilon_{log}(\sigma) - \frac{f_y}{E}$$

1) Modelled engineering stress–strain and true stress–logarithmic strain curves.

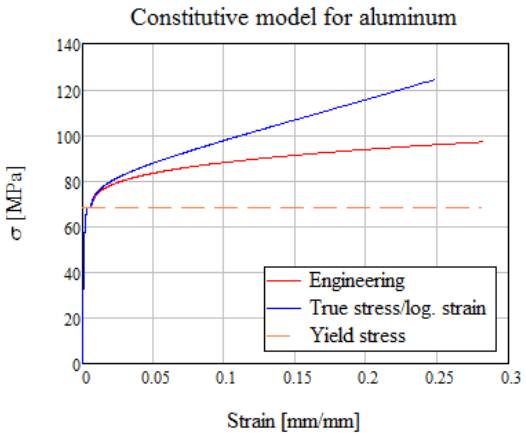

2) Modelled engineering stress–strain curve for comparison with the reference study.

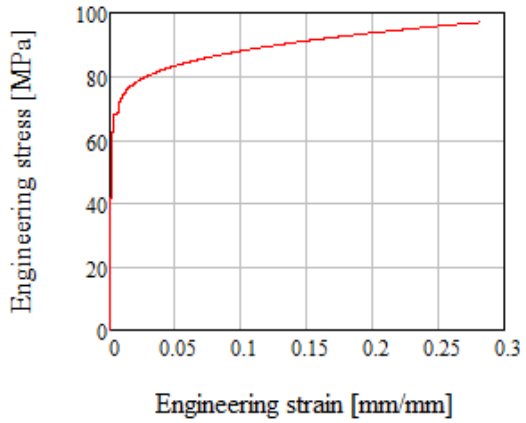

3) Engineering stress–strain curve from reference study [111].

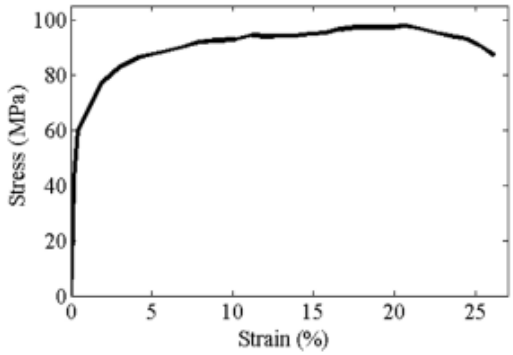

Fig. 2. Stress–strain curve of aluminum material.

APPENDIX 3: USED CROSS SECTIONS IN SQUARE HOLLOW SECTION FIRE DESIGN COMPARISON

50×50×3	100×100×5	160×160×6
50×50×4	100×100×6	160×160×8
50×50×5	100×100×8	160×160×10
60×60×3	110×110×4	180×180×6
60×60×4	110×110×5	180×180×8
60×60×5	120×120×3	180×180×10
70×70×3	120×120×4	200×200×5
70×70×4	120×120×5	200×200×6
70×70×5	120×120×6	200×200×8
80×80×3	120×120×8	200×200×10
80×80×4	120×120×10	200×200×12.5
80×80×5	140×140×5	250×250×6
80×80×6	140×140×6	250×250×8
90×90×3	140×140×8	250×250×10
90×90×4	140×140×10	250×250×12.5
90×90×5	150×150×5	300×300×6
90×90×6	150×150×6	300×300×8
100×100×2.5	150×150×8	300×300×10
100×100×3	150×150×10	300×300×12.5
100×100×4	150×150×12.5	

APPENDIX 4: 15 MIN STANDARD FIRE WITH UNPROTECTED AXIALLY LOADED EN 1.4301, EN 1.4571 AND S355 COLUMNS

Mild steel room temperature and fire design according to EN 1993-1-1 [115] and EN 1993-1-2 [106], respectively, stainless steel room temperature and fire design according to Design Manual for Structural Stainless Steel, 4th edition (2017) [3].

Buckling length 3000 mm. Room temperature ULS load kept constant at 100 kN, fire load 30…80 kN. Profile selection presented in appendix 3.

UR is utilization rate, RT is room temperature.

EN 1.4301 η_{fi}	UR @ RT [%]	UR @ fire [%]	Profile [mm]	Mass [kg]	max. UR [%]
0.3	99	55	80x80x3	7.2	99
0.4	99	73	80x80x3	7.2	99
0.5	99	91	80x80x3	7.2	99
0.6	76	89	90x90x3	8.2	89
0.7	62	88	100x100x3	9.1	88
0.8	59	88	90x90x4	10.7	88

EN 1.4571 η_{fi}	UR @ RT [%]	UR @ fire [%]	Profile [mm]	Mass [kg]	max. UR [%]
0.3	97	41	80x80x3	7.2	97
0.4	97	55	80x80x3	7.2	97
0.5	97	68	80x80x3	7.2	97
0.6	97	82	80x80x3	7.2	97
0.7	97	96	80x80x3	7.2	97
0.8	75	86	90x90x4	8.2	86

S355 η_{fi}	UR @ RT [%]	UR @ fire [%]	Profile [mm]	Mass [kg]	max. UR [%]
0.3	45	93	90x90x4	10.5	93
0.4	35	95	100x100x4	11.7	95
0.5	29	94	110x110x4	13.0	94
0.6	24	92	120x120x4	14.2	92
0.7	24	92	110x110x5	16.0	92
0.8	25	96	100x100x6	17.0	96

APPENDIX 5: 30 MIN STANDARD FIRE WITH UNPROTECTED AXIALLY LOADED EN 1.4301, EN 1.4571 AND S355 COLUMNS

Mild steel room temperature and fire design according to EN 1993-1-1 [115] and EN 1993-1-2 [106], respectively, stainless steel room temperature and fire design according to Design Manual for Structural Stainless Steel, 4th edition (2017) [3].

Buckling length 3000 mm. Room temperature ULS load kept constant at 100 kN, fire load 30…80 kN. Profile selection presented in appendix 3. UR is utilization rate, RT is room temperature.

EN 1.4301 η_{fi}	UR @ RT [%]	UR @ fire [%]	Profile [mm]	Mass [kg]	max. UR [%]
0.3	99	84	80×80×3	7.207	99
0.354	98.6	98.7	80×80×3	7.207	98.7
0.4	76	93	90×90×3	8.167	93
0.5	62	100	100×100×3	9.127	100
0.6	48	91	100×100×4	11.958	91
0.7	40	93	110×110×4	13.238	93
0.8	34	94	120×120×4	14.518	94

EN 1.4571 η_{fi}	UR @ RT [%]	UR @ fire [%]	Profile [mm]	Mass [kg]	max. UR [%]
0.3	97	52	80×80×3	7.207	97
0.4	97	70	80×80×3	7.207	97
0.5	97	87	80×80×3	7.207	97
0.555	96.9	97.0	80×80×3	7.207	97.0
0.6	75	83	90×90×3	8.167	83
0.7	75	96	90×90×3	8.167	96
0.8	60	91	100×100×3	9.127	91

S355 η_{fi}	UR @ RT [%]	UR @ fire [%]	Profile [mm]	Mass [kg]	max. UR [%]
0.3	24	91	120×120×5	14.246	91
0.4	20	98	120×120×5	17.550	98
0.5	15	91	140×140×5	20.690	91
0.6	13	97	150×150×5	22.260	97
0.7	11	94	150×150×6	26.402	94
0.8	10	96	160×160×6	28.284	96

APPENDIX 6: 15 MIN STANDARD FIRE WITH UNPROTECTED AXIALLY LOADED EN 1.4301, EN 1.4162 AND S355 MEMBERS WITH DIFFERENT BUCKLING LENGTHS

Critical length 2.0 m, 3.0 m, 4.0 m, 5.0 m, 6.0 m. Buckling length was assumed to be the member length. Room temperature compressive load 200 kN, elevated temperature load 110 kN.

L_{cr} (m)	S355 + regular paint	mass (kg)	price (€)
2.0	100×100×6	16.98	24.45
3.0	120×120×6	20.75	29.80
4.0	120×120×8	26.41	35.18
5.0	120×120×10	31.85	40.45
6.0	120×120×10	31.85	40.45

L_{cr} (m)	EN 1.4301	mass (kg)	price (€)
2.0	80×80×5	11.49	36.75
3.0	90×90×5	13.09	41.87
4.0	120×120×4	14.52	46.46
5.0	120×120×5	17.89	57.23
6.0	140×140×5	21.09	67.47

L_{cr} (m)	EN 1.4162	mass (kg)	price (€)
2.0	80×80×4	9.16	45.82
3.0	90×90×4	10.41	52.06
4.0	100×100×5	14.32	71.59
5.0	110×110×5	15.88	79.39
6.0	120×120×6	20.62	103.09